Geometry of Gene Regulatory Dynamics

David A. Rand[a], Archishman Raju[b,c], Meritxell Sáez[a,d], Francis Corson[e], and Eric D. Siggia[c,1]

[a]Zeeman Institute for Systems Biology and Infectious Epidemiology Research, University of Warwick, Coventry, CV4 7AL, UK; [b]Simons Centre for the Study of Living Machines, National Centre for Biological Sciences, Tata Institute of Fundamental Research, Bangalore, India; [c]Center for Studies in Physics and Biology, Rockefeller University, New York, NY 10065; [d]The Francis Crick Institute, 1 Midland Road, London, NW1 1AT, UK; [e]Laboratoire de Physique de l'Ecole Normale Supérieure, CNRS, ENS, Université PSL, Sorbonne Université, Université de Paris, 75005 Paris, France

This manuscript was compiled on May 25, 2021

Embryonic development leads to the reproducible and ordered appearance of complexity from egg to adult. The successive differentiation of different cell types, that elaborates this complexity, result from the activity of gene networks and was likened by Waddington to a flow through a landscape in which valleys represent alternative fates. Geometric methods allow the formal representation of such landscapes and codify the types of behaviors that result from systems of differential equations. Results from Smale and coworkers imply that systems encompassing gene network models can be represented as potential gradients with a Riemann metric, justifying the Waddington metaphor. Here, we extend this representation to include parameter dependence and enumerate all 3-way cellular decisions realisable by tuning at most two parameters, which can be generalized to include spatial coordinates in a tissue. All diagrams of cell states vs model parameters are thereby enumerated. We unify a number of standard models for spatial pattern formation by expressing them in potential form. Turing systems appear non-potential yet in suitable variables the dynamics are low dimensional, potential, and a time independent embedding recovers the biological variables. Lateral inhibition is described by a saddle point with many unstable directions. A model for the patterning of the Drosophila eye appears as relaxation in a bistable potential. Geometric reasoning provides intuitive dynamic models for development that are well adapted to fit time-lapse data.

Morse-Smale | Waddington landscape | bifurcation | Turing model | gene network

1. Introduction

Much of classical physics, chemistry, and by extension biology is represented by differential equations. Particularly in biology, the precise form of these equations and their parameters is poorly known. In addition, the long time behavior of these systems is typically opaque and one resorts to a case by case numerical solution. Mathematics sidesteps the question of solving a particular equation by using geometric methods to enumerate the discrete types of solutions. Then qualitative features of the biology may select a type and mathematics in some instances then supplies a minimal parameterization.

A most striking aspect of development is the extreme fidelity of the output in response to insults, which nicely aligns with the mathematical notion of genericity, i.e., simply by insisting all nearby systems are equivalent, eliminates exceptional cases that require parameter tuning and are unlikely to be relevant to biology. The assumption of genericity strongly constrains the dynamical behavior. Although the dynamics appropriate for development are simple, expressing a model in geometric language classifies its essential features. In particular Smale and his school have shown that models that plausibly encompass development all admit a potential that decreases as the system evolves. This potential derives from a graph representing which critical or decision points can flow to which others. Thus the potential is implicit in, and derived from, the dynamics. Then the differential equation model can be written effectively as a metric times the gradient of this potential all defined on a Riemann manifold. Thus the Waddington metaphor for development, as flow down a landscape with bifurcations signifying decisions between alternative cell fates, is literally true.

Geometric reasoning will typically reduce a genetic model to a few variables per cell, and thus the explicit connection of variables to genes is lost. But the typical network for cell communication involves tens of genes, and most gene centric models include only a subset of these, thus are to some degree phenomenological. Geometry takes this reduction to the extreme, and will deliver the minimum number of parameters that can not be eliminated by variable redefinitions, and the minimal phase space for representing the dynamics surrounding a cellular decision.

The results of Smale and colleagues do not apply through bifurcation points which is essential for applications. Thus we extend their results to encompass bifurcations, both local and global. We limit ourselves to at most three possible states per cell to capture a progenitor cell giving rise to two alternative fates. Within this class we enumerate all ways the cellular states can be arranged by two parameters. Our topological arguments yield global results in parameter and state spaces that link together locally described bifurcations.

Geometric methods are well suited to fitting time lapse data obtained when cells are poised among competing fates. A minimal parameterized topographic model with the correct

Significance Statement

Genetic screens have enumerated the genes that control the process of self-organization that converts a featureless fertilized egg into an embryo. Even the elementary steps may involve ten genes so models that attempt to represent each gene contain a plethora of unmeasured parameters. Mathematics has largely categorized the types of solutions that can arise from the equations governing gene networks. These representations are well suited to modern time-lapse imaging where a limited number of genetic markers are followed in time. Models with minimal parameters that focus on the nonlinear regime from inception to pattern maturation, simplify data fitting, and provide an intuitive and transparent representation for the dynamics of development.

All authors contributed to the calculations and composition of the paper.

Please declare any conflict of interest here.

[1]To whom correspondence should be addressed. E-mail: siggiaerockefeller.edu

geometry is essential to extract model parameters from the cells as they are transitioning. Merely enumerating terminal fates looses this information. When dealing with many cells, focusing on the saddle points that represent cellular decisions quantifies similarities among all models that use inhibition to define a pattern. Turing showed how chemical reactions plus diffusion can generate patterns in an otherwise uniform system. In geometric terms the Turing instability is represented as a saddle point and the trajectory from it to the terminal pattern can be represented by gradient dynamics in the tangent space of the saddle composed with a time independent sigmoid, thus revealing similarities to models of lateral inhibition by long-range contacts or diffusing factors. Geometric methods are optimal for bridging the time from the initiation of a pattern to its saturation, and thus extracting the essential dynamics of cell specification.

2. The mathematics of gene network models

A gene network model defines a differential equation that describes the changes on the system with time. The time integration of a differential equation or, equivalently a vector field defines a flow $x \to \phi^t(x)$ which tells us the state $\phi^t(x)$ at time t if the initial state at time $t = 0$ was x. Off of the bifurcation set, the restpoints p of these systems have well-defined stable and unstable manifolds i.e. (stable manifold) $W^s(p) = \{x | \phi^t(x) \to p \text{ as } t \to \infty\}$ and (unstable manifold) $W^u(p) = \{x | \phi^t(x) \to p \text{ as } t \to -\infty\}$, Fig.1. Moreover, these restpoints p are of three types: attractors ($W^u(p)$ empty, they attract all nearby points), saddles ($W^s(p)$ & $W^u(p)$ not empty) and repellors ($W^s(p)$ empty). We say a saddle has index λ if its unstable manifold has dimension λ.

If a system is not on the bifurcation set then small perturbations of it do not change its qualitative form (i.e. there is a homeomorphism of phase space sending the trajectories of one system onto the other). We say that such a system is *structurally stable*.

Relatively simple sufficient conditions have been found (1) for systems with a finite number of restpoints and periodic orbits to be structurally stable and these are called *Morse-Smale (MS) systems* (2). These assumptions exclude chaos but include models of development. In what follows, we exclude periodic orbits and insist that trajectories can not escape to infinity. This is entirely plausible for development and makes the point at infinity a repeller which is needed for certain topological arguments. In our applications the phase space M is the n-dimensional Euclidean space $\mathbb{R}^n$

The downhill structure of generic landscapes. The Waddington analogy of development to flow in a topography can be formalized mathematically. All MS systems possess a Liapunov function (a.k.a. potential function) defined on the phase space which decreases along trajectories and for which restpoints (and periodic orbits) are critical points. This formalizes the notion of height in a topography. We call such dynamical systems *gradient-like*. It is commonly thought that this is enough to specify dynamics but the Liapunov function is not enough to determine where a cell will go when it escapes an attractor, ie a small perturbation to Fig.1F will direct the unstable manifold from the upper saddle to either state B or C. Therefore extra information about the dynamics is necessary.

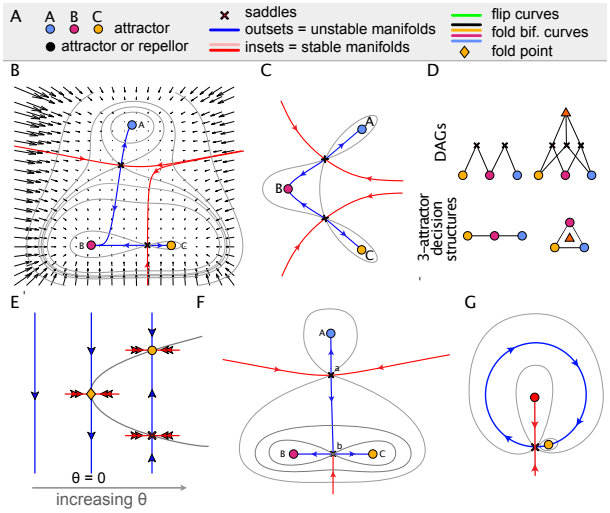

Fig. 1. Representations of Morse-Smale systems. **A.** The symbol set used consistently to describe elements of the phase space or parameter space (flip and fold bifurcation curves). **B.** A Morse-Smale system with three attractors and two saddles showing the stable (red) and unstable (blue) manifolds of the saddles. Contours of a potential are shown in grey. In this system the unstable manifolds meet at the attractor B in a cusp like shape. **C.** In this Morse-Smale system which also has 3 attractors, the unstable manifolds of the saddles make up a smooth curve. **D.** (Top row) Two examples of directed acyclic graphs (DAG) corresponding to the system in **B** (left) and the compactified elliptic umbilic of Fig.5D (right). (Bottom row) The decision structures associated with the DAGs above them. The filled circles represent the attractors and a connection between attractor A and B means that a cell whose state sits at A (resp. B) can transition to B (resp. A) via a saddle-node bifurcation that destroys A (resp. B). Thus the connections characterize the escape routes and possible decisions. The connections also correspond to the index 1 saddles in the system that connect A and B. Some escape routes wrap around an index 2 saddle as shown and indicated by a triangle. To minimize the numbers of decision diagrams we do not distinguish cases where multiple saddles connect the same two fixed points (see SI). **E,F.** The two simplest bifurcations: the local saddle-node and the global heteroclinic flip. These are the main events underlying decision-making in our dynamical systems. **E.** A saddle-node or fold bifurcation. As θ increases through 0 a saddle and an attractor are born which then separate with a distance of order $\sqrt{\theta}$. **F.** The configuration shown in **A** can flip to one where the saddle a is connected to C instead of B via a *heteroclinic flip*. To do this it passes through the intermediate state shown where there is a heteroclinic connection in which the unstable manifold of the saddle a connects to the saddle at b. **G.** An example of a compact landscape involving a repellor. We have taken a case where the attractor is close to the saddle to illustrate that the attractor can move around the circular unstable manifold and collide undergoing a saddle-node bifurcation and turning the unstable manifold into a limit cycle. This is called a SNIC bifurcation. Although it is important to be aware of such bifurcations we do not consider them anymore since the existence of a limit cycle moves us out of the gradient-like restpoint-only systems.

There are two essentially equivalent ways to specify the missing information. One way is to supply the stable and unstable manifolds of the saddle points. The unstable manifolds of the index one saddles for instance describe the transition routes between attractors.

The other way to augment the Liapunov function, is to note that MS systems are nearly *gradient systems*. In a gradient system a potential f together with a Riemannian metric g_{ij} completely defines the dynamical system:

$$\dot{x}_i = -\sum_j g^{ij} \frac{\partial f}{\partial x_j} \qquad [1]$$

where $(g^{ij}) = (g_{ij})^{-1}$. The restpoints of such a vector field are the critical points of f (g_{ij} is positive definite), and the metric rotates and stretches the potential gradient so it coincides with the vector field. Gradient-like MS systems are also

nearly gradient and the difference is just at the restpoints. By making adjustments of the restpoints in arbitrarily small neighbourhoods one can convert the system into a topologically equivalent gradient system ((3), SI App. A). The need to adjust the restpoints is because at such points the gradient system has a special structure (e.g. the eigenvalues are real), while the MS system allows complex eigenvalues with nonzero real parts. In applications, the model with its metric abstractly represents how signals distort the landscape and direct cells to the available fates or attractors.

A directed acyclic graph organizes cellular decisions. Now consider a MS system and the graph G whose vertices correspond to the restpoints and where two vertices β and β' are connected with a (downward) directional edge (denoted $\beta \succ \beta'$) if there is a trajectory going from β to β', Fig.1D. Then, the following non-trivial results hold (4): (i) it is never true that $\beta \succ \beta$; (ii) if $\beta \succ \beta'$ and $\beta' \succ \beta''$ then $\beta \succ \beta''$ (thus $\succ$ is a partial ordering) (iii) if $\beta \succ \beta'$ then $\dim W^s(\beta) \leq \dim W^s(\beta')$. The conditions (i-ii) that exclude $\beta \succ \beta'$ and $\beta' \succ \beta$ are crucial and eliminate heteroclinic cycles (these are not generic). By (iii) we can naturally attach levels to the nodes of G using the *index* $d = \dim W^u(\beta)$. The attractors are at the bottom level ($d = 0$), the repellors at the top and the index d saddles at level d. The graph G is a directed acyclic graph which we shall refer to as the *DAG*.

Using this we can allocate heights h_i to the restpoints which for consistency must satisfy that $h_i > h_j$ whenever $\beta_i \succ \beta_j$ and then find a Liapunov function h that takes these values at restpoints. Moreover, this function can be taken to be a Morse function (5). This means that near each restpoint β_i there is a coordinate system $x_1, \ldots, x_n$ such that in these coordinates $h = h_i + \sum \pm x_i^2$ with the number of minuses equalling the index of β_i.

This height function is unique in the following sense (5). If $\hat{h}$ is another Liapunov function such that the heights $h'_i = \hat{h}(\beta_i)$ are ordered in the same way as those of h, then h and $\hat{h}$ are qualitatively equivalent in the sense that there are homeomorphisms, ϕ of the phase space and ψ of the reals $\mathbb{R}$ such that $\hat{h}(x) = \psi(h(\phi(x)))$.

As we will see below a number of advantages flow from these results. Since motion is always downhill it gives a hierarchical structure to the dynamics and easier understanding of the eventual fates. Secondly, there is a powerful classification theory for the bifurcations of such systems that is aided by the existence of the potential, and, finally, it allows a better understanding of how complexity of such systems can be built up.

Parameterised landscapes. Our dynamical systems depend upon parameters that will be changed by the signals received by the cell. Changes in the parameters may cause bifurcations where the qualitative nature of the dynamics undergoes a discontinuous change and these lead to transitions between cell states.

For a given number of attractors or saddles there are a large number of topologies of landscape potentials. However, if we define a decision as the eventual attractor A reached after the state is freed from its initial attractor B either by a bifurcation destroying B or by stochastically escaping the basin of B then we can associate to a DAG a unique connected simple graph that we call *decision structure* (see Fig.1D) which encodes the possible decisions. The number of these is much smaller than the number of landscapes. All three and four-attractor decision structures are shown in Fig. 1D and the SI Sec I.7 respectively.

For applications to biology, we consider situations where a precursor cell decides between two alternative fates. Thus we classify decisions among three or fewer states that depend on two or fewer parameters. The fold bifurcations, Fig.1E, divide the parameter space up into components in which the restpoints vary smoothly with parameters. We call these *MS-components*.

In what follows, we leverage the continuity of MS dynamics within a MS component to arrive at global representation of the parameter space. The component boundaries consist of smooth fold bifurcation segments that meet in special points that we can enumerate under assumptions of genericity. The sequence of these points around the boundary of the MS-component classifies the component. This classification for gradient-like MS systems is global and, not only tells us what to expect in detailed mechanistic models, but also provides a class of archetypal models that can be parameterised and compared to experimental data (6–8) as described below.

Universality and normal forms. It is very useful to contrast our proposed construction of parameterized landscapes with the ideas of a universal unfolding and normal forms that are derived from Thom's theorem (9, 10) that gave rise to Catastrophe Theory (Fig. 2). This subject assumes strictly gradient dynamics. It then classifies, irrespective of the dimension of state space, the generic local bifurcations in parameterised dynamical systems where the number r of parameters θ (or codimension) is ≤ 5 ,Fig. 2. By smooth variable changes any function near the bifurcation can be reduced to a normal form polynomial in one or two dimensions ,Fig. 2. The dynamics in the other dimensions is just contraction onto the one or two effective dimensions, thus proving strong dimensional reduction. The parameters in the normal form are the minimum necessary to represent the bifurcation to within variable changes. On the other hand, in parallel with our discussion above about needing to know more than the Liapunov function, it does not classify the global bifurcations in such systems arising from heteroclinic connections (2, 11, 12) which need to be handled separately. Moreover, the results are local in that they only apply close to a bifurcation point.

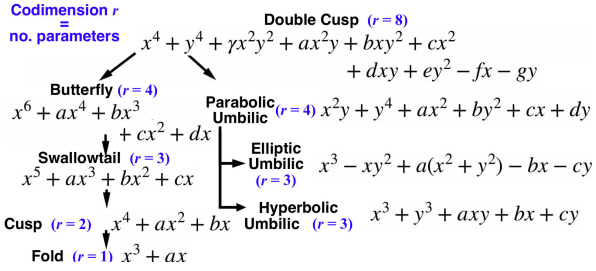

Fig. 2. The hierarchy of elementary catastrophes obtained by coupling two bistable systems. These describe all generic local bifurcations of potentials depending on $r \leq 4$ parameters. If h_θ is such a generic family then there are coordinates $(x_1, \ldots, x_n)$ on phase space such that $h_\theta = f_\theta(y) + \sum_{\rho+1}^{n} \epsilon_i x_i^2$ where $f_\theta(y)$ represents one of the elementary catastrophes in the figure, $\rho = 1$ *or* 2 and the remaining phase space variables can be reduced to a diagonal quadratic form where $\epsilon_i = \pm 1$. Several of these polynomials are prototypes for the parameterized landscapes below For a precise statement see (10).

We aim for results that are global in phase and parameter space and apply to generic parameterized families with a finite number of restpoints and no periodic orbits. Nevertheless the catastrophes of higher codimension are biologically relevant because even if the parameters that we can manipulate to control fates (morphogens) are fewer in number than the codimension, two-dimensional cuts through complete parameter space will occur in our enumeration. Figure 5A occurs as part of the butterfly (codim. $r = 4$), and Fig. 5D is essentially related to the elliptic umbillic (codim. $r = 3$).

In the following discussion we focus on generic systems and bifurcations and do not treat non-generic situations that occur because the system is restricted by, for example, invariant boundaries (e.g. the Lotka-Volterra systems) or symmetries.

Building up complexity: the simplest bifurcations. Any gradient-like MS system can be built up by using just three simple bifurcation types (13). Only two of these are relevant to our discussion: the *fold* (Fig. 1E), and the simplest global bifurcation, the *heteroclinic flip* (Fig. 1F). As we will see, these bifurcations are particularly important for development and using them provides a powerful method to build complexity that is available for evolution to work on (SI Sec I.2).

The *fold* (a.k.a. the *saddle-node*) bifurcation results in the appearance of an attracting or repelling restpoint and an index 1 saddle as a parameter θ is changed (supercritical case) or the disappearance of the same (subcritical case). More generally a fold results in the creation/destruction of a pair of saddles of index i and $i + 1$. The fold is local in that all the action takes place around a point in parameter and phase space.

When a heteroclinic flip occurs, the outset of a saddle flips between two different attractors by passing through a state where the unstable manifold of one saddle is the inset of the other i.e. we have a heteroclinic connection (Fig.1F).

Figure 3 shows the generic local ways we can build a system with three attractors starting from a bistable one within a two dimensional parameter space. Specifically we show all the ways that folds (codimension-1) defined by a smooth curve in the parameter space can intersect in codimension-2 cusps or crossings Fig.3C-F. Then Fig. 3G-H shows the two ways in which a curve of heteroclinic flips can terminate in a fold bifurcation curve, defining a second class of codimension-2 points in parameter space. From these locally described bifurcation sets, we can construct all 2d phase diagrams of MS systems. (Catastrophe theory enumerates higher codimension points, but all the codimension-2 points are contained in our list.)

Dimensional reduction characterizes transitions among landscapes. Repellors and higher index saddles can complicate the classification in Fig.3 e.g., each index-1 saddle can be replaced by two index-1 and one index-2 saddles. This is handled using the following result (SI Appendix A). As we have seen above, the developmental transitions and decisions are determined by the disposition of the unstable manifolds of the index 1 saddle points relative to the attractors. Thus a first useful result (see SI) is that for a MS system in our context one can always find an attracting ball B in phase space with smooth spherical boundary ∂B that contains all the N attractors, $N - 1$ index 1 saddles connected to them and also captures almost all the trajectories. There may be choices of B depending on which index 1 saddles are included which in turn define which decision structures are allowed within B.

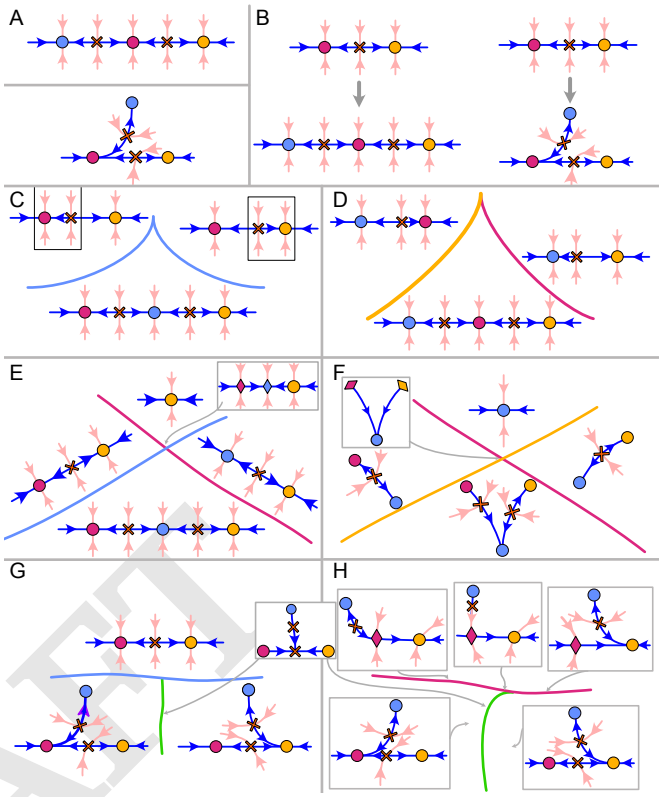

Fig. 3. Building complexity from bistable landscapes using one and two-dimensional perturbations. Symbols follow the key in Fig.1A.(A) We distinguish between these two 3-attractor systems even though they are topologically conjugate because in applications the allowed transitions are different. The red attractor can not undergo a saddle-node bifurcation when the outsets of the saddles merge in a cusp. The attractors represent biological states that are not equivalent, as they would be under topological conjugacy. (Top) All the restpoints lie on a smooth curve defined by the outsets of the saddles. (Bottom) The outsets of the saddles meet at a central sink in a cusp with a common tangency. (B) Fold bifurcations add an extra saddle-sink pair to the bistable system. The new attractor is marked in blue. (C-H) The allowed bifurcation sets for three and fewer fixed points when two parameters are varied. The colored curves denote fold bifurcations where the like colored attractor disappears. (C) Dual cusp. The new attractor in blue and saddle are inserted in the middle. For this to occur the fold bifurcation curve must contain at least one cusp point. (D) Standard cusp. A bistable system has a third attractor added. The cusps in (C,D) are defined by the discriminant of the same 3rd order polynomial representing either a source and two saddles or a saddle and two attractors (cf Fig.2). (E,F) Crossing points. Two fold bifurcation curves can intersect transversally creating a region with a single attractor and a region where there are three attractors. (E). One of the two bifurcation curves involves the central attractor and then the attractors must lie on a smooth curve. (F). In this case the curves correspond to peripheral attractors and then both smooth and cusped unstable manifolds are possible. (G,H). There can be a (codimension 2) point on the fold bifurcation curve where the outset of the top saddle undergoes a heteroclinic flip as shown. Generically these heteroclinic flips occur on a curve (green). (G). When the source saddle bifurcates away the flip curve in green intersects the fold bifurcation curve transversely. (H). When the target saddle is destroyed in a fold bifurcation the flip curve generically terminates in a cusp (see SI)

Under these conditions, we can find B above so that the stable manifolds of the index 1 saddles transversally intersect the spherical boundary of B in disjoint spheres of dimension $\dim B - 1$ and divide B into regions each of which is the basin of one of the attractors (see SI). The stable manifolds of the saddles define the boundaries of the basins of attraction for

each attractor. Two attractors in adjacent basins are joined by the unstable manifold of the saddle. Thus the entire MS component is controlled by its boundary

As a corollary, for such systems with 3 attractors, there are two index 1 saddles that connect them and they have a simple disposition: the unstable manifolds of each saddle each connect to two of the attractors and they join at one of the attractors (called the *central attractor*). It is fixed at crossings and cusps Fig. 3C-F, but interchanges at flip points. The other attractors are called *peripheral*. The union of the unstable manifolds is called the *connector*. At the central attractor, the unstable manifolds either join smoothly or in a non-smooth fashion. If non-smooth and this attractor is close to undergoing a fold bifurcation then the join has a cuspoidal shape as in Fig. 3 (SI Sect. I1). In either case the DAG linking the attractors is shown in Fig.1D (left).

The universal dimension independent topological structure of the attractors, index-1 saddles, and their unstable manifolds that comes from the existence of B is a statement of dimensional reduction derived purely from the dynamics. The restrictions on the orientation of the central attractor that derive from B lead to the results in Fig. 4 and severely constrain the bifurcations that can occur in the boundary of a MS component.

Global bifurcation structures. We want to understand the structure of the bifurcations and transitions as the parameters pass into and out of MS-components with ≤ 3 attractors. We start by discussing the compact ones Ω i.e. ones which do not intersect the boundary of the parameter domain. To get the corresponding characterisation for noncompact versions one just opens up the boundary of the MS component, $\partial\Omega$ at a crossing point.

For our discussion it is necessary to consider the so-called *catastrophe manifold* (SI Sec I.3),

$$\mathcal{M} = \{(x,\theta) | x \text{ is a restpoint of } \phi_\theta^t\}.$$

Then, a key point is that, if the parameter space is d-dimensional and the state-space n-dimensional, $\mathcal{M}$ is generically a submanifold of $\mathbb{R}^n \times \mathbb{R}^d$ having the same dimension d as the parameter space (10, 15). Thus, here it is a surface in $n+2$ dimensions. For our systems the topology of $\mathcal{M}$ is trivial (it is diffeomorphic to a disk, see SI Sec I.3) but the way it sits in $\mathbb{R}^n \times \mathbb{R}^d$ and the non-trivial structure of the projection $\chi(x,\theta) \mapsto \theta$ from $\mathcal{M}$ to parameter space is hugely informative.

A point $\mathbf{x} = (x,\theta)$ in $\mathcal{M}$ corresponds to a restpoint x of the parameterised landscape at θ and we will be particularly interested in the subset where x is either a fold or cusp point. Generically this consists of smooth curves $\mathcal{C}$ (called *fold curves*) which can either be open and connecting to the boundary of $\mathcal{M}$ or they can be circles (called *fold circles*). The part of the bifurcation set corresponding to folds and cusps consists of the sets $B_\mathcal{C} = \chi(\mathcal{C})$ in parameter space, called fold bifurcation curves, where χ is the projection defined above. Although $\mathcal{C}$ is smooth, $B_\mathcal{C}$ will typically have cusp points as in Figs.3 and 5. A smooth piece of a fold bifurcation curve is called a fold bifurcation segment. If $\mathcal{C}$ is a fold circle then $B_\mathcal{C}$ is a closed curve without self-intersections (SI Sec II.3).

Now a key result that will lead to our characterisation of MS-components is the following: If $\mathbf{x} = (x,\theta) \in \mathcal{M}$ is on a fold curve $\mathcal{C}$ then through x there is a center manifold (2) and as $\mathbf{x}$ moves along $\mathcal{C}$ the tangent $\ell(\mathbf{x})$ to this center manifold varies in a smooth fashion. At x the time evolution determines a definite positive direction and orientation on $\ell(\mathbf{x})$ (Fig. 4B). Generically, as $\mathbf{x}$ moves along a fold curve $\mathcal{C}$ this orientation flips only at cusps and so counting orientation flips gives the number of cusps in $\mathcal{C}$ (SI Sec. I.4).

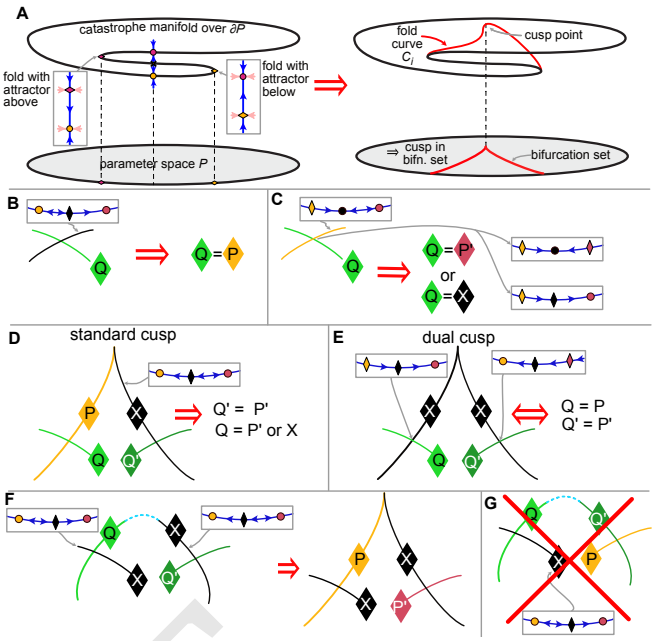

Fig. 4. Legend as in Figs.1A and 3. **A.** Over part of the boundary ∂P of a 2-dimensional domain of parameter space P we assume we have an S-shaped bistable section and that the system is monostable over the rest of ∂P. Then it follows that under very mild conditions (SI Sect. I4E) inside P there must be at least one cusp (see (14) for $n = 1$ case). This is because there must be a fold curve joining the two folds shown and on this fold curve the two folds shown have opposite orientations. (B-G) Local rules governing the disposition of cusps and crossings in the boundary of a 3-attractor MS component. X is always the central attractor, P, P' peripheral. **B.** The orientation of the fold bifurcation involving the central attractor determines the possible transverse crossings of the fold bifurcation curve. On the black fold bifurcation curve the central attractor bifurcates with the saddle to its right (connected to red), thus the only allowed crossing is the bifurcation of the yellow attractor with its saddle. **C.** The peripheral attractor involved in the fold constrains the possible crossings of the fold bifurcation curve. **D. Standard cusp.** Fold bifurcation curves crossing the cusp's branches satisfy the conditions in (B) and (C). **. E. Dual cusp.** Fold bifurcation curves crossing the cusp's branches satisfy the conditions in (B) and (C) and the crossings imply the existence of the cusp. **F.** The opposite orientations of the folds of the central attractor on the two fold bifurcation curves as shown imply the existence of a cusp. **G.** If $Q - Q'$ is a single fold bifurcation curve, certain consecutive crossings are not possible. By (B) $Q = P$ but P can not intersect itself, so if $Q' = X$ then the next intersection can only be with P' via (D).

From this observation we readily get all the results in Fig. 4 and these provide tight constraints on what can happen in the boundary of a 3-attractor MS-component (Ω in parameter space) as we now explain. By definition the attractors vary smoothly in Ω with the parameters and maintain their identity.

As one proceeds around $\partial\Omega$ there is a sequence of codimension 2 points $\theta_1 \ldots \theta_N$ with $\theta_N = \theta_1$ as described in Fig.3, namely cusps, dual cusps, crossings and the two types of endpoints of flip curves. If we know these then we know all the bifurcation structures associated with Ω and $\partial\Omega$. The points θ_i and θ_{i+1} are joined by a smooth fold bifurcation segment ℓ_i.

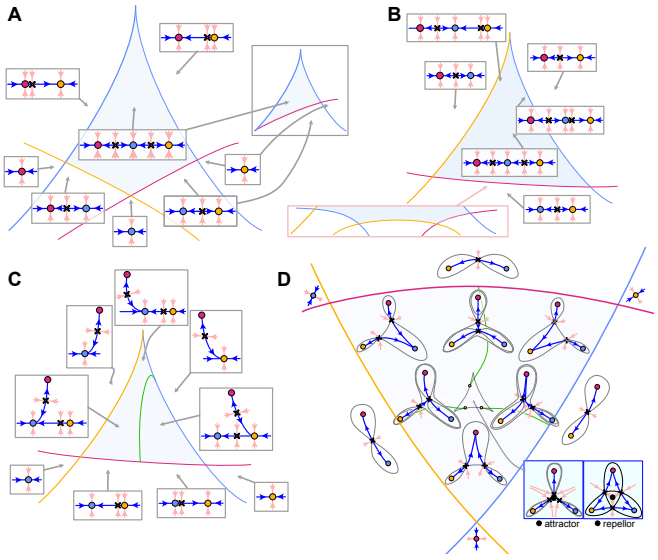

Fig. 5. Minimal 3-attractor MS-components (light blue). Legend as in Fig. 1A or 3. The color of a fold bifurcation curve indicates the attractor that bifurcates on it. (A) The minimal MS-components containing a dual cusp. The inset figure shows the minimal system involving a dual and standard cusp. The MS components with $\leq$ 2 attractors are a subset of this for the dual cusp case. (B) Minimal MS-component for a standard cusp. Inset in pink box shows a simple alternative configuration replacing the red curve at the bottom of the cusp. (C) Ditto for a standard cusp and a flip curve. Note that for parameters near a cusp point the connector among the three attractors will be smooth. The intersection of the flip curve (green) is cusped when it hits the fold for the central attractor and transverse when the peripheral, red, attractor disappears. There is a second curve emanating from the cusp in the flip curve where the connector changes from smooth to cusped. (D) The compactified elliptic umbilic. Inside the MS component boundary and outside the triangular hypocycloid $B_{\mathcal{C}}$ there are three attractors and two saddles. This dynamical system can be obtained by taking the gradient dynamical system of the potential associated with the potential $f_\theta(x,y) = x^4+y^4+x^3-2xy^2+a(x^2+y^2)+\theta_1 x+\theta_2 y$. with respect to a generic Riemannian metric. The term x^4+y^4 is added to the usual polynomial for Thom's elliptic umbilic in order to make the dynamical system compact. It has the effect of adding the three attractors and the outer fold bifurcation curves to the 3 saddles. The sign of the parameter a controls whether the central rest point is an attractor or repellor. By the MS inequalities (4) this is a minimal effect.

The bifurcations on this segment involve one of the attractors X_i and we say that the attractor identity of ℓ_i is X_i.

Figure 5 contains the simplest MS-components that involve all three attractors and are not decomposable into two attractor systems. Panel A is the minimal system with a dual cusp (SI Sec. I.5). In this case, if the parameters are inside Ω and the state starts in the central attractor (blue), then it stays there unless the parameters cross the curves through the cusp. Then it transitions to either peripheral attractor depending upon the branch crossed. For this reason we regard this as an *all or nothing landscape* because a population of cells with their initial state at the central attractor would all transition to the same new state upon bifurcation. An intimately related minimal MS component is shown in the Fig. 5A(inset). This involves a dual and a standard cusp joined together.

The simplest MS-components containing a standard cusp are those in Fig. 5B,C. The difference between them is the existence of the flip curve (green) shown in Fig. 5C. The transitions allowed using the landscape in Fig. 5B are rather limited. If parameters start in Ω one can only transition between a peripheral attractor and the central one or visa-versa.

The transitions are richer with the flip curve as it enables bifurcations that can change the central attractor and the escape routes available to cells. On this curve there is a heteroclinic connection from the saddle connected to the red peripheral attractor (the source) to the other saddle (the target). The flip curve joins tangentially to the side of the cusp where the central attractor (blue) and target saddle disappear in a fold. The flip curve must either terminate on the same fold bifurcation segment or end on the fold bifurcation curve where the source saddle and red peripheral attractor disappear as in Fig.5C. If one considers populations of cells in each of the three attractors, then on the boundaries of Ω transitions out of red are possible and between blue and yellow but not into red. This landscape illustrates a *downhill flexible choice*. Near the lower, red, fold bifurcation curve, a signal that repositioned the flip curve would control the fractions that populated the other two attractors (SI Sec. 5).

More complex structures involving combination of these cusps and more crossing points are possible but these also are highly constrained as described in the SI. These more complex versions are unlikely to occur in experiment since morphogens are apt to act monotonically on cell fates, and the new complexity is just multiple appearances of the same fold bifurcation.

Finally, we need to consider the case where there are no cusps in the MS component boundary $\partial\Omega$; then only crossing points are involved. The case of two crossing points is trivial and is decomposable in the sense that it is a 2-attractor MS-component with a non-bifurcating attractor added. However the case of three crossing points is already extremely interesting.

This gives the configuration shown in Fig. 5D with three smooth fold bifurcation curves corresponding to each of the attractors. The simplest example with such a MS component boundary is what we call the *compactified elliptic umbilic* (CEU) (Fig. 5D) and one can show that any 3-attractor MS component with such a boundary consisting of smooth fold bifurcation curves is just a more complex version of the CEU. It automatically has non-trivial monodromy because if one traces around a simple closed curve γ just inside of this boundary the two saddles are interchanged. Together with an analysis of the curves of heteroclinic connections that must occur, this implies that γ contains a bifurcation curve $\Omega_{\mathcal{C}}$ where $\mathcal{C}$ is a fold circle containing an odd number of cusps in three groups corresponding to the three cusps in the CEU (SI I.6).

We emphasize that these results follow from the properties of a gradient-like MS system, we do *n*ot assume a gradient system.

Note that biology takes place around $\mathcal{M}$. Thus in the vicinity of the cusp in Figs.4A, 5B it is possible to find a path in parameter space along which a population of cells in one attractor transitions smoothly to a second attractor without crossing a fold bifurcation curve. Thus although one is crossing a fold point in parameter space, if there are no cells at the attractor that disappears, it is invisible in an experiment.

3. Models for fate specification and embryonic patterning

The parameter spaces of a number of published 3-state models exemplify the categories in Fig.5. A model for the mouse blastocyst places a weakly stable inner cell mass state between the primitive endoderm and epiblast (16). They find a dual cusp in the parameter space comprising the growth

factor FGF that can be tuned externally, and one of many parameters defining the mutual inhibition between the two terminal states (their Fig. S4). The development of the vulva in *C.elegans* is a clear example of three cell fates and an elliptic umbillic, (6), and also fit as Fig.5C in (7). The specification of embryonic stem cells into neural and mesodermal fates was described by Fig.5A coupled to a sector of Fig.5D (8).

We next explicitly solve a gene network model for mutual inhibition among three states to show specifically that it conforms to Fig.5D. We then recast in potential form, a number of models for patterning an array of cells, to illustrate how our results extend to interacting cells with details in SI Sec II.

A. Three state system has elliptic-umbillic parameter space. The discussion surrounding Fig.5, envisioned multiple states for one cell. But the examples would apply equally well to a model of three interacting cells each with a single binary state with mutual repression among the active forms. The mathematics is agnostic to the biological interpretation, Fig.6. We chose to work around a point in parameter space with permutation symmetry in the three cells to simplify the parameter search, but the result persists so long as the three boundary curves have the topology shown, Fig.5D.

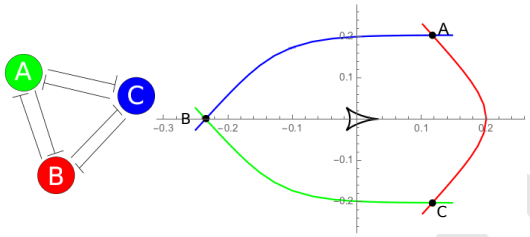

Fig. 6. A symmetric three cell or gene network with mutual repulsion and the elliptic umbillic conformation Fig.5D. The outer colored lines are the fold curves when one of the states disappears (three attractors become two). At the points A,B,C there is one stable restpoint and four with eigenvalues $\sim(-1,0,-1)$ (ie the intersection of two fold lines). The inner black contour consists of three fold lines and inside it is an index 2 saddle, three index 1 saddles and three attractors.

B. A flow defines a potential. Consider a typical two variable activator-inhibitor system, $\dot{a} = f_a(a,h) - \nu a, \dot{h} = f_h(a) - h$, which are ubiquitous in signaling pathways. They pose an ostensible challenge to represent in potential form since we have $\partial_a f_h > 0$, the activator turns on h; while $\partial_h f_a < 0$, the inhibitor represses a. Thus the cross derivatives have opposite sign, so it's of interest to reduce these to potential form. The system has two stable fixed points and a saddle. There is a general construction which defines the potential as Euclidean distance near the fixed points, insets and outsets of saddles and then glues the various functions together (17). A more intuitive construction in 2D is given by defining the potential to be the vector field integrated along the trajectory to the stable fixed points and then making the two functions smooth across the inset to the saddle. This is shown in Figure 7. The inverse metric is defined as the sum of two projection operators, one which projects the potential stream lines along the direction of the flow and one which projects it in a direction tangent to the contour (SI Sec II.2). Together they define a proper metric that aligns the potential gradient to the flow, except near the restpoints where a separate construction is necessary and the two pieces then glued together.

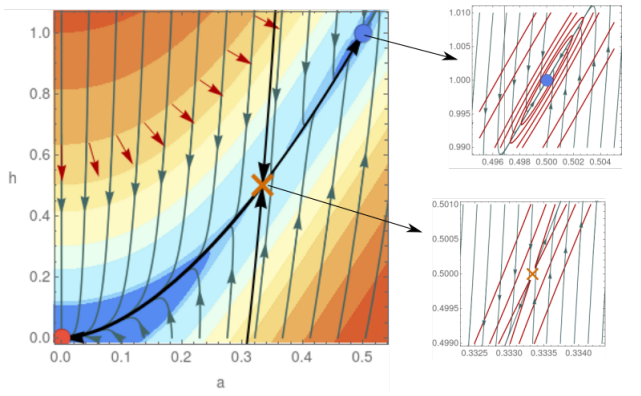

Fig. 7. The system has two stable fixed points and a saddle in between with flows shown in green. Contours of the potential, which is defined as the integral of the vector field along the trajectory to the stable fixed point, are shown going from low (blue) to high (red) potential. The red arrows on one of the contour lines show the flow from the potential gradient. Evidently, the inverse metric is needed to rotate the flow which derives from the potential into the actual flow. The construction does not work near the fixed points but the potential can be defined there locally and glued to the global potential. Plots of the contour lines in red and flow magnified near the upper fixed point and the saddle are also shown.

C. Patterning by lateral inhibition. Inhibition is ubiquitous in biology and is manifest on the epidermis of many animals as a sparse array of hairs, feathers, or sensory bristles . How are these patterns established? A recent model for sensory bristle patterns in a fly (18) nicely illustrates the organization of restpoints into the DAG of Fig. 1D, and the process of gluing local potential representations around critical points to model the complete system.

Each cell i is described by a single variable $0 \le a_i \le 1$ where the value 1 corresponds to the neural fate that will develop into a bristle. In the terminal state the bristles are spaced by 4-5 cell diameters in all directions. Cells are initialized with $a_i \sim 0$ and are confined to a strip by inhibition from the surroundings so that the initial pattern formation is one dimensional along the strip and then extends laterally. We generalize Fig.6, three cells that mutually inhibit, to a periodic ring of N cells with long range inhibition represented as:

$$\begin{aligned} \dot{a}_i &= \sigma(a_i - h_i) - a_i, \\ h_i &= \sum_{j \neq i} K_{i,j} d(a_j) \end{aligned} \qquad [2]$$

where $\sigma(a)$ and $d(a)$ are sigmoidal functions of their arguments varying between 0 and 1. The kernel $K_{i,j}$ is a Gaussian function of the distance between cells i,j, so the sum h_i is the net inhibition seen by cell i.

The qualitative behavior of the model can be understood from Fig.8a. When $h < 0.37$ only $a = 1$ is stable while for $h > 0.63$ only $a = 0$ is stable, with bistability in between. Initially $h = 0$, all the a_i grow from 0, and cells inhibit their neighbors with the result that trajectories peal off from a common envelope. Which cells turn on is a sensitive function of initial conditions and noise, but the kernel will keep neural precursor cells well separated.

The first 'decision' is defined by the principal saddle point on the diagonal $a_i = a$, where a varies from ~ 0.9 for $N = 2$ cells to ~ 0.51 for N large. At this point the number of unstable directions scales $\sim N$. For $N = 8$ in Fig. 8B, there are 5 unstable directions with nearly identical eigenvalues, 3 stable ones and the Jacobian matrix is symmetric. Proceeding down the DAG from the most unstable saddle, we find a state $\sim (1, 1, 1, 0, 1, 1, 1, 0)$ that has 4 unstable directions, as does a second less symmetric state with only cells $4, 7$ off and the others on to varying degrees. States with fewer unstable directions and various patterns of ON/OFF cells can all be found. Thus for very physical reasons this model generates a rich DAG. There are also stable terminal states that are not reflection invariant on the circle such as $\sim (1, 0, 0, 1, 0, 0, 0, 0)$, but these were not found as the endpoint of the dynamics when initializing with small randomized a_i.

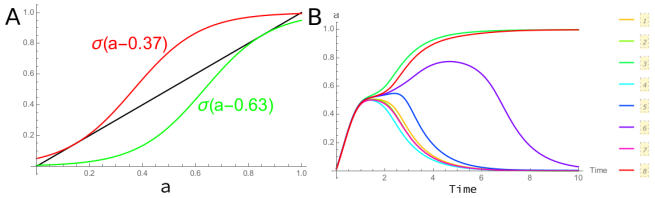

Fig. 8. Behavior of Eq. 2. (A) Values of inhibition h for which the $\dot{a}$ equation has saddle-node bifurcations. When h from neighboring cells is < 0.37 only the $a = 1$ state is stable, bistability persists for $0.37 < h < 0.63$, and only the $a = 0$ state exists for larger h. The diagonal is shown in black. (B) Eight cells on the circle with a kernel chosen to allow only two cells with $a = 1$ at the end. The time to reach steady state can vary by 2x depending on whether a third cell hangs close to the saddle point as seen here vs Fig.9

To reproduce the flow around the principle saddle point on the diagonal from a potential, we propose what is essentially an antiferromagnet but with a diagonal inverse metric (n.b. $d(a)$ in Eq. 3 is identical to Eq. 2)

$$\begin{aligned} \dot{a}_i &= -g(a_i)\nabla_{a_i} F, \\ F &= \sum_i V(a_i) + \frac{1}{2}\sum_{i\neq j} d(a_i) K_{i,j} d(a_j). \end{aligned} \qquad [3]$$

In the SI we show that we can match both the location of the principle saddle point on the diagonal, $a_i = \bar{a}(N)$, and the Jacobian for any number of cells N by fixing two functions of a single variable, g and V. The solution for g near the origin behaves as $g(a) \sim a$ in contrast to the Eq. 2 where the velocity is $\mathcal{O}(1)$ (compare Fig. 8b with Fig. 9. But since the saddle point is restricted to $a > 0.51$ we can easily correct the inverse metric for smaller a.

The dynamics derived from these potential models are shown in Fig. 9 where it is obvious comparing with Fig. 8b that we have corrected the dynamics around the origin with the two part inverse metric, at the expense of now making the decrease of single a_i in response to the antiferromagnetic repulsion too abrupt. But that can plausibly be fixed by adjusting the metric in a separate region of the phase space.

Putting the original model in potential form shows the extent to which the entire pattern formation process is controlled by the saddle point on the diagonal. Analytic calculations for how small differences amplify are facilitated by knowing the stable and unstable manifolds of the saddle.

We started from a very idealized model, but if it were elaborated to include a more realistic description of the Notch-

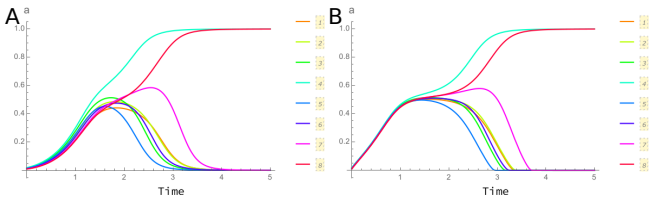

Fig. 9. Two potential models for Eq. 2 run with the same initial conditions. (A) The potential in Eq. 3 with the inverse metric extending to the origin. (B) The inverse metric near the origin now matches Eq. 2.

Delta signaling that is responsible for the inhibition or a more complete account of the neural fate, we suspect that the principal saddle point will retain its unstable directions but add many more stable ones. The best estimate for how much those additional details disappear from the dynamics is in fact the stable eigenvalues at the saddle point.

One may object that any model with contact inhibition is unrealistic since signals have to travel diffusively. That point is somewhat debated in *Drosophila* after cellularization (19, 20), but nevertheless we show in the next section, when diffusion is responsible for communication between cells, the underlying potential models have the structure discussed here. Finally representing a biological 'decision' as a saddle point in a high dimensional space applies during mesoscopic times, from when the pattern first emerges, to when it is close to saturation.

D. The Turing Model in potential form. While the terminology 'Turing system' and reaction-diffusion are used somewhat interchangeably, we focus in this section on the narrow use of the term to mean an activator inhibitor pair a, h where the inhibitor diffuses much more rapidly than the activator. The system is formally infinite dimensional since the fields are defined in continuous space, so not strictly a MS system, but practically so, as we will see. The crucial property is existence of a saddle point for uniform non-zero values of a, h that evolves into a nonuniform state where concentrated regions of a produce inhibitor that spreads rapidly and confines the activator. In a truly homogeneous-isotropic system there is a huge degeneracy of patterns all with a common characteristic scale, with very slow rearrangements among them. This space-time scale is of no biological relevance, and again we wish to focus our modeling effort on mesoscopic times, after some small biases trigger the basic instability and until the localized patches of activator are stably formed, i.e., the unstable manifold or Waddington valley leading from the initial stability to the terminal patch of activator. Thus it suffices to consider Turing systems on a circle with parameters that give a single localized state, modulo symmetries. The question is how to describe the dynamics on the unstable manifold of the saddle point as it tends to the stable state.

Consider a system of the form,

$$\begin{aligned} \dot{a}(x,t) &= f_a(a,h) - \nu a + D_a \partial_x^2 a, \\ \dot{h}(x,t) &= f_h(a) - h + D_h \partial_x^2 h. \end{aligned} \qquad [4]$$

The spatially uniform version of this model was the subject of the example in Sec 3B that derived a potential from the flow in spite of the fact that the cross derivative have opposite sign.

Any matrix with real eigenvalues can be represented as the product of two symmetric matrices one positive definite (21). However for Eq. 4 at the saddle point, that would require the inverse metric to contain the Laplace operator which we consider overly cumbersome (SI Sec II.4). Fortunately the resolution of the cross derivative problem in the continuum is both more interesting and useful in fitting data.

To be most explicit, consider a discrete version of Eq. 4 with N cells and a Laplacian obtained by differentiating an expression of the form $\sum_i D_y(y_i - y_{i+1})^2/2$, where $y = a, h$. With $D_{a,h} = 0$ the phase space for fixed x was shown in Fig.7, where we made the origin stable by assuming $f_{a,h} \sim a^2$ in Eq. 4. This definition separates the linear Turing instability caused by the diffusive coupling when $D_h \gg D_a$ from the patterning system defined by the lateral inhibition model where the activator in all cells increased from 0 at a constant rate.)

Now linearize around the saddle point of the discrete form of Eq. 4. There will be $2N$ modes that generally occur in pairs when reflection symmetry connects two inequivalent states that vary in space (i.e., with cell index i). Due to the large value of D_h/D_a there will be $N-1$ very stable modes centered on the h_i, one modestly stable one for uniform h. In the a sector of the spectrum, the uniform mode is stable by the definition of a Turing system (the first unstable mode is nonuniform and defines the scale of the terminal pattern) and among the remaining, a few will be positive in pairs. The most stable eigenvalue for both a and h may be a singleton or in a pair depending on whether N is even or odd.

Figure 10 shows the case of $N = 7$ with one unstable pair of modes. The dynamics can be projected on the (linear) tangent space of the unstable modes at the saddle point. The unstable manifold is 7-fold symmetric, compact, and flat enough that its projection onto the tangent space is 1:1. At the boundary of the unstable manifold there are 7 fixed points, related by rotational symmetry, and between them 7 saddles each with one unstable direction Fig. 10.

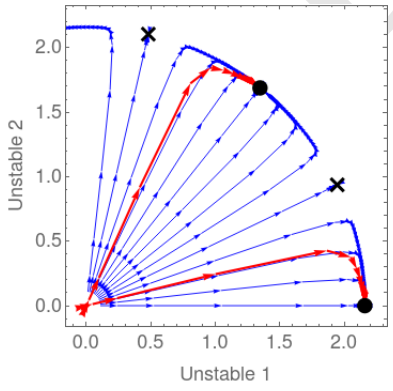

Fig. 10. A sector of the tangent plane to the unstable manifold at the saddle for a discrete version of Eq. 4 with $N = 7$ cells. The blue arrows show the trajectories of the potential fit with different initial conditions chosen at equally spaced angles. The red arrows show the projection of the actual equations on the tangent plane. Arrows are plotted at equal times and so give the approximate velocity.

The dynamics on the tangent plane can be accurately parameterized in polar coordinates relative to the central saddle by the system:

$$\begin{aligned} \dot{r} &= \lambda r - \beta r^3, \\ \dot{\theta} &= g(r)\sin(7(\theta - \theta_0)), \end{aligned} \qquad [5]$$

where $g(r)$ is a Gaussian tightly centered at $\sqrt{\lambda/\beta}$, the system is $2\pi/7$ periodic, and θ_0 is a phase shift. The Eqs.5 are potential with $g(r)$ acting as an inverse metric. However, the precise form of $g(r)$ is not crucial since as N increases, the number of fixed points increases accordingly and the angle dependence disappears leaving an invariant circle on which the radial motion terminates.

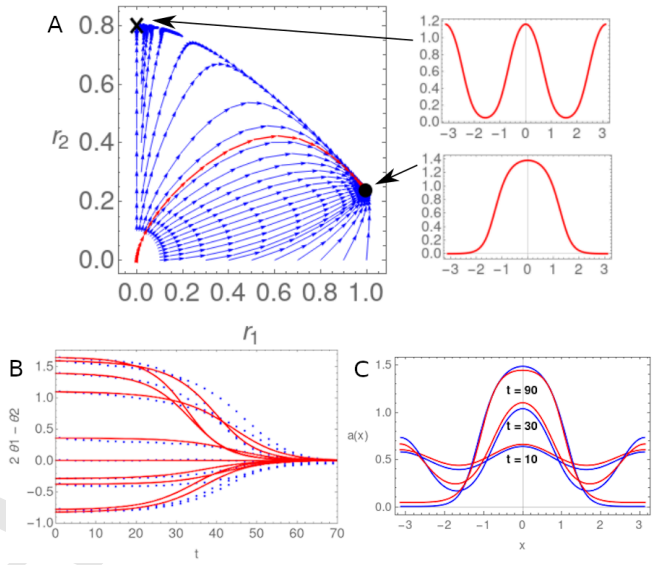

Fig. 11. The continuous Turing PDE is solved and projected on to the variables z_1 and z_2 in Eq. 6 by simply doing a linear projection onto the Fourier modes ($z_i = r_i e^{i\theta_i}$). (A) The streamlines of Eq. 6 in the space of the two radii with the angles set to 0 showing a 2 dimensional projection of the 4 dimensional unstable manifold. The call outs show the terminal profiles of $a(x)$ at the saddle with two peaks and the fixed point with one. The initial condition is $a(x) = 0.01\cos(2x) + 0.001\cos(x)$ (B). Equation. 6 implies that the angles stably lock together with $2\theta_1 - \theta_2 = 0$. This is shown with blue dots for the actual Turing model and red for the potential fit for various initial conditions. (C) A saturation function is required to match the solution in the tangent space in (a,h) to $a(x)$ in physical space x. The solution of the continuous system (blue) is compared with a sigmoidal saturation of the tangent space flow (red) for the red cross-over trajectory in (a).

Of greater interest is that we have reduced the dynamics from the $2N$ dimensions to the two dimensions of Fig. 10, with a rate parameter λ and a limiting radius. All the complexity of $f_{a,h}$ in Eq. 4 is reduced to these two numbers, and manifestly could not be made any simpler. This describes the entire unstable manifold from the linear instability to the finite amplitude stable state. Still missing is the embedding of the radius variable r in the tangent space into the fields a, h that we will deal with after properly treating the continuous case. However this embedding is by definition time independent, all the dynamics lives in r, and we thus have a very compact representation of a time dependent field with accuracy at the few percent level, more than adequate for biology.

Guided by the discrete case we represent the continuum equations around the saddle point as a linear term that we can Fourier transform on the circle and a nonlinear term local in position that we expand to third order. Our restriction to mesoscopic times makes it entirely reasonable to work on

a compact space. Call the most unstable Fourier mode k_1 and if we close the system with cubic nonlinearity within this space we must obtain an equation of the form $\dot{z}_1 = \lambda_1 z_1 + f_3 z_1 |z_1|^2$ where z_1 is the complex coefficient of that Fourier mode. If a second unstable mode $|k_2| = 2|k_1|$ exists then we find couplings between the modes as in:

$$\begin{aligned} \dot{z}_1 &= \lambda_1 z_1 - \beta z_1(|z_1|^2 + 2|z_2|^2) - 2\gamma z_1^* z_2, \\ \dot{z}_2 &= \lambda_2 z_2 - \beta z_2(|z_2|^2 + 2|z_1|^2) - \gamma z_1^2. \end{aligned} \quad [6]$$

The k_2 mode describes two incipient blobs on the circle that under our assumptions are unstable to a single blob (i.e., the k_1 mode grows faster). The unstable manifold is now four dimensional and goes to a fixed point through a series of saddle points each with one less unstable mode. The first and second of these saddles correspond to a state with two blobs and is inaccessible for typical initial conditions. Thus we have described the dynamics of the cross over between two blobs and one on the circle with four modes and dynamics derived from a potential. One consequence of these equations is that the angles of the two modes are locked as shown in Fig 11. We note that the model is potential with trivial metric only to cubic order and higher order Taylor series would induce a nontrivial metric.

To map the modes $z_{1,2}$ back to the continuum a, h we have to interpolate between the Fourier modes for the linear system and the static solution for a which is a single blob. The simplest way to model this constraint is to simply add the Fourier modes linearly and saturate them with a sigmoidal function $\sigma(x)$ at medium and late times reflecting the high and low values of a. Thus one needs to fit the parameters in Eq. 6 as well as the sigmoidal function shape as a function of z_1 and z_2 to map our potential to continuum a. The comparison is plotted in Fig11c with details in SI.

To illustrate the utility of this reduced representation for fitting experimental data consider a 2-d continuum periodic rectangular system which leads to the formation of three blobs. Each of these blobs are slightly different because of a long range gradient as well as randomness in the microscopic equations. However, our reduced representation captures the essential nature of the dynamics and the different blobs can be fit to with different parameter in the radial mode in Eq.5 as shown in Fig. 12.

When presented with time-lapse data for a Turing system, we would take the radial profile of each blob as a function of time and fit to a single time independent sigmoidal function composed with a solution to $\dot{r}$ in Eq. 5, with parameters and initial conditions specific to each blob. We expect this procedure will collapse considerable variability among the dynamics of the blobs to universal functions with minimal parameters as in Fig.12.

We conclude this section by generalizing the lateral inhibition model, Eq. 2 to one with a diffusing inhibitor which is instructive to compare with the Turing system. Consider the system for N cells periodically continued (suppressing constants),

$$\begin{aligned} \dot{a}_i &= f_a(a_i) - h_i d'(a_i), \\ \dot{h}_i &= d(a_i) - h_i + D_h(h_{i+1} + h_{i-1} - 2h_i). \end{aligned} \quad [7]$$

where $d(a)$ is again a sigmoidal function mapping a into the interval $[0, 1]$. There is no loss of generality in making the coupling between h and a in $\dot{a}_i$ the derivative of the source of h in $\dot{h}_i$ since we can redefine a to make this true. For illustration we assume $f_a(a) \sim a$ around the origin to make that point unstable. If we solve $\dot{h}_i = 0$ for h_i, substitute into the $\dot{a}_i$ equation, we obtain the contact (rapid diffusion) form of the equations with the Greens function appropriate to the circle i.e., Eq. 3. The cross derivatives $\partial_h \dot{a}$ and $\partial_a \dot{h}$ are equal and opposite in sign as we expect for inhibition.

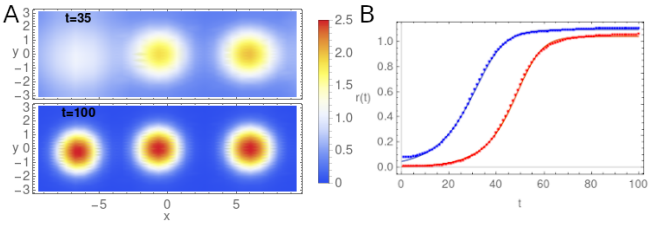

Fig. 12. (A) A model in 2 spatial dimensions leads to the formation of three blobs each of which are slightly different because of randomness in the parameters and initial conditions. The blobs are shown at two different time points demonstrating that the left and right end form at different times. Since the blobs have spherical symmetry, the profile is first averaged over angles and then projected on to the Bessel Function $J_0(R)$ being the first term in a Fourier-Bessel series, where R is a scaled radial coordinate in space. (B) The simulated 2D dynamics is projected onto the tangent plane (dots) for the left (red) and right (blue) blobs in (A). The data is fit very well by the radial part of Eq. 5 (curve) with parameters specific to each blob. The space-time profiles in (A) are then fit by a sigmoid depending on $r(t)$ from Eq. 5 and $J_0(R)$ (SI Sec II.4)

For an example with all constants order one, and the D_h adjusted to produce the desired spacing between the active cells; there is again a saddle point along the diagonal with $\sim N$ stable directions corresponding to the h_i and a few additional ones with weight in the a_i directions. A few of the stable eigenvalues can be complex reflecting the nonzero antisymmetric terms in the Jacobian matrix. The unstable eigenvalues are numerically very close to those of the system with h_i eliminated and the dynamics within the a_i subspace is identical for practical purposes (SI).

So in comparison with the Turing system, there are now many unstable modes all deriving from the same saddle point along the diagonal in a_i. The origin is unstable rather than stable and the dynamic competition that generates the pattern derives from the saddle point on the diagonal. We believe the geometric view point provides the clearest characterization of these two systems with diffusing inhibitors.

E. Spreading the pattern by a wave. When a two dimensional area is to be patterned, the process often proceeds from a boundary which provides the template. One such system is the morphogenic furrow in the fly eye. It moves as a wave with constant velocity from posterior to anterior across the eye imaginal disk, leaving behind the hexagonal crystal of ommatidia that characterize the insect eye (22).

We follow the ideas of (23) who modeled this system with effectively three modes: a cell localized activator a, an intermediate range inhibitor that is responsible for the spacing between successive rows of ommatidia, and a long range activator, b, that destabilizes the $a = 0$ state ahead of the furrow to allow the cells to compete as described in Eq. 7. We will replace the dynamic inhibitor in our reformulation with static lateral inhibition which we just showed to be functionally equivalent.

We can directly formulate our model as a potential since

there is no sign conflict when integrating two activators. We thus propose in one dimension,

$$u(a,b) = v(a) + (b-a^2)^2/2 - ab,$$
$$U = \sum_{i=1}^{N} u(a_i,b_i) + D_b(b_i - b_{i-1})^2/2 + \frac{1}{2}\sum_{i\neq j} d(a_i)K_{i,j}d(a_j) \quad [8]$$

where constants are omitted, $v(a)$ is a bistable potential, and the double sum copies Eq. 2. The boundary conditions are open, and we fix $b_0 = 1$ so the left end of the lattice is activated and the wave propagates towards $i = N$. The only condition on the one cell potential $u(a,b)$ is that the origin $a,b = 0$ is stable and the saddle point occurs around $a,b \sim 0.1$ in units where the final state shows $a \sim 1$ in the active cells, zero elsewhere, and $b \sim 1$, i.e., the value of the saddle point is small but not tiny and stabilizes the cells at $a = 0$ until the leading edge of the wave of b arrives by diffusion and kicks them over the saddle. The static inhibition controls the spacing between the active cells, and the diffusion constant governs the speed within limits, Fig. 13.

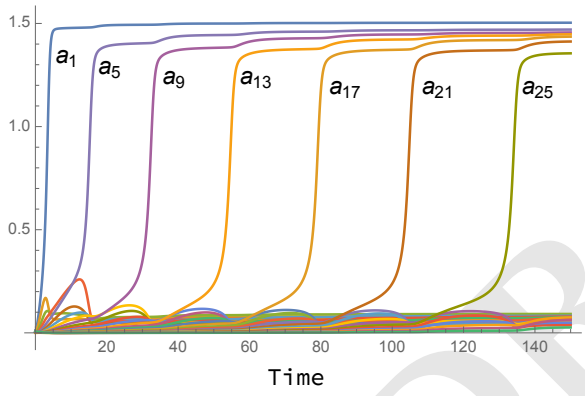

Fig. 13. Dynamics for the 1D morphogenic furrow from Eq. 8 for N=30 where every 4th cell is active. The wave appears to slow towards the end since the long range activator b is diffusing out the right hand boundary. For the same reason the plateau in a_i is a bit lower at the end.

The potential formulation makes it obvious that the moving solution in Fig. 13 is just an instance of relaxational dynamics for a field with two minima, the simplest instance being, $\int_x (sa - a^2/2 + a^4/4 + D(\partial_x a)^2/2), s \ll 1$ where an interface between locally stable solutions at $a \sim \pm 1$ moves to replace the higher potential solution with the lower potential one, and does so with constant velocity. For the parameters of Fig. 13 all solutions of period 2 to 5 have negative potential U and thus lie below the initial conditions with $U > 0$. However only the period 4 solutions is realized as the wave spreads.

F. A static morphogen gradient and adaptive systems. We note in closing two instances where the components are few enough in number and well enough characterized that gene centric models are informative and quantitative, yet the geometric viewpoint poses questions that are often neglected (see SI).

A morphogen is a diffusible factor whose level defines cell fate. Morphogen systems like any other dynamical model may be multistable implying hysteresis in the pattern. An informative geometrical representation is given in the SI.

An adaptive system has one variable that responds to an external signal, yet whose value is signal independent under static conditions. Adaptation is common in biology from sensory systems to signaling pathways where its a more rapid way to connect position to fate than reading a static signal (24). This property is succinctly expressed in the form of a potential and metric (SI Sec II.7).

4. Discussion

We have given a tight argument that in the absence of periodic behavior, robust (i.e. structurally stable) gene regulatory dynamics satisfy the Morse-Smale assumptions and thus can be described by a downhill gradient-like system where the rest-points can be organized into a directed acyclic graph (DAG) defining the allowed transitions between them. Moreover, we observed that such dynamics can reasonably be represented as a true gradient system given by a potential and a Riemannian metric. The mathematics achieves such sweeping results by imposing genericity: system properties are unchanged in a neighborhood of the system in question. In analogy, embryonic development is robust against environmental noise.

In geometric terms, the inhibition among cells that produces a sparse array of neural progenitors, is simply a high index saddle point that initiates the DAG. Turing pattern formation begins from the linear instability of a uniform state, making it a saddle point. Its nonlinear development is just the unstable manifold of the saddle that we represented as a MS system. There was a cascade of saddle points with decreasing index to the terminal pattern.

A representation of the flow as a metric and potential continues to work around saddle node bifurcations and heteroclinic flips, the two operations needed to grow any MS system from the trivial one (13). These operations are thus the only topology changing 'mutations' that are needed to computationally evolve gene regulatory networks(25).

The results of Catastrophe Theory (CT) are clearly of relevance to our analysis but they are local and, since they only study the potential, they do not capture the stable and unstable manifolds of the dynamics or the heteroclinic flips. Our study shows that the latter are crucial to understanding developmental dynamics and the study of them opens up new ways to extend the theory from local to global.

In particular, we borrowed from the mathematics that Smale developed for his proof of the high-dimensional Poincare conjecture, to rigorously deduce a new form of dimensional reduction in which for generic systems like ours the topological relationship between index 1 saddles and attractors is effectively independent of dimension and can be represented by 2-dimensional systems. The *canalization* of Waddington is simply the focusing of the dynamics onto the unstable manifolds of the saddles. The results in Fig.5 depend upon this understanding which is very different to the dimension reduction that CT supplies which only applies locally in state and parameter space.

A network model represented by activating and inhibitory arrows among genes has little relation to the geometry of the flow, that is the ultimate representation of the dynamics. We expect that such models with two parameters and ≤ 3 attractors will produce the bifurcation diagrams in Fig. 5.

Recent examples of modeling development have taken a more geometric approach from the start. The first several steps in the differentiation of mouse embryonic stem cells were decomposed into two coupled three way decisions. The first involving an all or nothing decision that deposits all cells into either adjoining state depending on a morphogen used the landscape in Fig. 5A. The second used a flip bifurcation to flexibly allocate cells to one of two attractors (8), corresponding to part of 5D. In (26) the so called triple points in the phase diagram of the *C. Elegans* vulva plausibly correspond to Fig.5D, and a related study (7) used Fig.5C. If embryonic stem cells can transition directly to ectoderm, mesoderm, and endoderm, then Fig.5D is a possible model with the pluripotent state being the fourth attractor in the center.

Cartoons of development commonly represent the succession of fates as a binary tree, suggesting the existence of three attractor systems at the nodes. Left implicit is a developmental clock that biases fate progression in one direction. This could be a competence window that limits the response to signals to a temporal interval combined with epigenetic changes.

There is no reason that our analysis cannot be generalized to periodic systems where the structurally stable dynamics are also MS. All the key ingredients regarding MS systems are available (with obvious changes such as a constant potential on the periodic orbit) (5), but the generic bifurcations are more numerous and complex and that makes this a substantially more challenging task. When a developmental system is subject to an autonomous periodic signal, such as might be the case with the cell cycle, the relevant dynamics is represented by a map rather than by a flow as we have assumed so far, and opens up a richer corpus of behavior.

In applications the states in question are rarely terminal, thus parameters are not static. When systems are not steady, do all the other degrees of freedom have time to relax to the two dimensions necessary to represent all three way decisions? This question can only be resolved by fitting data, and in examples we have seen that high index saddles can also have multiple stable directions, which is then the recipe for quantifying the neglected variables.

The geometric description is compact since all reference to specific genes is lost, yet experiments commonly mutate genes and observe changes in patterning dynamics and outcomes. Clearly each mutant requires at least one parameter to fit, but is there any way to predict a double mutant from each of the single ones? An interesting ansatz was used in (6), where a single vector sigmoid function was wrapped around the non-compact polynomial equations for the dynamics. A linear force added to the sigmoid rendered the dynamics bounded, but the dependence on the two morphogens was entirely linear inside of the sigmoid. The double mutant was thus the sum of the single ones. Nevertheless the model captured the essential genetic interactions. While the qualitative details of the problem dictates the geometry, how it is parameterized is very germane for applications.

We have concerned ourselves exclusively with representing gene networks as potentials, but not with morphogenesis for which forces and potentials are natural. Morphogenesis and fate assignment are tightly coupled in development as exemplified the ordered expression of the HOX genes during the unfolding of the anterior-posterior axis (27), but it is as yet unclear how to unify potentials for fates and forces.

Acknowledgements

The authors thank James Briscoe, John Guckenheimer, and David Lubensky for discussions. EDS was supported by NSF grant No. 2013131, DAR thanks Ian Stewart for very helpful early discussions. DAR and MS were funded for this work by EPSRC grant EP/P019811/1. MS was also supported by the Francis Crick Institute, which receives its core funding from Cancer Research UK, the UK Medical Research Council and Wellcome Trust (all under FC001051). FC was supported by the ANR grant ANR16-CE13-0003-02. DAR, FC and EDS participated in the 2019 Kavili Institute Program on quantitative biology supported by NSF Grant No. PHY-1748958, NIH Grant No. R25GM067110, and the Gordon and Betty Moore Foundation Grant No. 2919.02 . AR acknowledges support from the Simons Foundation.

1. Smale S (1961) On gradient dynamical systems. *Annals of Mathematics* pp. 199–206.
2. Guckenheimer J, Holmes P (2013) *Nonlinear oscillations, dynamical systems, and bifurcations of vector fields*. (Springer Science & Business Media) Vol. 42.
3. Newhouse S, Peixoto M (1976) There is a simple arc joining any two morse-smale flows. *Asterisque* 31:15–41.
4. Smale S (2000) Morse inequalities for a dynamical system in *The Collected Papers of Stephen Smale: Volume 2*. (World Scientific), pp. 596–602.
5. Meyer KR (1968) Energy functions for morse smale systems. *American Journal of Mathematics* pp. 1031–1040.
6. Corson F, Siggia ED (2012) Geometry, epistasis, and developmental patterning. *Proceedings of the National Academy of Sciences* 109(15):5568–5575.
7. Camacho-Aguilar E, Warmflash A, Rand DA (2021) Quantifying cell transitions in c. elegans with data-fitted landscape models. *bioRxiv*.
8. Sáez M, et al. (2021) A quantitative landscape of cell fate transitions identifies principles of cellular decision-making. *bioRxiv*.
9. Thom R (1969) Topological models in biology. *Topology* 8(3):313–335.
10. Zeeman C (1976) The classification of elementary catastrophes of codimension ≤ 5 in *Structural stability, the theory of catastrophes, and applications in the sciences*. (Springer), pp. 263–327.
11. Guckenheimer J (1973) Bifurcation and catastrophe in *Dynamical systems*. (Elsevier), pp. 95–109.
12. Khesin BA (1990) Bifurcations in gradient dynamic systems. *Journal of Soviet Mathematics* 52(4):3279–3305.
13. Newhouse S, Peixoto M (1976) There is a simple arc joining any two morse-smale flows. *Asterisque* 31:15–41.
14. Stewart IN (1980) Catastrophe theory and equations of state: Conditions for a butterfly singularity. *Mathematical Proceedings of the Cambridge Philosophical Society* 88(3):429–449.
15. Arnold VI, Afrajmovich V, Il'yashenko YS, Shil'nikov L (2013) *Dynamical systems V: bifurcation theory and catastrophe theory*. (Springer Science & Business Media) Vol. 5.
16. De Mot L, et al. (2016) Cell fate specification based on tristability in the inner cell mass of mouse blastocysts. *Biophysical journal* 110(3):710–722.
17. Nitecki Z, Shub M (1975) Filtrations, decompositions, and explosions. *American Journal of Mathematics* 97(4):1029–1047.
18. Corson F, Couturier L, Rouault H, Mazouni K, Schweisguth F (2017) Self-organized notch dynamics generate stereotyped sensory organ patterns in drosophila. *Science* 356(6337).
19. Alexandre C, Baena-Lopez A, Vincent JP (2014) Patterning and growth control by membrane-tethered wingless. *Nature* 505(7482):180–185.
20. Kornberg TB (2019) Scripting a place in time. *Developmental biology* 447(1):24–27.
21. Bosch A (1986) The factorization of a square matrix into two symmetric matrices. *The American Mathematical Monthly* 93(6):462–464.
22. Baker NE (2007) Patterning signals and proliferation in drosophila imaginal discs. *Current opinion in genetics & development* 17(4):287–293.
23. Lubensky DK, Pennington MW, Shraiman BI, Baker NE (2011) A dynamical model of ommatidial crystal formation. *Proceedings of the National Academy of Sciences* 108(27):11145–11150.
24. Sorre B, Warmflash A, Brivanlou AH, Siggia ED (2014) Encoding of temporal signals by the tgf-β pathway and implications for embryonic patterning. *Developmental cell* 30(3):334–342.
25. François P (2014) Evolving phenotypic networks in silico in *Seminars in cell & developmental biology*. (Elsevier), Vol. 35, pp. 90–97.
26. Corson F, Siggia ED (2017) Gene-free methodology for cell fate dynamics during development. *Elife* 6:e30743.
27. Iimura T, Pourquié O (2007) Hox genes in time and space during vertebrate body formation. *Development, growth & differentiation* 49(4):265–275.

Supplementary Information

This manuscript was compiled on May 25, 2021

In the following, we provide technical details and various supplementary illustrations to those provided in the main paper that hereafter is referred as **I**.

Contents

Part I
Mathematical concepts

Throughout this note we restrict attention to the generic case. A generic property is one that holds for almost all systems. This means that the systems for which the property holds form an open and dense subset of the relevant function space. We will be a little cavalier in not mentioning the function spaces we are using but generally it should be clear.

1. Morse-Smale Systems

The time integration of a differential equation $\dot{x} = X(x)$ or, equivalently the vector field X defines a flow $x \to \varphi_X^t(x)$ on the phase space P. If $x \in P$ then $\varphi^t(x)$ is the solution with initial condition x.

Throughout we shall be considering vectorfields X and their associated flows $\varphi_X^t(x)$ on a domain $P \subset \mathbb{R}^n$ in which there is a globally attracting ball B i.e. a region B which is a n-dimensional ball (i.e. diffeomorphic to $\{x \in \mathbb{R}^n : ||x|| < 1\}$) with a boundary ∂B that is a smooth* sphere (i.e. diffeomorphic to $\{x \in \mathbb{R}^n : ||x|| = 1\}$) such that every trajectory of X starting in P outside B enters B eventually and X is transverse to ∂B.

A point x of P is called chain recurrent for the flow provided that for any $T, \epsilon > 0$ there are points $x_i \in P$ and real numbers $t_i > T$, $i = 0, 1, \ldots, N$, such that $x = x_0 = x_N$, and $d(\varphi^{t_i}(x_i), x_{i+1}) < \epsilon$.

A Morse-Smale (MS) flow is one satisfying the following properties:

(a) the set of chain recurrent points consists of a finite number of hyperbolic rest points and hyperbolic closed orbits (see (1) for definitions);

*Throughout smooth means C^2.

(b) the unstable manifold of any closed orbit or rest point has transversal intersection with the stable manifold of any closed orbit or rest point.

We study generic parameterised families in which the structurally stable systems are MS flows X that only have rest points. We call these *gradient-like* Morse-Smale flows because by (2) they always have a smooth Liapunov function i.e. a function $L : P \to \mathbb{R}$ such that its derivative is zero at rest points and $X(L) < 0$ otherwise, where $X(L) = dL \cdot X$.

A. Saddle-attractor configurations. Consider for a moment the planar case where $n = 2$ and the above conditions apply so that the boundary of P is a smooth simple closed curve and the flow is inwardly transverse to it. Then one can always find a smooth simple closed curve γ such that the flow is inward transverse to γ and so that the interior Ω of γ contains all the m attractors of the system, $m-1$ saddles and no other rest points. Moreover, γ can be chosen so that the stable manifolds of the saddles inside γ intersect the boundary in two points and do so transversally. They thus divide Ω into m components each of which is the basin of one of the attractors and, moreover, the unstable manifold of each saddle intersects the basin of two attractors. The possibilities with $m = 3, 4$ are shown in Fig. S1(A-C) and we see that the $m = 3$ case is particularly simple.

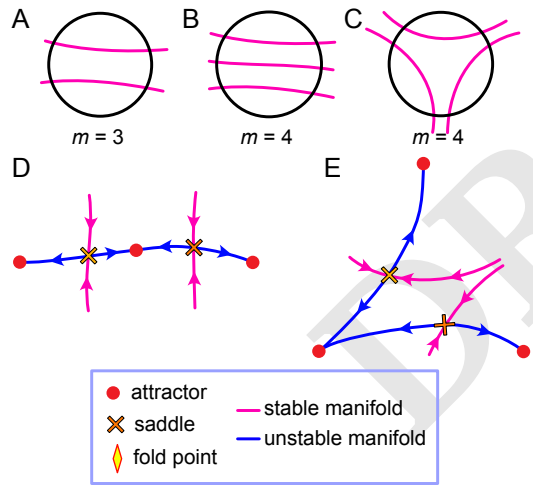

Fig. S1. (A-C) These illustrate some of the different possibilities (the most important for us) for the configuration of the stable manifolds of the saddles in the attractor disk region R defined above which is represented by the interior of the circle. All cases for 3 and 4 attractors are shown. (D-E) These illustrate the smooth (D) and cuspoidal (E) versions of the connector (blue curve) which is made up of the unstable manifolds of the two saddles in each case. Other non-smooth configurations are possible such as with a spiral due to non-real eigenvalues at the central attractor.

There is a corresponding decomposition in n dimensions. In Appendix A we explain the following result: For a gradient-like MS system on a region P in $\mathbb{R}^n$ with attracting ball B as above one can always find an attracting n-dimensional disk R in P with smooth spherical boundary ∂R that contains all the m attractors plus $m-1$ index 1 saddles but no other rest points. It captures almost all the trajectories in the following sense: if W^s is the union of all stable manifolds of rest points outside R and $x \in R \setminus W^s$ then for t large $\varphi^t(x) \in R$. Moreover, R has the property that the stable manifolds of the index 1 saddles inside R transversally intersect the spherical boundary of R in disjoint spheres of dimension $n-2$ and divide R into regions each of which is the basin of attraction of one of the attractors.

We are interested in regions like R above because in applications to developmental biology the index 1 saddles play a particularly important role: their unstable manifolds determine the escape routes by which cells change their state by escaping one attractor and moving to another.

As a corollary to the above result, for such systems with 3 attractors, associated with the 3 attractors are two saddles s_1 and s_2 with a disposition as in Fig. S1D,E i.e. we can label the attractors A, B and C so that $s_1 \succ A, B$ and $s_2 \succ B, C$ where $s \succ X$ means that the unstable manifold of s intersects the stable manifold of X.

Thus the unstable manifolds of these two saddles join at one of the attractors. The attractor at the joint is called the *central attractor* and the other attractors are said to be *peripheral*. The union of the parts of the unstable manifolds which connect the attractors is called the *connector*. The joint can either be smooth (Fig. S1D) so that the connector is a smooth curve or it can be non smooth (e.g. as in Fig. S1E).

Consider such a situation where we have two index 1 saddles s_1 and s_2 whose unstable manifolds intersect the stable manifold of an attracting rest point at x. If the latter is close to undergoing a fold or cusp bifurcation then there is a line ℓ through x and a $n-1$-dimensional submanifold W^{ss} (the strong stable manifold) intersecting ℓ tranversally at x such that all trajectories starting near x and not starting in W^{ss} approach x in a direction tangent to ℓ. Consequently, it is generic that the unstable manifolds of the two saddles in the connector approach x tangent to ℓ. If they approach in opposite directions relative to ℓ then the connector is smooth (Fig. S1D) but if they approach from the same direction relative to ℓ then the connector is not smooth and has what we call a *cuspoidal* structure (Fig. S1E).

If the attractor x is not close to a fold then there can be other non-smooth connectors. One obvious example is where the linearisation of the system about x has eigenvalues with non-zero imaginary part so that the unstable manifolds spiral into x. The reader should note that in order to keep our figures to a minimal size we never illustrate such cases but we do take them into account in our arguments.

In Lemma 6 of Appendix B we show that if the joint is cuspoidal at an attractor then that attractor cannot undergo a fold bifurcation involving either of the saddles s_1 and s_2. For the other non-smooth cases this is obvious. Thus such a joint involving s_1, s_2 and x can only undergo a fold bifurcation involving x and s_1 or s_2 if the joint is smooth.

2. Fold and cusp bifurcations

We consider the bifurcations between gradient-like MS systems in families of differential equations given by a family of vector fields X_θ parameterised by $\theta \in \mathbb{R}^c$. Throughout this discussion we restrict to the case $c = 2$.

When $c = 2$ for gradient-like systems the only local bifurcations that can occur generically are the *fold* (or *saddle-node*) and the *cusp* bifurcation. There are other codimension 2 bifurcations for dynamical systems (1, 3) such as the Takens-Bogdanov bifurcation but these introduce periodic orbits and therefore move us outside gradient-like systems that we focus on here.

At such a fold or cusp bifurcation point θ there is an invariant 1-dimensional smooth center manifold $W^c(x_0)$ through the point x_0 in phase space where the bifurcation is taking place and the system on this submanifold may be transformed into one of the following families via a $C^{N(r)}$ change of coordinates ((3) Chap. 1, Sect. 3 and Chap. 2, Sect. 5.7):

$$\text{(fold) } \dot{x} = \pm x^2 + \theta_1 \qquad [1]$$

or

$$\text{(cusp) } \dot{x} = \pm x^3 + \theta_1 x + \theta_2. \qquad [2]$$

In fact, if the original system is C^∞ then for each $r > 1$ one can find a neighbourhood U of x such that there is a C^r center manifold of x in U.

If the system is n-dimensional then the dynamics near x_0 are topologically conjugate to

$$\begin{aligned} \text{(fold) } \dot{x} &= x^2 + \varepsilon_1(\theta); \\ \dot{v} &= -v;\ \dot{w} = w; \end{aligned} \qquad [3]$$

or

$$\begin{aligned} \text{(cusp) } \dot{x} &= \pm x^3 + \varepsilon_1(\theta)x + \varepsilon_2(\theta); \\ \dot{v} &= -v;\ \dot{w} = w \end{aligned} \qquad [4]$$

where $v \in \mathbb{R}^{n_s}$, $w \in \mathbb{R}^{n_u}$ and n_s (resp. n_u) is the number of eigenvalues of the linearisation of the system at x_0 with negative (resp. positive) real part.

Consider the set of eigenvalues λ_i, $i = 1, \ldots, n$, of the linearisation $\dot{x} = Ax$ of the system $\dot{x} = X(x)$ at an equilibrium x_* and let r_i be the real part of λ_i. A *resonance* is a relation of the form $r_s = \sum_i m_i r_i$ with the m_i positive integers with $\sum_i m_i \geq 2$. We say this equilibrium is non-resonant if no such resonance exists.

Consider a fold x_0 as above in n dimensions. Then if it is non-resonant for $r > 2$ one can find C^r coordinates $(x, y) \in \mathbb{R} \times \mathbb{R}^{n-1}$ on some neighbourhood U of the fold point in which the differential equation takes the form

$$\begin{aligned} \dot{x} &= \pm x^2 + a(\theta)x^3 + \theta_1 \\ \dot{y} &= A(x, \theta)y \end{aligned} \qquad [5]$$

((3) Part I, Chap. 2, Sect. 5.7). Without loss of generality we can assume that the bifurcation takes place at $\theta = 0$. In the systems we study the y direction is stable and the matrix $A(0, 0)$ has all its eigenvalues with negative real parts.

A. Center manifolds. Center manifolds will play a key role in our considerations. Our use of the term *center manifold* will be a little more general than usual as normally it is discussed when the systems is at a bifurcation and we will want to use it when we are only near a bifurcation. For example, we want to be able to associate a center manifold to an attractor that is close to undergoing a fold bifurcation. Also we need to consider the smoothness of the variation in the center manifold as parameters are changed.

For relevant information about center manifolds see (4) Sect. 5A. In particular note that by Theorem 5A.3 of (4), if W^c is a center manifold through a rest point x and W is a backward invariant set containing x then, near x, W is contained in W^c. Thus, for example, if the unstable manifold of a saddle is asymptotic to a fold point, then close to the fold point it is in the center manifold. Center manifolds are not necessarily unique but their tangent space is. We will use this fact below.

We now consider what we call *pseudo-hyperbolic* rest points x. At such rest points x there is $a > b > 0$ such that the Jacobian of the vector field at x has eigenvalues λ that either have their real part $\leq -a$ or $\geq -b$. Then pseudo-hyperbolic index 1 saddles and attractors have 1-dimensional center manifolds $W^c(x)$ that vary smoothly with parameters (Sect. 5 (4), especially Theorems 5.1, 5.5 and 5A.1). If φ^t is the flow, this manifold is characterised by the fact that $z \in W^c(x) \iff ||\varphi^{-t}(z) - x||/e^{ct} \to 0$ as $t \to \infty$ for any c with $a > c > b$. There is a complementary submanifold $W^{ss}(x)$ transversal to $W^c(x)$ at x characterised by $z \in W^{ss}(x) \iff ||\varphi^t(z) - x||/e^{-ct} \to 0$ as $t \to \infty$ for such a c. This we call the *strong stable manifold*. Note that our use of the term *center manifold* is a little more general than usual as in that case one commonly takes $b = 0$.

Index 1 saddles are always pseudo-hyperbolic and attractors are if they are close to having a fold bifurcation. For an index 1 saddle, part of the unstable manifold containing the saddle can be taken for a center manifold.

According to Theorems 5.1 of (4), $W^c(x)$ has C^r dependence upon parameters provided $e^{jb-a} < 1$ for $1 \leq j \leq r$. Thus the center manifold for saddles always is smooth and that for attractors is smooth provided they are close enough to having a fold bifurcation. The later point is true because the closer an attractor is to being a fold, the closer one can take b to zero.

3. Catastrophe Manifold

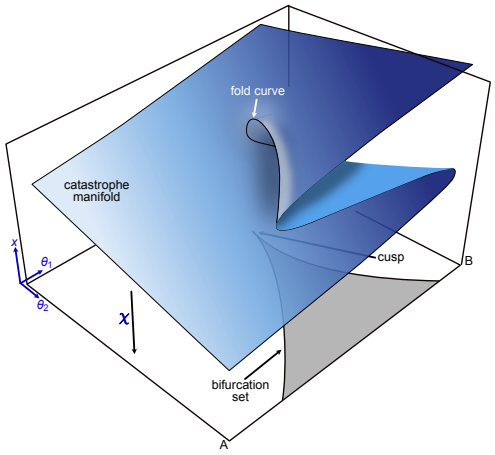

Fig. S2. The catastrophe manifold $\mathcal{M}$ for the cusp catastrophe. Notice that although the bifurcation set has a cusp and hence is not smooth the corresponding fold curve in $\mathcal{M}$ is smooth.

We now consider a family of flows parameterised by $\theta \in \mathbb{R}^c$ given by the family of vector fields $X_\theta = X_\theta(x)$. The catastrophe manifold is defined as

$$\mathcal{M} = \{(x, \theta) : x \text{ is a rest point of } X_\theta\}.$$

Generically, (see (3), I Sect. 1.4), this is a c-dimensional submanifold of $\mathbb{R}^n \times \mathbb{R}^c$. We denote by $\chi : \mathcal{M} \to \mathbb{R}^c$ the projection $\mathbf{x} = (x, \theta) \mapsto \theta$ and let $\mathcal{S}$ denote the set of singularities of χ i.e. the set of points $\mathbf{x} \in \mathcal{M}$ where χ is not a local

diffeomorphism. Then $\mathcal{B} = \chi(\mathcal{S})$ is the set of local bifurcation points. In the generic case this consists of fold and cusp points and the only other bifurcation points are where heteroclinic connections occur. The latter are considered to be global bifurcations because their effect is not restricted to a small neighbourhood.

Since in our discussion $c = 2$, $\mathcal{M}$ will be a surface in $\mathbb{R}^{n+2}$ and χ will be a projection into the plane. Fig. S2 is useful to see the form of cusps and folds in this case.

If $\theta \in \mathbb{R}^2$ is a fold bifurcation point and $x \in \mathbb{R}^n$ is the corresponding rest point then $\mathbf{x} = (x, \theta)$ is in $\mathcal{M}$ and, by (3), I Sect. 1.4 (cf. Theorem 8.1 of (5)), generically there is a smooth curve C in $\mathcal{M}$ through $\mathbf{x}$ that consists of fold points. At $\mathbf{x}$ there are local coordinates (x_1, x_2) on $\mathcal{M}$ and (θ_1, θ_2) on $\mathbb{R}^2$ such that χ is locally given by $(\theta_1, \theta_2) = (x_1^2, x_2)$.

A universal unfolding[†] of the cusp is $\dot{x} = \pm x^3 + \theta_1 x + \theta_2$ and, in the minus sign case the catastrophe manifold $\mathcal{M}$ is given by $x^3 - \theta_1 x - \theta_2 = 0$. Therefore, the map $(\theta_1, x) \mapsto (x, \theta_1, \theta_2 = -\theta_1 x + x^3)$ from $\mathbb{R}^2$ to $\mathcal{M}$ parameterises $\mathcal{M}$ in terms of x and θ_1. Thus, in this parameterisation χ is given by $(\theta_1, x) \mapsto (\theta_1, \theta_2 = -\theta_1 x + x^3)$ and this is singular when $\theta_1 = 3x^2$ which defines a smooth curve C in $\mathcal{M}$. The bifurcation set B_C is its image under χ, which is the set of points given by $\theta_1 = 3x^2, \theta_2 = -2x^3$ i.e. $4\theta_1^3 = 27\theta_2^2$. The + case is entirely analogous.

In Appendix C we prove the following result telling us that in a broad range of cases of interest to us the catastrophe manifold has trivial topology. On the other hand, as we will demonstrate, the mapping χ has a highly non-trivial structure.

Proposition 1. *Suppose there are no bifurcation points near the boundary of the parameter domain P and that P is diffeomorphic to a 2 dimensional disk. Then the connected components of $\mathcal{M}$ are diffeomorphic to the disk D^2.*

Standing hypothesis 1. We therefore assume throughout that the connected components of $\mathcal{M}$ are diffeomorphic to 2 dimensional disks. This is the case for a far more general set of circumstances than those given in Prop. 1.

It follows from this hypothesis that any simple closed curve Γ in one of these components $\mathcal{M}_0$ separates $\mathcal{M}_0$ into two connected components, one of which contains the boundary of $\mathcal{M}_0$. This component we call the *exterior* of Γ and the other component the *interior*.

In the discussion below we often lift to the catastrophe manifold $\mathcal{M}$ smooth curves of the form $\theta = \gamma(t)$, $0 \le t \le \tau_0$ in the parameter space that do not meet any bifurcation points. A lift is a curve $\mathbf{x} = \Gamma(t)$ such that $\chi(\Gamma(t)) = \gamma(t)$ and to ensure it is uniquely determined we will need to fix a point $\Gamma(t_0)$ such that $\chi(\Gamma(t_0)) = \gamma(t_0)$. Often the curve will be closed so that $\gamma(0) \equiv \gamma(\tau_0)$ and then Γ can be taken to be closed although one may have to extend the domain of t because the period of Γ is a multiple of τ_0. The lifts exist because γ meets no bifurcation points.

In some other cases we are able to lift curves from parameter space to $\mathcal{M}$ even though they intersect bifurcation curves. An example is the lift of curves around a cusp in Sect. D, p. 5 and Fig. S3. These lifts can be carried out because the process is local and we can use the universal unfolding of the bifurcation to check that the lift is possible.

[†] See (5) for a definition of universal unfolding.

A. Fold curves and bifurcation sets. It follows from the above (cf. (5), Theorem 8.1, (3), I Sect. 1.4) and the fact that our parameters are 2-dimensional that generically the set of singularities of χ (i.e. $\mathcal{S}$) consists of a finite number of 1-dimensional submanifolds of $\mathcal{M}$. Moreover, if C is one of these submanifolds then every point on C is either a fold point or a cusp point. We call these submanifolds *fold curves* and those that are circles *fold circles*. Clearly, since the closure of $\mathcal{M}$ is compact, a fold curve that does not meet the boundary of $\mathcal{M}$ must be a fold circle.

Standing hypothesis 2. We always assume that our parameterised system is generic in the sense discussed above i.e. that the fold curves are smooth curves in $\mathcal{M}$.

Proposition 2. *Generically, if C is a fold circle then the associated bifurcation set $B_C = \chi(C)$ is a closed curve without any self crossings and $\chi|C : C \to B_C$ has degree one. It is smooth except possibly at a finite number of cusp points and B_C separates $\mathbb{R}^2$ into exactly two components, one of which (denoted B_C^{int}) is a disk.*

Proof. See Appendix D for details.

Terminology 1. *The* bifurcation set *is the subset in parameter space of all bifurcation points. A* bifurcation curve *is any curve contained in the bifurcation set. A* fold curve *is a smooth curve of fold points in the catastrophe manifold $\mathcal{M}$ and this is called a* fold circle *iff it is a closed curve. A* fold bifurcation curve *is any set of the form $B_C = \chi(C)$ where C is a fold curve. A* bifurcation segment *or* segment of a bifurcation curve *is a connected smooth curve contained in a set of the form $B_C = \chi(C)$ where C is a fold curve.*

A very useful construct associated with fold curves and circles that we will use a number of times involves an analysis of their neighbourhoods. Suppose C is a fold circle. Consider a small tubular neighbourhood N of C. By definition of a tubular neighbourhood there is a retraction $q : N \to C$ making (q, N, C) a vector bundle whose zero section is the inclusion $C \to N$. Then $N \setminus C$ has two components one of which is contained in the interior of C. We denote this component by N_C^{int}. If N is sufficiently small then N_C^{int} meets no other fold circles and $\chi|N_C^{\text{int}}$ is injective. This injectivity follows from the fold structure given by equation (5). Let N_C^{ext} denote the other component of $N \setminus C$.

The following result follows from this discussion.

Lemma 1. *If C is a fold circle then χ restricted to the interior $\check{C}$ of C has degree 1 and at all points in $\check{C}$ near C, χ is injective.*

B. Heteroclinic connections and flips. We will be interested in systems where there are two or more index 1 saddles. In such a system a codimension 1 global bifurcation that can occur involves a heteroclinic connection. This occurs when the unstable manifold of one of the saddles s_1 intersects the stable manifold of another saddle s_2. In this case we call s_2 the *target saddle* and s_1 the *source saddle*. If this occurs at a parameter θ then we call this parameter value a *flip point* and we refer to such bifurcations as *flip bifurcations* or just flips.

Generically, in 2-parameter families these bifurcations occur on smooth curves which we call *flip curves* and these curves end on fold bifurcation curves in ways described below in Sect. B.

4. Counting cusps on fold curves & circles

A. The fold orientation. Consider the fold equation (1). Close to $x = 0$ the $\dot{x}$ is always ≥ 0 or ≤ 0. Thus close to a fold point there is a definite direction of flow on a center manifold and this induces an orientation on the center manifold and its tangent space $\ell(\mathbf{x})$. Moreover, $\ell(\mathbf{x})$ varies smoothly with $\mathbf{x} \in C$.

Using this smoothness we have that this orientation is locally consistent on any segment of a fold curve C which contains no cusp points but it switches at cusp points as can be verified by looking at the normal form (2). Thus we have the following proposition.

Proposition 3. *Consider a fold curve C whose endpoints are not cusps. Then, for a generic parameterised system, the number of cusps in C equals the number of orientation switches in C.*

B. Saddle & near-fold bundles. Now consider a smooth closed curve Γ in $\mathcal{M}$ such that, for each point $\mathbf{x} = (x, \theta) \in \Gamma$, x is either an index 1 saddle point or a pseudo-hyperbolic attracting rest point (Sect. A). In this case we say that such a curve Γ is *pseudo-hyperbolic*.

Then we can associate to such a point $\mathbf{x}$ the 1-dimensional tangent space $E^c(x)$ to the center manifold $W^c(x)$ of the rest point at x. These vary smoothly with $\mathbf{x}$ and so we have a bundle $\pi : E^c_\Gamma \to \Gamma$ over Γ with fibre the line $E^c(x)$. Clearly this bundle E^c_Γ must be either a cylinder or a Möbius band and the topology of this bundle encodes important information.

C. Fold circle bundle. For the special case where Γ is a fold circle C we call the bundle E^c_C the *fold circle bundle* and denote it $\mathcal{C}_C$.

Now if C is a fold circle and we start at a point $\mathbf{x} \in C$ which is not a cusp point and traverse the circle, when we arrive back at $\mathbf{x}$ the orientation will have changed a number of times. If this number is odd when we arrive back at $\mathbf{x}$, the orientation will be the opposite to when we started out. Thus for the fibres of $\mathcal{C}_C$ to glue smoothly at $\mathbf{x}$ and for the orientation to be constant on fibres near to $\ell(\mathbf{x})$ (since $\mathbf{x}$ is not a cusp point), $\mathcal{C}_C$ must be a Möbius band. Conversely, if $\mathcal{C}_C$ is a Möbius band then the number of switches must be odd. Thus, for a generic parameterised system, we have the following.

Proposition 4. *If C is a fold circle, $\mathcal{C}_C$ is a Möbius band if and only if C contains an odd number of cusps.*

We call such fold circles *Möbius* fold circles.

D. Conditions for a fold circle to be Möbius. We now investigate the immediate neighbourhood of a Möbius fold circle in $\mathcal{M}$. In particular, we demonstrate that a simple closed curve Γ in $\mathcal{M}$ has the bundle E^c_Γ a Möbius band if and only if it contains an odd number of Möbius fold circles, and we show that, if C is a Möbius fold circle, then on the exterior of C close to C, χ has degree two. As a corollary we see that although a fold circle can contain simple fold circles, it cannot contain a Möbius one.

Proposition 5. *Suppose that Γ is a smooth simple closed pseudo-hyperbolic curve in $\mathcal{M}$ with E^c_Γ a Möbius band. Then in the generic situation, Γ contains an odd number of Möbius fold circles in its interior. Moreover, if C is one of these Möbius fold circles one can find another such curve Γ' such that C is the only fold circle contained in the interior of Γ' except possibly for simple fold circles contained in the interior of C.*

Proof. See Appendix E. □

Now consider a Möbius fold circle C. Then C contains an odd number of cusps. Suppose that the folds in C involve a saddle and an attractor with the interior of C consisting of points $\mathbf{x} = (x, \theta)$ where x is an attractor. Let B^{int}_C be the open disk bounded by B_C.

Now consider a closed curve γ that has one self intersection inside B_C near each cusp (temporarily called nodes), loops around the cusps as shown in Fig. S3C, and otherwise lies entirely in the interior B^{int}_C of B_C near to B_C. Provided it is sufficiently close to B_C this curve can be lifted to a smooth curve Γ in $\mathcal{M}$ so that (i) $\chi(\Gamma) = \gamma$, and (ii) if $(x, \theta) \in \Gamma$, x is an attractor of X_θ which we denote by $x(\theta)$.

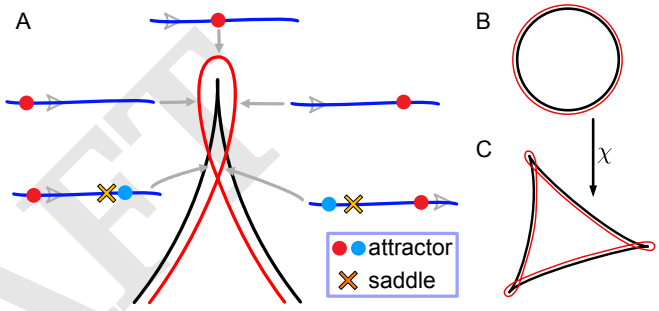

Fig. S3. This shows how the disposition of the rest points involved in a standard cusp vary as one follows the projection into parameter space under χ of a closed curve (red) of attractors in $\mathcal{M}$ which approximates the fold curve giving the cusp. Since the red curve is close to the bifurcation set there is a center manifold through the red attractor. The grey arrow shows the orientation on the center manifold. The cusp shown is a standard one and going round the loops swaps the attractors; for a dual cusp the roles of saddles and attractors are interchanged.

Since the curve γ lies close to B_C, the attractor $x(\theta)$, $\theta \in \gamma$, lies on a smoothly changing center manifold. Since the center manifold varies smoothly, we can give it a consistent orientation $\mathcal{O}$ for all $\theta \in \gamma$. At each node and at all points of γ in B^{int}_C, the unstable manifold of the saddle intersects the stable manifold of the attractor created in the fold bifurcation of B_C.

We define the *relative orientation* of the saddle at $\theta \in \gamma \cap B^{\text{int}}_C$ to be the relative orientation of the saddle to the attractor using the orientation $\mathcal{O}$. Note that although the orientation $\mathcal{O}$ is constant the relative orientation of the saddle can change. In fact, this relative orientation is constant along any segment of γ wholly inside B^{int}_C but flips as θ moves around the loops going from the node around the cusp (Fig. S3A). As a consequence, if there are an odd number of cusps then starting from a node and doing one revolution around γ back to that node results in a flip in the relative orientation. But at the node θ, since it is in B^{int}_C and is close to the cusp, the system has two attractors and a saddle. Thus traversing γ results in the attractors swapping.

A similar picture holds for dual cusps with the roles of the attractors and saddles interchanged and with the unstable manifold of the saddle replacing the role of the center manifold.

Now let U_C be an open set in $\mathcal{M}$ that contains C in its interior and meets no other fold curves in the exterior of C and consider $\chi_1 = \chi|U_C$. The choice of nodes above was arbitrary apart from being in B_C^{int} close to a cusp. Consequently, we deduce that there is a neighbourhood U of the node such that $\chi_1^{-1}(U)$ consists of two disks on each of which χ_1 is orientation preserving (for reasons given below). Consequently, χ_1 has degree 2. This gives the following lemma and its very useful corollary.

Theorem 1. *Consider the following conditions on a fold circle C. (i) C is a Möbius fold circle; (ii) C contains an odd number of cusps; (iii) there is a simple closed pseudo-hyperbolic curve Γ in $\mathcal{M}$ that contains in its interior C and no other fold circles that are in the exterior of C such that (a) under χ, Γ double covers a curve γ in the parameter space and (b) E^c_Γ is Möbius; and (iv) C is contained in an open disk $\mathcal{G}$ in $\mathcal{M}$ on which χ has degree 2. Generically, (i) $\iff$ (ii) $\iff$ (iii) $\Rightarrow$ (iv).*

Proof. We already proved (i) $\iff$ (ii) in Prop. 4. That (i) implies (iii) follows from the above discussion. The curve Γ discussed there double covers the curve γ (cf. Fig. S3). Moreover, since γ can be taken arbitrarily close to B_C, Γ can be taken arbitrarily close to C. Thus the fibres of the bundles $\mathcal{C}_C$ and E^c_Γ will be close and consequently $\mathcal{C}_C$ and E^c_Γ will both have the same Möbius band topology.

To see that (iii) implies (i) we need to use Prop. 5. This asserts that we can modify the curve Γ in (iii) so that it contains in its interior the fold curve C and no other fold points in the exterior of C. Then the modified Γ is homotopic to curves Γ' arbitrarily close to C but exterior to C. Since they are connected by a homotopy, E^c_Γ and $E^c_{\Gamma'}$ are homeomorphic, and since Γ' is close to C, $E^c_{\Gamma'}$ and $\mathcal{C}_C$ are homeomorphic.

To see that (iii) implies (iv) note that χ is a local diffeomorphism at points of Γ and, moreover, since there are no fold points on Γ the sign of the Jacobian of χ at two points on Γ is the same. It follows immediately that if Γ' is any simple closed curve containing Γ in its interior then χ has degree 2 on the interior of Γ' which is a disk. □

Corollary 1. *If C is a fold circle then there are no Möbius fold circles contained in its interior.*

Proof. This follows from part (iv) of the Theorem and the fact that the restriction of χ to the interior of a fold circle has degree 1 by Lemma 1. □

More generally, if $\mathcal{G}$ is a subset of $\mathcal{M}$ diffeomorphic to a disk and $\chi|\mathcal{G}$ has degree 1 then $\mathcal{G}$ contains no Möbius fold circles.

E. Cusps and bifurcation diagrams. In applications it is common to plot bifurcation diagrams in which the position of the rest points is plotted against a single bifurcation parameter θ_1. For example for bistable systems one obtains a S or Z shaped multivalued graph over the parameter. If there is another parameter θ_2 involved in the system it is then of interest to know whether the 2-parameter bifurcation system contains cusps.

Now we extend the cusp index for use in such a situation to determine the number of cusps. We restrict to fold bifurcations between attractors and index 1 saddles but it will be clear that it applies to other fold bifurcations.

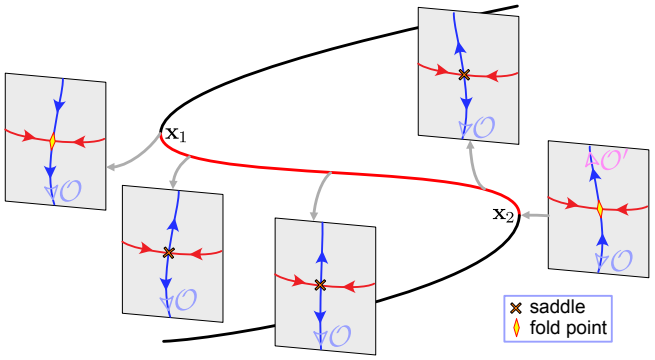

Fig. S4. The black and red curve is a curve in the catastrophe manifold such as that over the line AB in Fig. S2. The red part corresponds to saddles. The left hand fold point determines the orientation on the center manifold shown using the hollow arrow. This induces the corresponding orientation on the saddle points in the systems corresponding to the points along the red curve. Then all the systems on the red curve close to the right hand fold point have the opposite orientation to that fold point. This implies that on any fold curve joining the two fold points shown there are an odd number of cusps.

Suppose that $\Gamma(t)$, $0 \le t \le 1$ is a smooth curve in $\mathcal{M}$ that connects two fold points $\mathbf{x}_i$, $i = 1, 2$, and except at its endpoints consists of index 1 saddles. Suppose moreover that the tangent $E^u(\mathbf{x})$ to the unstable manifold of these saddles $\mathbf{x}$ varies smoothly as t varies.

Given this, we can compare the orientation of $\ell(\mathbf{x}_1)$ with that of $\ell(\mathbf{x}_2)$. Use the orientation of $\ell(\mathbf{x}_1)$ at the fold point $\mathbf{x}_1$ to put an orientation on $E^u(\Gamma(t))$ for t close to 0 using the fact that $E^u(\Gamma(t))$ converges to $\ell(\mathbf{x}_1)$ as t tends to 0 and extend this to all $0 \le t \le 1$ by continuity. Since $E^u(\Gamma(t))$ converges to $\ell(\mathbf{x}_2)$ as t tends to 1 this produces an orientation $\mathcal{O}$ on $\ell(\mathbf{x}_2)$ and the question is whether this is the same as that $\mathcal{O}'$ induced by the fold at $\mathbf{x}_2$ (see Fig. S4).

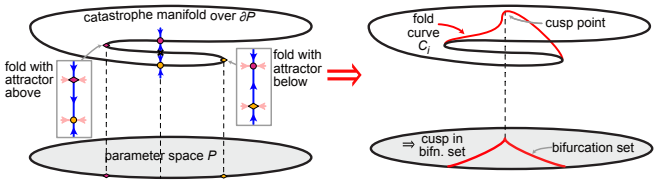

Fig. S5. Over part of the boundary ∂P of a 2-dimensional domain of parameter space P we assume we have an S-shaped bistable section and that the system is monostable over the rest of ∂P. Then if Condition (*) holds it follows that inside P there must be at least one cusp. This is because there must be a fold curve joining the two folds shown and on this fold curve the two folds shown have opposite orientations.

Proposition 6. *If $\mathbf{x}_1$ and $\mathbf{x}_2$ are on a common fold curve C and the orientations $\mathcal{O}$ and $\mathcal{O}'$ of $\ell(\mathbf{x}_2)$ are incoherent then there is an odd number of cusps on C between $\mathbf{x}_1$ and $\mathbf{x}_2$.*

In a number of applications of CT (e.g. (6)) one is given the behaviour on the boundary of the parameter domain and one wants to deduce the bifurcation behaviour inside. By far the most considered situation in this regard is where the boundary behaviour is as in Fig. S5(Left) i.e. one has a parameter space P which is a 2-dimensional disk-like region and the catastrophe manifold over the boundary ∂P is bistable over part of ∂P. In this case one would like to know if there is a cusp inside P.

Suppose the boundary ∂P is given by $\theta = \theta(s)$, $0 \leq s \leq 1$, and that the interval where there is bistable behaviour is given by $\theta(s)$, $s_1 \leq s \leq s_2$, so that there are folds at $s = s_1$ and $s = s_2$. To obtain the required result about cusps we need the following condition on the two attractors involved in the two folds: (*) for at least one of these attractors, the attractor varies smoothly with s in (s_1, s_2) and for all s in (s_1, s_2) the unstable manifold of the saddle point intersects the basin of this attractor. This condition is automatic if the state space is 1-dimensional but not so in higher dimensions. To understand why see Fig. S17 in Appendix F. Note that we are not assuming that the saddle and attractors that are involved in the fold bifurcations are all the rest points in the system. If they are then Condition (*) is redundant. An example of a bistable 1-parameter system that swaps orientation but where the two folds are not on a common fold curve is given by taking a straight line in the parameter space in Fig. S10 which is roughly parallel to one of the boundary curves and does not meet the deltoid $\mathcal{B}$. Then we have the following theorem:

Theorem 2. *If the two fold points in $\mathcal{M}$ corresponding to the two folds at $\theta = \theta(s_1)$ and $\theta = \theta(s_2)$ are on a common fold curve in $\mathcal{M}$ and condition (*) holds then generically there are an odd number of cusps in P.*

Proof. By Condition (*), as s moves between the folds at s_1 and s_2 the unstable manifold of the saddle must intersect the basin of the smoothly varying attractor. The identity of this attractor remains constant for all s and we call it A. The unstable manifold can also be involved in heteroclinic bifurcations but, in generic systems, for all but a finite number of s values, it will also intersect the basin of a different attractor of the system at $\theta(s)$ which we denote by $B(s)$. At these finite number of s values the identity of $B(s)$ may change. In the generic case when s in (s_1, s_2) is close to s_1 or s_2 the attractors A and $B(s)$ vary smoothly and they are connected by the unstable manifold of the saddle. If for $\mathbf{x}_1$ in Prop. 6 we take the fold involving A, then $\mathcal{O}$ points away from A when s is near the bifurcation value. Since the unstable manifold of the saddle and A vary smoothly, $\mathcal{O}$ remains doing this for all $s \in (s_1, s_2)$ and therefore is incompatible with the orientation at the fold involving $B(s)$ since this orientation points away from $B(s)$. Thus the odd number of cusps follows from Prop. 6. □

Historical Note. Results similar to Theorem. 2 for the case where $n = 1$ were obtained by Stewart in (7) using entirely different methods based on singularity theory. Ian Stewart pointed out to us a paper of Tim Poston (8) that discusses the problem in Theorem. 2 and mentions a preprint by E. C. Zeeman (*A boundary value problem involving cusps*) in which this problem is treated. However, in Poston's discussion the need to check the incompatibility of the orientations $\mathcal{O}$ and $\mathcal{O}'$ is not mentioned. If it existed this manuscript seems to have disappeared and is not listed in the Zeeman Archive (www.lms.ac.uk/2015/zeeman_archive). One of us (DAR) recalls Zeeman mentioning that someone else had proved this result but we cannot trace such a paper.

5. Characterising 3-attractor MS components

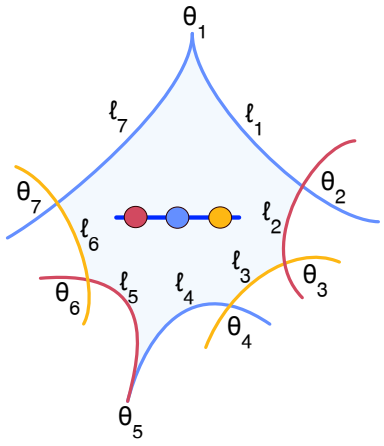

Fig. S6

Now we consider 3-attractor MS components Ω in 2-parameter systems with compact dynamics. Our aim is to understand the bifurcations in the boundary of Ω and we will do this by deducing a set of rules for the way in which cusps, crossings and flip end points are disposed around the boundary.

We denote the attractors by A, B and C. Since they do not bifurcate in Ω they vary smoothly with the parameters and maintain their identity.

As one proceeds around the boundary $\partial\Omega$ of Ω there is a sequence of codimension 2 points $\theta_1 \ldots \theta_N$ with $\theta_N = \theta_1$ as described in Fig. 2 of **I**, namely cusps, dual cusps, and crossings (see Fig. S6). (The other relevant codimension 2 points, namely, the two types of endpoints of flip curves are dealt with in Sect. B.) If we know these then we know all the bifurcation structures associated with $\partial\Omega$. The points θ_i and θ_{i+1} are joined by a smooth fold bifurcation curve segment ℓ_i. The bifurcations on this segment involve one of the attractors $X \in \{A, B, C\}$ and we denote this by $\ell_i \in \mathcal{L}_X$ or say that the attractor identity of ℓ_i is X. For a sequence $\ell_i, \ldots, \ell_{i+j}$ with ℓ_k having attractor identity X_k we write $\ell_i, \ldots, \ell_{i+j} \in \mathcal{L}_{X_i,\ldots,X_{i+j}}$. There are strong constraints on what sequences can occur as we now describe.

A. Crossings of bifurcation curves. In general when two bifurcation curves cross, the two bifurcations may be completely independent. However, this is not the case when the corresponding rest points are both on the same smooth connector and are adjacent. This is because, when it is smooth, the connector is contained in any center manifold of a fold point on the connector and hence the fold orientations (Sect. A) of the two folds provide orientations for the connector that must be the same for the simultaneous bifurcations to be allowed. See Figs. S7 and S8.

Now consider the case where the system has 3 attractors P_1, P_2 and X, and two saddles, where X is the central attractor. Assume all these are on a smooth connector.

Firstly, note that there is only one possibility for the orientation of a fold involving a peripheral attractor. The vector field near the fold point must point along the connector towards the other rest points on the connector. In particular,

the orientations $\mathcal{O}_1$ and $\mathcal{O}_2$ of folds involving the two peripheral attractors P_1 and P_2 are opposite. Given this, when considering a fold curve or fold bifurcation curve involving the central attractor X we say *the fold of X is compatible with P_i* (with $i = 1$ or 2) to indicate that the orientation of the fold involving X is $\mathcal{O}_i$.

Now consider two smooth segments ℓ_1 and ℓ_2 of fold bifurcation curves that cross each other. Suppose that the segment ℓ_i, $i = 1, 2$, involves the attractor $A_i \in \{P_1, P_2, X\}$. Then the following lemma follows immediately from the above discussion.

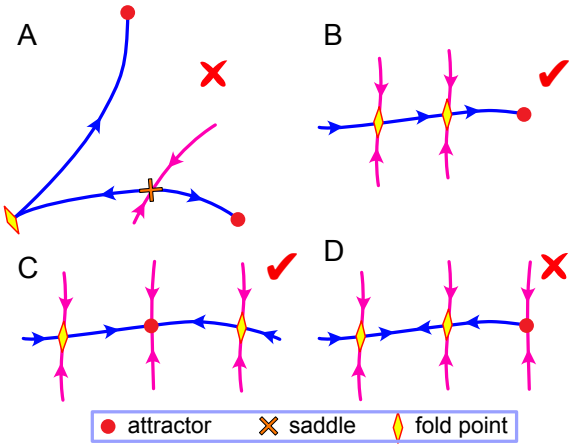

Fig. S7. (A) If at the central attractor the connector has a cuspoidal structure then a fold bifurcation of this attractor is impossible. This is proved in Lemma 6 Appendix B and basically follows from the incoherence of the two arrows on the branches approaching the fold point. (B-D) This illustrates examples of what dynamics on the connector are possible and impossible at points where bifurcation curves cross. The orientations of two folds at adjacent rest points must be the same. There are no restrictions on the way the blue connector approaches the red attractor. (B) allowed since the arrows are consistent, (C) allowed since the folds are not adjacent, (D) not allowed as center and bifurcating peripheral have opposite orientations.

Lemma 2. *The only restrictions on crossings concern the case where one of the A_i is the central attractor X. In this case the folds on ℓ_1 and ℓ_2 all have the same orientation.*

A.1. Crossings near cusps. A key fact in this section is that since a bifurcation curve B_C is the image of a single fold curve in $\mathcal{M}$, as one moves along B_C, either the attractor or the saddle that is bifurcating remains constant.

The bifurcation curve through a cusp is the projection under χ of a fold curve in $\mathcal{M}$. Near the cusp point the bifurcation curve in parameter space Ω consists of two smooth segments ℓ and ℓ' joined at the cusp. In a neighbourhood of the cusp point in Ω there is a smooth center manifold containing the rest points involved in the bifurcation because at the cusp point the central manifold is normally hyperbolic and hence varies smoothly with the parameters and contains the bifurcating rest points.

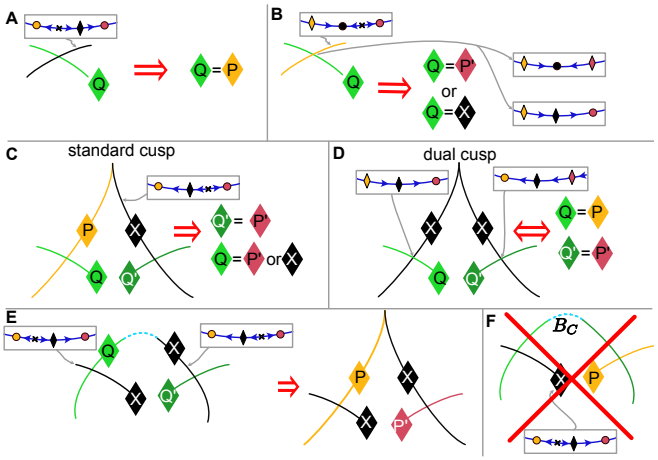

Fig. S8. Illustration of Lemma 2 and Theorem 3. **A.** The orientation of the fold bifurcation involving the central attractor determines the possible crossings of the fold curve. **B.** The peripheral attractor involved in the fold constrains the possible crossings of the fold curve. **C. Standard cusp.** Fold curves crossing the cusp's branches satisfy the conditions in (A) and (B). . **D. Dual cusp.** Fold curves crossing the cusp's branches satisfy the conditions in (A) and (B) and the crossings imply the existence of the cusp. **E.** The orientations of the folds of the central attractor imply the existence of a cusp. **F.** Certain consecutive crossing are not possible. **Legend**: A diamond shape denotes a fold bifurcation of the specified attractor. Bifurcation curves are coloured accordingly.

For a dual cusp the folds along both of the segments ℓ and ℓ' involve the central attractor and they have opposite orientations on the two segments (Fig. S8D). For a standard cusp the two smooth segments either side of the cusp correspond to a common saddle and two different attractors. One of them is the central attractor $X \in \{A, B, C\}$ and the other a peripheral attractor $P \in \{A, B, C\}$ (Fig. S8C).

As a corollary of Lemma 2, if C is a fold curve with such a standard cusp involving P and X compatible with the other peripheral attractor P', then a fold curve crossing the P side involves the bifurcation of P' or X compatible with P, and a fold curve crossing the X side involves the bifurcation of P' (Fig. S8C).

Now consider a fold curve C in $\mathcal{M}$ such that $B_C = \chi(C)$ is contained in the boundary of a 3-attractor MS component and which is such that moving out of the component across B_C involves the loss of an attractor. Suppose that the attractors in the MS component are (central) X, (peripheral) P_1 and P_2. Suppose that on B_C there are two crossing points at θ_1 and θ_2 and none in between them and suppose the fold bifurcation curves which cross at these points are ℓ_1 and ℓ_2 respectively.

Theorem 3. *1. ℓ_1 and ℓ_2 are associated with different peripheral attractors if and only if C is a fold curve for X and it contains an odd number of dual cusps (Fig. S8D).*
2. If the folds in ℓ_1 at θ_1 and in B_C at θ_2 involve the central attractor X and the former (resp. latter) have orientation compatible with P_1 (resp. P_2) then there is an odd number of standard cusps in B_C between θ_1 and θ_2 and the fold in ℓ_2 at θ_2 involves P_2 (Fig. S8E).
3. It is not possible that the fold in ℓ_1 at θ_1 involves X with orientation compatible with P_1 and the one in ℓ_2 at θ_2 involves P_1 (Fig. S8F).

Proof. Proof of 1. If C is a fold curve for X and it contains an odd number of dual cusps, then the orientation of the X fold is different at $\mathbf{x}_1 = (x, \theta_1)$ and $\mathbf{x}_2 = (x, \theta_2)$. Hence, by

lemma 2 the crossing curves involve the bifurcation of different peripheral attractors.

Conversely, assume that the crossing curves involve different peripheral attractors and in particular that ℓ_1 at θ_1 involves P_1. Then, B_C at θ_1 involves either X compatible with P_1 or P_2. Assume that it is P_2. Since the fold in ℓ_2 at θ_2 involves P_2 there must be a cusp in C that changes the bifurcating attractor. This cusp is a standard cusp that involves X compatible with P_1, which again can not cross ℓ_2 at θ_2. Therefore, C at θ_1 involves X compatible with P_1. Similarly, C at θ_2 involves X compatible with P_2. Therefore, C is a curve of X folds with different orientations at θ_1 and θ_2 and therefore it contains an odd number of cusps between these two points.

Proof of 2. By lemma 2 the fold along B_C near θ_1 involves P_1 and the fold along ℓ_2 near θ_2 involves P_2. Therefore B_C contains an odd number of dual cusps between these two points.

Proof of 3. The condition at θ_1 implies that at that point in B_C the saddle between P_1 and X bifurcates with P_1. Thus there cannot be a crossing by P_1 at θ_2 as this would also have to involve the same saddle to create the additional fold. □

B. Heteroclinic bifurcations (flips) and flip curves. Before proceeding we need to discuss flip curves and how they end. This relates to the question of whether or not the connector is smooth. As one moves along a bifurcation curve such smoothness can change. This happens at certain endpoints of flip curves.

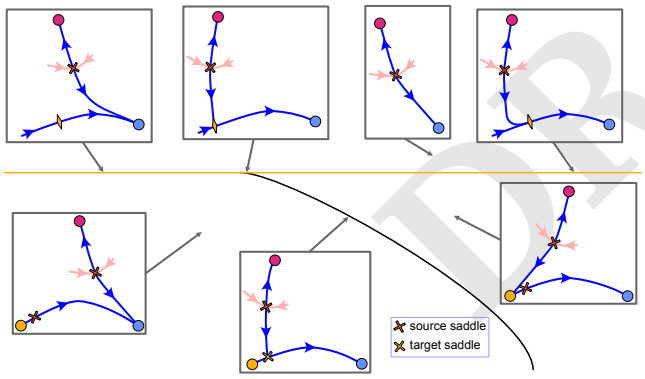

Fig. S9. This shows how a generic flip curve (black) meets a fold curve (yellow) when the fold occurs at the central attractor. See (9).

B.1. Target saddles. The first way that flip curves can end is by a bifurcation of the corresponding target saddle.

Proposition 7. *Consider a smooth fold bifurcation segment ℓ involving the attractor $X \in \{A, B, C\}$. Suppose that at a point θ_0 on ℓ the connector changes from smooth to non-smooth. Then, generically, X is central at θ_0 which is the end-point of a flip curve where the target saddle is destroyed in a fold bifurcation with X. There is a neighbourhood U in ℓ of such a point θ_0 such that for θ in one component of $U \setminus \{\theta_0\}$ the connector is smooth and X is central, while for θ in the other component the connector is non-smooth and another attractor Y is central. The third attractor Z is the source attractor. In this situation the only fold bifurcation curves that can cross the $U \setminus \{\theta_0\}$ must involve the attractor Z.*

Proof. For the first part of the proposition see Theorem I.3 and Corollary I.4 of (9). Strictly speaking the results quoted are for gradient systems but it is clear that the arguments used apply to our situation. According to this, the generic situation is as follows. On a neighbourhood of θ_0 there are coordinates (μ_1, μ_2) such that θ_0 is given by $\mu_1 = 0, \mu_2 = 0$, the fold bifurcation curve through θ_0 is given by $\mu_2 = 0$ and the flip curve is given by $\mu_2 = \mu_1^2$, $\mu_1 \geq 0$. Along $\mu_2 = 0$ the connector is smooth for $\mu_1 > 0$ and non-smooth otherwise.

To see the result about crossing fold bifurcation curves note that in the component of $U \setminus \{\theta_0\}$ where the connector is smooth, the orientation at the fold is compatible with Z and not Y. In the other component, the central attractor is Y which is therefore not able to undergo a fold bifurcation. Thus any crossing must be by a curve involving Z. □

It follows that if there are no flip curves then the connector is always smooth or always non-smooth. Also a corollary is that in terms of its connections with crossing points and cusps such a bifurcation segment with a single such target flip curve endpoint behaves exactly as one that has a smooth connector all along its length.

The above result raises the question of how the transition from a smooth to a cuspoidal connector takes place in the region where there are three attractors. If the attractors involved are as in Fig. S9 then the transition involves the yellow attractor i.e. the attractor that is close to bifurcation. When the system is sufficiently close to the fold curve the yellow attractor x has a center manifold and a strong stable manifold $W^{ss}(x)$ as described in Sect. A. The transition takes place when the unstable manifold from the source saddle s_S intersects $W^{ss}(x)$ and flips from joining smoothly at x to the unstable manifold of the other saddle, to having a cuspoidal joint to it at x.

B.2. Source saddles. The other way a flip curve can end is via a fold bifurcation that destroys the source saddle. This is more straightforward and needs no special consideration. It meets the fold curve transversally.

B.3. Crossings sequences. Recall that if the connector is not smooth at the point where two fold bifurcation curves cross then the two crossing curves must involve both peripheral attractors as a fold bifurcation of the central attractor is impossible in this case (see Appendix B).

Lemma 3. *Consider an adjacent pair of crossing points involving the smooth segments ℓ_{i-1}, ℓ_i and ℓ_{i+1} where these respectively involve the attractors Y, X and Z. Assume that for each segment, if it contains more than one target flip curve endpoint then they all involve the same target saddle. Then if X is central at some point on ℓ_i, $Y = Z \neq X$.*

Proof. Firstly, suppose that there are no flip curves along ℓ_i. Then as you move along the fold curve ℓ_i the central attractor remains the same and the orientation $\mathcal{O}$ of the fold at the central attractor stays constant. At a crossing of ℓ_i by a fold bifurcation curve corresponding to P the orientation induced by the bifurcation of P must be compatible with $\mathcal{O}$ and this is the case for only one peripheral attractor. If there is a flip curve ending then the result follows from Prop. 7. □

Lemma 4. *With the same assumption as in the previous lemma, suppose that $\ell_i, \ldots, \ell_{i+j}$ is a sequence of crossing*

points and $X_i, \ldots, X_{i+j}$ is the corresponding sequence of attractors. Then if we replace all triples of the form PXP (where X is central and P peripheral) by P, the resulting sequence just alternates between P and P' where P' is the other peripheral attractor.

Proof. This follows from the fact that by Lemma 3 if $\ell \in \mathcal{L}_X$ has X central for some $\theta \in \ell$ then the crossings are of the form PXP. Thus replacing the PXP triples by Ps removes all Xs. Moreover, a PXP triple is adjacent either to a XP pair or a P'. So repeating this process produces a sequence alternating between P and P'. □

C. Simplest/minimal MS components. Given the constraints outlined above it is clear that for a given configuration of cusps the first four of the following give the minimal complexity examples. The fourth is more complex (see Sect. 6). In the first three the connector is always smooth and there are no flip curves. The first two can be obtained as a 2 dimensional section through the butterfly catastrophe.

1. With a dual cusp and no other cusps: **I** Fig. 5A.
2. With a dual cusp and a standard cusp: **I** Fig. 5A(inset).
3. With a standard cusp and no other cusps: **I** Fig. 5B.
4. With a standard cusp and a flip curve: **I** Fig. 5C.
5. With no cusps and only smooth bifurcation segments: **I** Fig. 5D & see Sect. 6 below.

6. Topological charge and the elliptic umbilic

Our goal in this section is to explain why the boundary behaviour in Fig. S10 necessitates the complex dynamics inside. This is a particularly striking boundary value problem and we introduce the notion of a phase or *topological charge* into the analysis. In physics an optical vortex has a topological charge. This is observed by interfering an optical vortex with a plane wave of light. This reveals the spiral phase of the vortex as concentric spirals. The number of arms in the spiral equals the topological charge.

In our case the topological charge of a fold circle is the number of cusps it contains. It is topological because when measured mod 2 the even and odd cases correspond to the topology of the various line bundles we have introduced. One can recognise the presence or not of mod 2 charge by topology. Lastly, non-zero mod 2 charge is rigid and cannot be perturbed or homotoped away while zero charge fold curves can.

We are concerned with a system where the boundary behaviour is as shown in Fig. S10, and described as follows:
Compact Elliptic Umbilic boundary behaviour assumption is that there are three smooth curves ℓ_A, ℓ_B, and ℓ_C which intersect as shown in Fig. S10 and on which the indicated attractor undergoes a fold bifurcation that destroys the attractor. On a neighbourhood of the three curves we have the bistable and monostable behaviour shown in Fig. S10.

We denote by Δ the open region enclosed by ℓ_A, ℓ_B, and ℓ_C. Clearly, it is diffeomorphic to the 2-dimensional disk. Since we are interested in characterising 3-attractor MS components we also assume that inside Δ we have three attractors A, B and C that have smooth dependence upon the parameters.

We show that given this boundary behaviour the system in Δ contains all the ingredients of the compact elliptic umbilic (CEU) that we now introduce.

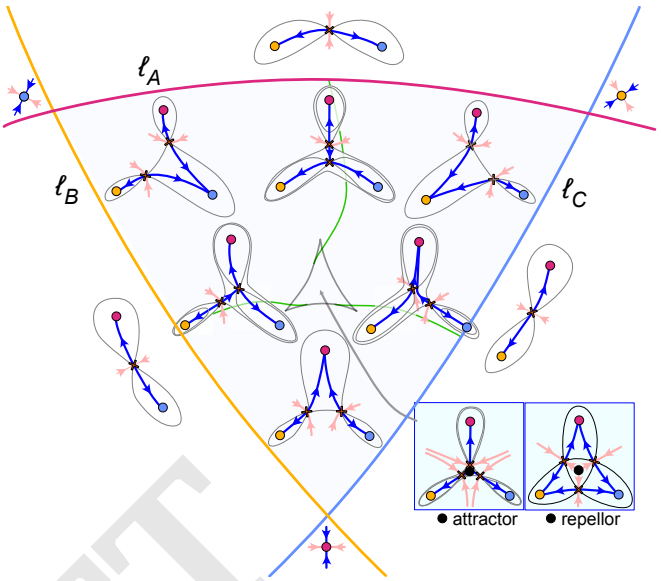

Fig. S10. The compact elliptic umbilic. See text for description.

A. The compact elliptic umbilic. This is the set of gradient systems associated with the potential

$$f_\theta(x_1, x_2) = x_1^4 + x_2^4 + x_1^3 - 2x_1x_2^2 + \theta_3(x_1^2 + x_2^2) + \theta_1 x_1 + \theta_2 x_2. \quad [6]$$

These parameterised families of gradient systems are given by $\dot{x}_i = -\sum_j g^{ij} \partial f_\theta / \partial x_j$ where g_{ij} is a Riemannian metric and $(g^{ij}) = (g_{ij})^{-1}$.

We illustrate the case where θ_3 is fixed at 0.1 but we will see this provides a ubiquitous landscape structure. There are three curves ℓ_A, ℓ_B, and ℓ_C in the parameter space $\mathbb{R}^2$ of fold bifurcations as shown in Fig. S10. For $X \in \{A, B, C\}$ the curve ℓ_X is where the attractor X is destroyed in a fold bifurcation. These curves enclose a triangular shaped region which we denote by Δ. There is a hypocycloid $\mathcal{B}$ with three cusps (a *deltoid*) inside Δ such that for θ inside Δ but outside $\mathcal{B}$ the system has three attractors that we label A, B, and C plus two saddles. Inside $\mathcal{B}$ it has an extra saddle and either an extra attractor (if $\theta_3 > 0$) or an extra repellor.

For a given Riemannian metric g_{ij} the corresponding gradient system also has three flip curves in Δ as shown on Fig. S10 on which heteroclinic bifurcations occur. These start on ℓ_A, ℓ_B, and ℓ_C and end on the hypocycloid $\mathcal{B}$. The configurations shown are for a generic metric; for the standard one the situation is not generic and the curves end at a cusp point (10).

Let $\mathcal{M}$ be the catastrophe manifold over Δ i.e. $\mathcal{M} = \{\mathbf{x} = (x, \theta) : x \text{ a critical point of } f_\theta, \theta \in \Delta\}$. Since the attractors A, B and C vary smoothly, the components $\mathcal{M}_A$, $\mathcal{M}_B$ and $\mathcal{M}_C$ of $\mathcal{M}$ corresponding to them are graphs over Δ that form disjoint components. Thus we focus on $\mathcal{M}_0$ which is the remaining component of $\mathcal{M}$ after $\mathcal{M}_A$, $\mathcal{M}_B$ and $\mathcal{M}_C$ have been removed. Let $\chi_0 = \chi|\mathcal{M}_0$.

If $\mathcal{B}^{\text{int}}$ denotes the interior of $\mathcal{B}$ then $\mathcal{M}_1 = \chi_0^{-1}(\Delta \setminus \mathcal{B}^{\text{int}})$ is an annulus that under χ_0 double covers the annulus $\Delta \setminus \mathcal{B}^{\text{int}}$

i.e $\chi_0|\mathcal{M}_1$ is equivalent to the map: $\mathbb{S}^1 \times (-1,1) \ni (\theta, t) \mapsto (2\theta \bmod 2\pi, t) \in \mathbb{S}^1 \times (-1,1)$.

To obtain $\mathcal{M}_0$ we take the inner boundary of $\mathcal{M}_1$ which is a circle and glue in to it a disk correponding to the new non-saddle rest point that is created by the fold bifurcation that occurs on $\mathcal{B}$. This $\mathcal{M}_0$ is diffeomorphic to a disk but the mapping χ_0 is non-trivial.

B. Boundary conditions. Now we show that if we have the same boundary conditions as for the CEU then we have dynamics closely similar to those of the CEU inside. Indeed the only change is the possible addition of one or more simple fold circles inside the Möbius fold circle corresponding to $\mathcal{B}$ that then add extra rest points to the dynamical system that bifurcate in and out maintaining the architypal CEU structure.

For the rest of this section we assume the CEU boundary behaviour defined above in Sect. A.

Since there is a neighbourhood U of $\partial\Delta$ that contains no bifurcation points in $U \cap \Delta$, then by Proposition 1, each connected component of $\mathcal{M}$ over Δ is diffeomorphic to a disk. As above, since the attractors A, B and C vary smoothly, the components $\mathcal{M}_A$, $\mathcal{M}_B$ and $\mathcal{M}_C$ of $\mathcal{M}$ corresponding to them are graphs over Δ that form separate components. We denote by $\mathcal{M}_0$ the remaining component of $\mathcal{M}$ after $\mathcal{M}_A$, $\mathcal{M}_B$ and $\mathcal{M}_C$ have been removed. Let $\chi_0 = \chi|\mathcal{M}_0$. This is the connected component of the catastrophe manifold that involves the saddles.

In the following sections we will deduce the following results which mirror similar results for the CEU. We now show that close to $\partial\Delta$ it has the same double covering annular structure as this CEU. This will involve analysis of the flip curves in Δ. From this we will deduce the existence of a Möbius fold circle C in $\mathcal{M}$. Further analysis of the flip curves will show that C is unique and that $B_C = \chi(C)$ plays the role of the deltoid $\mathcal{B}$ of the CEU and has a 3-fold cusp structure.

C. Using flip curves.

C.1. Flips ending on ℓ_A, ℓ_B and ℓ_C. In the following subsections X, Y and Z are always distinct elements of $\{A, B, C\}$.

Proposition 8. *The CEU boundary behaviour assumption implies that*

1. *there is a neighbourhood U of $\ell_Y \cap \ell_Z$ such that if $\theta \in U \cap \Delta$ then X is the central attractor.*

2. *there is a neighbourhood V of ℓ_X such that for all $\theta \in V \cap \Delta$ either there is a heteroclinic connection or the system is MS with X a peripheral attractor.*

Proof. Firstly, note that the CEU boundary behaviour assumption implies that there is a neighbourhood U of the boundary such that if $\theta \in U \cap \Delta$ then X_θ has three attractors and two saddles all of which vary smoothly with $\theta \in U \cap \Delta$.

Since the curves ℓ_X, ℓ_Y, and ℓ_Z are smooth and since ℓ_Y meets both ℓ_X, and ℓ_Z then Y is peripheral along ℓ_Y by Lemmas 2 and 3. Similarly, Z is peripheral along ℓ_Z. Thus at $\ell_Y \cap \ell_Z$, X is central. It follows that X is also central close to $\ell_Y \cap \ell_Z$ for $\theta \in \Delta$ and X is peripheral for all θ in Δ near to ℓ_X. □

Corollary 2. *The CEU boundary behaviour assumption implies that for $X \in \{A, B, C\}$ there are generically an odd number of flip curves starting on the intersection of ℓ_X with the closure of Δ. On each of these the central attractor changes from Y to Z or vice-versa.*

Proof. The result follows because in moving along ℓ_X from $\ell_X \cap \ell_Y$ to $\ell_X \cap \ell_Z$ is to move from Z being the central attractor to Y being central. □

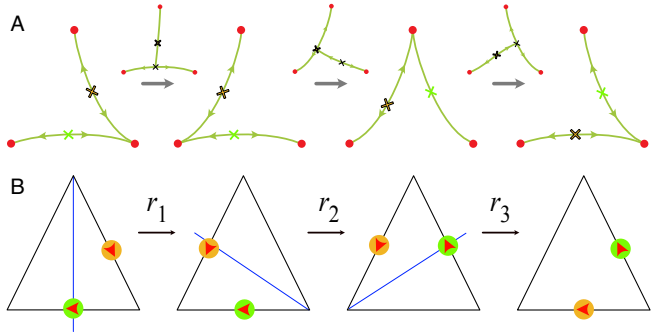

Fig. S11. A series of flips that results in the saddles swapping. The r_i are all reflections in the thin blue line that is shown.

C.2. Algebra of three-way flips. To each generic configuration of three attractors and two saddles as above we can associate a triangle with vertices marked A, B and C. We label the saddles g (green) and y (yellow). See Fig. S11A. Then we associate to each MS 3-attractor system the corresponding marked equilateral triangle as in Fig. S11B. The vertices correspond to the attractors A, B and C and we mark an edge with green or yellow if the corresponding unstable manifold of g or y joins the corresponding two attractors. The meaning of the red arrows in Fig. S11 is explained below.

To each flip we can associate a corresponding reflection as shown in Fig. S11. This is an element of the Dihedral group D_3 which can be represented as the group of symmetries of the equilateral triangle consisting of reflections and rotations through $2\pi/3$ radians.

Thus, consider an oriented loop $\gamma(t)$ in Δ with a given orientation and starting point (not in a flip curve), that does not meet any fold or cusp points and which is transversal to the flip curves. To this we can associate a sequence σ_γ of elements of D_3. This is the product $r_k r_{k-1} \cdots r_1$ where r_i is the reflection that occurs when the curve crosses the ith flip. The reduction of this product is $r_{i_r} r_{i_{r-1}} \cdots r_{i_1}$ which is what is left when we iteratively delete all products in the product of the form $r_i r_i^{-1}$ or $r_i^{-1} r_i$. It is then easy to see that the resulting product is

$$r_{\sigma(1)} r_{\sigma(2)} r_{\sigma(3)} \cdots r_{\sigma(1)} r_{\sigma(2)} r_{\sigma(3)} = \left(r_{\sigma(1)} r_{\sigma(2)} r_{\sigma(3)}\right)^k$$

for some cyclic permutation σ of $\{1,2,3\}$ and some $k \geq 0$. This is because the starting and ending configurations are the same and since once all the terms $r_i r_i^{-1}$ or $r_i^{-1} r_i$ have been removed the sequence of indices must be periodic of the form $\cdots\sigma(1)\sigma(2)\sigma(3)\sigma(1)\sigma(2)\sigma(3)\cdots$ since only two r_is can be applied to any given configuration and if that configuration has been achieved then the inverse of one of these was applied to get it.

We call (σ, k) the *flip index* of γ. Note that k does not depend on the starting point and that, for k even, when evaluated the product is the identity and otherwise is a non-trivial reflection.

When the unstable manifolds of the saddles undergo the transformations shown in Fig. S11 the unstable manifolds undergo interesting changes in orientation. Similar things occur for the stable manifolds but we only consider unstable manifolds here as we are interested in index 1 saddles and then the unstable manifold is 1-dimensional even in n-dimensional systems.

Put an orientation on the two saddles. This is indicated in Fig. S11 by the red arrow. As the flips occur this orientation is propagated as shown. (Note that this is not what you get by applying the geometric reflections. Instead follow what is happening in the top row.) After applying them once, the two saddles have switched and one of the unstable manifolds has opposite orientation. From this we see that applying the flips corresponding to $r_{\sigma(1)}r_{\sigma(2)}r_{\sigma(3)}$ twice we reverse the orientation of both unstable manifolds and the saddles switched twice. Thus we have the following result.

Proposition 9. *Suppose that γ is a closed curve in Δ that contains no fold or cusp bifurcation points. Put an orientation on the unstable manifolds of the two saddles. The flip index of γ has k odd if and only if this orientation is reversed in one of the unstable manifolds when γ is traversed once.*

Consider a simple closed curve $\gamma(t)$ in Δ that has a lift $\Gamma(t) = (x(t), \theta(t))$ $0 \le t \le 1$ to a smooth closed curve in $\mathcal{M}_0$. Assume that it meets no fold points. Then the unstable manifold $W^u(x(t))$ of the saddle $x(t)$ varies smoothly with t. Thus as $t \to 1$ from below $W^u(x(t))$ converges as a point set to $W^u(x(0))$. Thus if we fix an orientation on $W^u(x(0))$ and use the smooth dependence of $W^u(x(t))$ on t to propagate this orientation to all $W^u(x(t))$ we can ask whether as $t \to 1$ from below the orientation on $W^u(x(t))$ converges to that on $W^u(x(0))$. Clearly, this is the case if and only if the saddle bundle of Γ is a cylinder.

On the other hand, from the above discussion, this is not the case if the flip index of Γ has k odd and is the case otherwise. Thus we deduce the following result

Proposition 10. *The flip index of Γ is odd if and only if the bundle E^c_Γ is Möbius.*

Proof. By the above, the flip index is odd if and only if a complete revolution around Γ causes any orientation put on the unstable manifolds of the saddles to be reversed and this is the case if and only if the bundle E^c_Γ is Möbius. □

C.3. Flips at $\partial\Delta$ imply a Möbius fold circle. Cor. 2 above tells us that there are an odd number of flip curves along each of the edges ℓ_X, $X \in \{A, B, C\}$, and these flip curves induce the same element or its inverse when calculating the flip index of a simple closed curve γ close to $\partial\Delta$. We denote the corresponding element r_X. If the curve is sufficiently close to $\partial\Delta$ then the elements must alternate between r_X and r_X^{-1} with a total contribution of r_X. Thus, in the notation analogous to Cor. 2, the resulting product for the whole curve is of the form $r_{\sigma(Z)}r_{\sigma(Y)}r_{\sigma(X)}$ and we deduce that $k = 1$.

Since γ is a closed curve we can parameterise it as $\theta = \gamma(t)$, $t \in \mathbb{R}$, with $\gamma(t+1) \equiv \gamma(t)$. Since there are no bifurcation points in Δ close to $\partial\Delta$, we can lift this to a closed curve $\mathbf{x} = \Gamma(t)$ in $\mathcal{M}$ so that if $\Gamma(t) = (x(t), \theta(t))$ then $x(t)$ is one of the two saddles. If $0 \le t < 1$ it follows from the above discussion that $\Gamma(t)$ and $\Gamma(t+1)$ are two distinct points in $\mathcal{M}$ that are interchanged when t is increased by one. This is because $k = 1$ and therefore going once round γ flips the saddles as explained in Sect. C.2. Let $\mathcal{M}_0$ be the connected component of $\mathcal{M}$ containing Γ and $\chi_0 = \chi|\mathcal{M}_0$.

Proposition 11. *There is a neighbourhood U of $\partial\Delta$ such that $U \cap \Delta$ and $\chi_0^{-1}(U \cap \Delta)$ are annuli and the latter is a double cover of the former on which χ_0 has degree 2.*

Proof. Take a small tubular neighbourhood N_X of each curve ℓ_X, $X \in \{A, B, C\}$ so that (i) there are no bifurcation points in N other than in $\partial\Delta$ and (ii) so that if $N = N_A \cup N_B \cup N_C$ then $U = N \cap \Delta$ is an annulus and such that for any point $\theta \in U$ there is a curve γ as above with $\theta \in \gamma$. Then χ is a local diffeomorphism and, from the above discussion every point in U has two preimages in $V = \chi_0^{-1}(U)$ under χ_0. Put an orientation on V so that the degree of χ is non-negative. Then if $\mathbf{x}_1$ and $\mathbf{x}_2$ are the two preimages of θ, since we can move from $\mathbf{x}_1$ to $\mathbf{x}_2$ by moving along a closed curve in U, χ_0 is orientation preserving at both points. Thus the degree of $\chi_0|V$ is two. □

Now we can prove one of our main results.

Theorem 4. *Suppose that the configuration of the smooth bifurcation curves ℓ_A, ℓ_B, and ℓ_C is as in the CEU boundary behaviour assumption (cf. Fig. S10) and that Δ is the open region enclosed by these curves. Then Δ contains $B_C = \chi(C)$ where C is a Möbius fold circle.*

Proof. Let γ be a smooth simple closed curve in Δ close to the boundary of Δ. Lift γ to a closed curve Γ in $\mathcal{M}_0$. Then by Cor. 2 the flip index of γ is odd and therefore the same is true for Γ. Therefore, by Prop. 10, the bundle E^c_Γ is Möbius. It follows by Theorem 1 that there is a Möbius fold circle C in the interior of Γ. Since C is in the interior of Γ, B_C is contained in Δ. □

C.4. Flip curves in $\mathcal{M}$. In order to understand the way in which flip curves end on fold bifurcation curves in the parameter space we need to lift the flips to $\mathcal{M}_0$. Whereas in $\mathcal{M}$ a lift of a flip curve can only meet fold curves at its end points, in parameter space a flip curve can meet a fold bifurcation curve at other points (see e.g. Fig. S10).

If $\theta \in \Delta$ is a flip point then we associate to it two points $\mathbf{x} = \mathbf{x}(\theta) = (x, \theta) \in \mathcal{M}_0$ where x is either the target saddle x_T or the source saddle x_S. Thus a flip curve $\theta = \varphi(t)$, $0 \le t \le 1$, in Δ can be lifted to two smooth curves $\mathbf{x} = \Phi_T(t)$ and $\mathbf{x} = \Phi_S(t)$ in $\mathcal{M}_0$ that we respectively call *the target flip curve* and *source flip curve*.

If such a flip curve in $\mathcal{M}_0$ meets a fold curve in $\mathcal{M}_0$ it involves a fold in which the target or source saddle is destroyed. It follows that a flip curve in $\mathcal{M}_0$ only meets fold curves at its end points. As we will see this is different from flip curves in Δ which can cross fold bifurcation curves. We call a flip curve a target-source one if one end point is a target one and the other a source one. Source-source and target-target curves are possible but here we are only interested in target-source ones

If Γ is a lift to $\mathcal{M}_0$ of a closed curve γ in Δ then there is a 1-1 correspondence of points where they meet target flip curves and the intersections are ordered identically as in γ. Therefore, if one defines the flip index of such a closed curve Γ in $\mathcal{M}_0$ analogously to that of γ but only using the target flip curves in $\mathcal{M}_0$, then the flip indices of Γ and γ are equal.

Of course, instead of using target flip curves one could use source flip curves.

Now suppose that the closed smooth curve Γ' is obtained from Γ by a smooth homotopy and that both are transverse to the flip curves. Assume also that the homotopy does not cross any fold curves.

Proposition 12. *The reduced products* $(r_{\sigma(1)}r_{\sigma(2)}r_{\sigma(3)})^k$ *obtained from* Γ *and* Γ' *are the same.*

Proof. The homotopy Γ_t can be chosen so that the curve Γ_t is always transversal to the flip curves except at a finite number of t and at these it touches a single flip curve quadratically. The only changes in the sequence of flips occur at such t but then this just adds or removes a term of the form $r_i^{-1}r_i$ and therefore does not change the reduced form. □

Consider a closed curve Γ in $\mathcal{M}$ that contains a fold circle C in its interior. Suppose, moreover, that C is the only fold circle contained in the interior of Γ' except possibly for fold circles contained in the interior of C. We call such a curve Γ a *primary flip container* for C.

Proposition 13. *The fold circle* C *is Möbius if and only if there is a primary flip container* Γ *for* C *for which the flip index has* k *odd.*

Proof. Let N be a tubular neighbourhood of a fold curve and r be the associated retraction. One can use a homotopy to move Γ into $N \setminus C$ so that the new curve Γ' has degree 1 with respect to r. Moreover, by Prop. 12, Γ' has k odd if and only if Γ does.

If N is sufficiently small, C is Möbius $\iff$ its cusp bundle is a Möbius band $\iff$ $E^u_{\Gamma'}$ is a Möbius band $\iff$ k is odd. □

Theorem 5. *Suppose that* Γ *is a smooth simple closed curve in* $\mathcal{M}$ *consisting of index 1 saddles. If its flip index is odd then in the generic situation,* Γ *contains an odd number of Möbius fold circles in its interior. Moreover, if* C *is one of these Möbius fold circles one can find a primary flip container* Γ' *for* C *for which the flip index has* k *odd.*

Proof. One uses a construction as in Appendix E to show that if Γ is a simple closed curve in $\mathcal{M}$ then it contains at least one fold circle and that Γ can be modified so that it only contains any one of these that is Möbius. One firstly removes the fold circles with k even and then pairs of fold circles with k odd. Having modified Γ in this way one can use a homotopy to move it arbitrarily close to C and use Prop. 12. □

Corollary 3. *Under the CEU boundary behaviour assumption,* Δ *contains a unique Möbius fold circle.*

Proof. By Cor. 2 the lift Γ to $\mathcal{M}_0$ of any closed curve in Δ close to $\partial\Delta$ has k odd. Thus by Theorem 5 there is a Möbius fold circle C in the interior of Γ and a primary flip container Γ' for C for which the flip index has k odd. This means that for each $X \in \{A, B, C\}$ there is a flip curve ℓ'_X connecting the boundary component ℓ_X to Γ'. If C' were another Möbius fold circle in the interior of Γ it would also have a primary flip container Γ'' with similar connections ℓ''_X to ℓ_X. Since ℓ'_X and ℓ''_X cannot meet as they are flip curves, this is impossible. Thus C is unique. □

7. Decision structures

We identify a cell state with an attractor in the dynamical system. We say that a cell takes a decision when it changes state and transitions to another attractor. This transition happens when the cell crosses an index 1 saddle and follows the corresponding unstable manifold towards another attractor. Therefore, we identify a *decision* with an index 1 saddle and its unstable manifold, which connects two attractors: the two options for the decision.

The complete dynamical system can be represented by a DAG as explained in **I**. Since we want to focus only on the decisions, we will simplify the DAG in order to retain only the information on the possible decisions as per our definition above (that is, attractors and index 1 saddles).

Given a DAG we define the *decision graph* (see Fig. S12) as the undirected graph with as many nodes as attractors in the dynamical system and an edge connecting two nodes (or a node to itself) if there is a saddle whose unstable manifold connects the corresponding two attractors (or the attractor to itself). The loops in this graph correspond to index 2 saddles in the DAG (in the dynamical system).

If the edges in the decision graph define a loop, then there is an index two saddle in the dynamical system that connects to the index 1 saddles that define it. This a consequence of the Morse-Smale inequalities for the n-sphere. A compact dynamical system (with a repeller at infinity) needs to satisfy $M - s + m \geq 1$ where M is the number of index 2 saddles, s is the number of index 1 saddles and m is the number of attractors. If a dynamical system defines a loop in the decision graph, then $s = m$ and therefore $M \geq 1$. Hence,there is an index two saddle and in particular, if the system is planar, there is a repeller that connects to those saddles. We mark with a triangle the loops in the graph to emphasize the existence of such a higher index rest point.

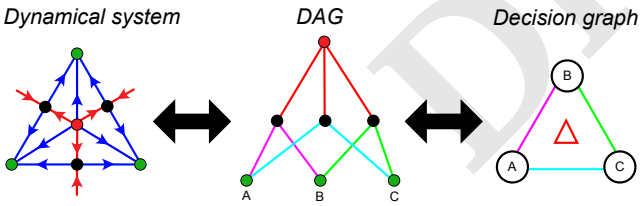

Fig. S12. Example of the correspondence between Dynamical systems, DAGs and decision graphs.

The decision graph may not be a simple graph, that is, it may have self-edges and parallel edges. We can remove the self-edges and keep only one edge from a set of parallel edges (see Fig. S13) and obtain the simple graph associated to a decision graph. An edge connecting a node to itself does not define a proper decision as we defined it since there is no change of states in such transition. Several parallel edges are defining the same decision, so they are redundant in this context.

We call a *decision structure* a simple decision graph. Its nodes correspond to attractors, the edges to unstable manifolds connecting them, and the loops correspond to index 2 saddles in the dynamical system. It encodes the essential information regarding the decision making process. Note that we will not specify the correspondence between attractors and

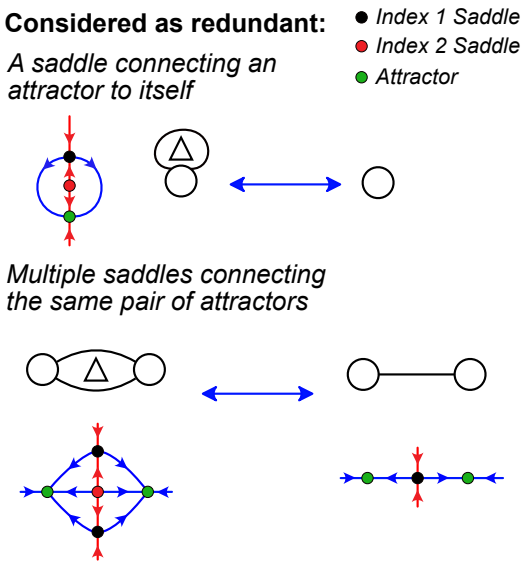

Fig. S13. Types of edges modified when computing a decision structure from a decision graph or DAG.

nodes, hence the same decision structure corresponds to any dynamical system with three attractors and two saddles irrespective of the particular central attractor. Any decision graph can be reduced to a unique decision structure graph as explained above. The possible decision structures given a number of attractors are in one-to-one correspondence with the connected simple graphs with that number of nodes (see Fig. S14). Decision structures define equivalence classes for decision graphs and they are the simplest representatives of the different classes.

The different decision structures correspond to a dynamical system structure that can correspond to several potential functions. The decision graph is independent of the specific saddle hierarchy in any possible potential structure associated with it. Note that as shown in (2) we can find a potential function corresponding to any decision structure such that all saddles have the same height (first column in example potentials). Figure S15 shows examples of dynamical structures and potentials corresponding to the decision structures with 2, 3 or 4 attractors.

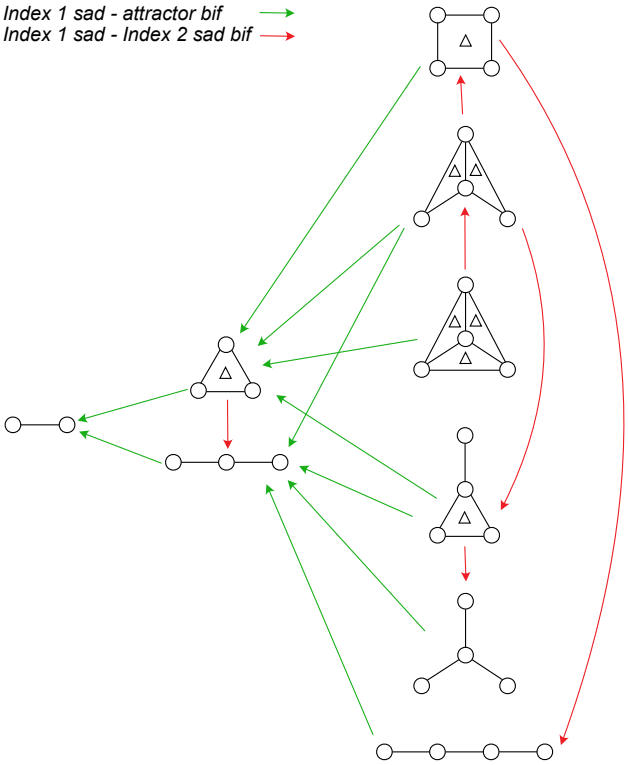

Fig. S14. Decision structures with 2, 3 or 4 nodes. The possible decision structures with a given number of attractors are in one-to-one correspondence with the connected simple graphs with that number of nodes.

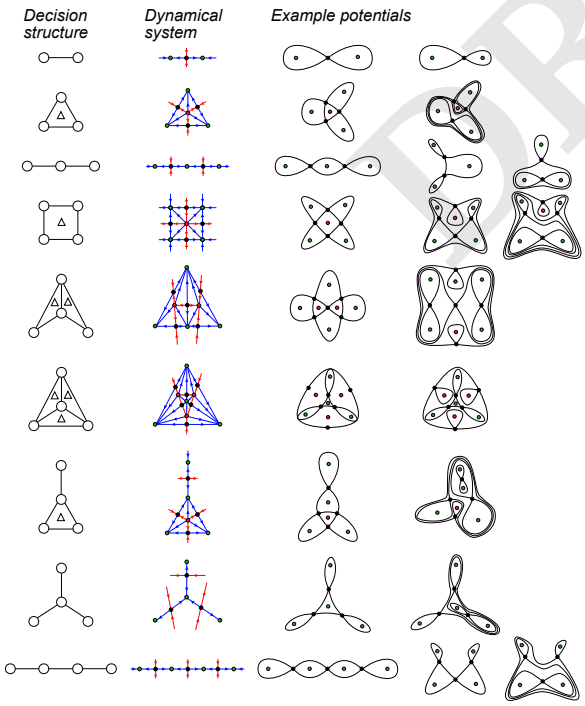

Fig. S15. Dynamical structure and potential functions examples for the decision structures with 2, 3 or 4 nodes. Legend as in Figure S13.

Appendices

A. Existence of decision regions R

This result relies on some results in Smale's proof of the higher dimensional Poincaré conjecture (11) and his h-cobordism theory (12) as expounded in Milnor (13).

It will be important that for the studied vectorfields X there is a region B with spherical boundary ∂B such that the X is transversal to ∂B and all trajectories cross ∂B into B.

The following lemma that is taken from (14) will be particularly useful. In it we are particularly interested in controlling the changes in the connection between the index 1 saddles σ_i, $i = 1, \dots, M$ and the attractors α_j, $j = 1, \dots, m$. Consider an index 1 saddle $p = \sigma_i$ with unstable manifold $W^u(p)$. Then $W^u(p) \setminus p$ has two components. Let γ be one of these, and assume γ is asymptotic to the attractor α_j. We call such curves *connecting trajectories* of σ_i to α_j. The set of all such pairs (i, j) is denoted by $\mathcal{C}_X$ and the corresponding connecting trajectory is denoted by $\gamma_{i,j}$.

Lemma 5. *Suppose that X is a gradient-like MS vectorfield with attracting region B as above and that we are given a small neighbourhood U_k of each rest point β_k and a small neighbourhood $U_{i,j}$ of $\gamma_{i,j}$ for all $(i, j) \in \mathcal{C}_X$. Then for any $\varepsilon > 0$ one can find smoothly varying MS vectorfields X_t, $0 < t < 1$ with $X_0 = X$ such that (i) the X_t all have the same rest points and they all agree outside the U_k for all k; (ii) for some $0 < t_0 < 1$, X_0 only differs from X_{t_0} inside the U_i and this is by less than ε in the C^1 topology; (iii) the connections $(i, j) \in \mathcal{C}_{X_t}$ do not vary with t and the connecting trajectories $\gamma_{i,j}$ are inside $U_{i,j}$ for all t; and (iv) X_1 is a gradient vector field with a smooth potential.*

This lemma allows us to modify a gradient-like MS X in a controlled way in small neighbourhoods of each rest point so as to produce a gradient vectorfield, at the same time controlling how the unstable manifolds of the index 1 saddles change. If f is a smooth Liapunov function for X, then one can do the modification so that X_1 is the gradient flow for f with respect to some Riemannian metric g.

Proof. This is Lemma 2 of (14). The fact that the X_t all agree outside the neighbourhood U_i is not stated in the lemma but is clear from the proof.

To see why the results about connectors are true, consider the process used to modify the dynamics at the rest point p in the last paragraph of the proof of Lemma 2 in (14). The vectorfields ξ_t constructed there all have the same stable manifold inside the neighbourhood $\varphi^{-1}U_2$ used there and they are independent of t outside $\varphi^{-1}U_2$. This is because (in the notation of the proof in (14)) in U_2, $\varphi_*^{-1}\xi_t$ is a linear combination of $\varphi_*^{-1}X_1$ and X_t both of which are tangent to the curve $x = 0$ in the coordinates (x, y) used there. As a consequence the connecting trajectory is independent of t. Therefore, the only perturbations to it occur when (in the notation of (14)) the vectorfield X_1 is modified so that it is equal to its linear part near p (an ε-small amount in the C^1-topology) and inside the region when the corresponding attractor is modified. Thus we deduce that the constructed family of vectorfields has the required property. □

Proposition 14. *Suppose that X is a gradient-like MS flow on $\mathbb{R}^n$ with an attractor region B as above with a smooth spherical boundary on which X is inward transverse. There is an open subset R in phase space with smooth boundary ∂R with the following properties (i) the flow is inward transverse on ∂R which is a sphere; (ii) R contains all the attractors of the flow and no rest points of index > 1; (iii) the stable manifolds of the index 1 saddles in R intersect ∂R in disjoint spheres of dimension $n - 2$. These index 1 saddles escape to two distinct attractors contained in distinct connected components of $R \setminus W^s$ where W^s is the union of the stable manifolds of the index 1 saddles in R.*

Proof. Denote the M saddles and m attractors of X by σ_i and α_j as above.

This step is only necessary if the number M of index 1 saddles is greater than m. Fix such an index 1 saddle s of X and let Σ be a set of $M - m + 1$ saddles that does not contain s. By (15) we can find a Liapunov smooth function L_Σ for X that takes the value 0 at attractors, 1 at the saddles in Σ and $1/2$ at all the saddles not in Σ. Let R_Σ denote the region in phase space given by $L_\Sigma < \eta$ where $1/2 < \eta < 1$ is a regular value of L_Σ. Then R_Σ contains all the attractors and the $m - 1$ index 1 saddles not in Σ together with their unstable manifolds. Moreover, X is transverse to the smooth codimension 1 submanifold ∂R_Σ. Let $R_{s,\Sigma}$ be the connected component of the intersection of the R_Σ for which Σ does not contains s. This is open and contains s and its unstable manifold.

We use Lemma 5 to modify our vectorfield X to obtain the vectorfields X_t given by Lemma 5. For the index 1 saddles σ_i we choose the $U_{i,j}$, $(i, j) \in \mathcal{C}_X$, so that they are contained in R_{σ_i} and so that $U_i \subset U_{i,j}$ and $U_j \subset U_{i,j}$ where U_k is the modification region of the saddle σ_i and the attractor α_j respectively. This ensures that the modifications of the saddle σ_i and the attractor α_j do not affect ∂R_Σ for all Σ not containing σ_i. We also want to ensure that the modification of the rest points do not change the vectorfields near any of the submanifolds R_Σ. So we choose the $U_{i,j}$ so that they meet none of these.

Then X_1 is a MS gradient flow with the same rest points as X and with the same connections between index 1 saddles and attractors as X all of which are held in a $U_{i,j}$ for some $(i, j) \in \mathcal{C}$.

Choose a small n-disk D_j around each attractor α_j with boundary $V_j = \partial D_j$ a smooth $n-1$ sphere so that the flow is transverse on V_j towards α_j and so that there are no other rest points in D_j. If the U_j of Lemma 5 were chosen sufficiently small we can assume that the closure of U_j is contained in V_j. Then since X and X_1 agree outside the U_j they are both inward transverse on the boundary of the V_j.

Let $V' = \partial B$, the flows of X and X_1 are also inward transverse on this since they agree there. Let $W = B \setminus D_0$. Then W has boundary $V_0 \cup V'$ and in the terminology of (13) (W, V_0, V') is a cobordism with trivial relative (singular) homology $H_*(W, V_0) = H_*(W, V') = 0$.

Now we consider the flow of the gradient system X_1. Using Theorem 8.1 of (13) and its proof we deduce that for each of the attractors α_j, $j = 1, \dots, m$, there is an index 1 saddle $s_j = \sigma_{i(j)}$ such that the unstable manifold of the saddle intersects V_j.

Since the flow is inward towards the attractor on each V_j this intersection point is unique. Let γ denote the part of the unstable manifold between the saddle s_j and α_j. We can then use Morse's cancellation lemma (Theorem 5.4 of (13))

to modify X_1 in an arbitrary small neighbourhood W_j of γ contained in $U_{i(j),j}$ to remove this attractor-saddle pair so that (i) the modified flow X_2 has no rest points in W_j and every trajectory that enters W_j also leaves it, and (ii) so that the modified flow X_2 is a gradient-like MS flow that equals X_1 outside W_j. As noted in (13) there is no restriction on dimensionality for connections between index 1 saddles and attractors. This process essentially involves a fold bifurcation.

We firstly do this for $j = m$. As a result we end up with a MS system with one less saddle-attractor pair that equals the original system X_1 outside $U_{i(j),j}$. Applying Theorem 8.1 of (13) again we have that for each of the attractors α_j, $j = 1, \dots, m-1$ there is an index 1 saddle such that the unstable manifold of the saddle intersects V_j. Now we can use Morse's cancellation lemma again and continue inductively until all the attractors $\alpha_1, \dots \alpha_m$ are removed. We end up with the single attractor α_0 remaining and this is inside the ball D_0.

If this process does not delete all the index 1 saddles (i.e. $M > m-1$) then proceed as follows. Let Σ denote the set of index 1 saddles that have not been deleted and let R be R_Σ. Since all modifications to bifurcate away the attractors took place inside sets $U_{i,j}$ where the saddle was not in Σ, X_1 and X_2 agree on a neighbourhood of ∂R_Σ. It follows from Theorem 3.4 of (13) that the cobordism $(R \setminus D_0, \partial R, \partial D_0)$ is a product cobordism and therefore that ∂R and ∂D_0 are diffeomorphic. Consequently, ∂R is a smooth $(n-1)$-dimensional sphere.

Since all modifications to X to produce X_1 took place in the U_i, X and X_1 agree on a neighbourhood of ∂R and we have found an appropriate smooth sphere containing the appropriate rest points.

If $M = m-1$ we take a Liapunov function L for X that takes the value i at each rest point of index i and take for R the connected component of $L < \eta$ for $1 < \eta < 2$ a regular value of L and demand that the U_i and $U_{i,j}$ for $(i,j) \in \mathcal{C}$ have closures in R. Then we deduce that ∂R is a smooth sphere in a similar fashion.

In either case we obtain a smooth sphere ∂R on which the flow is inward transverse and which contains all the m attractors of the flow, $m-1$ index 1 saddles and no rest points of index > 1. We also obtain a Liapunov function L for X for which ∂R is a level manifold.

The stable manifolds of the index 1 saddles in R intersect ∂R transversally in spheres of dimension $n-2$ since in some neighbourhood of each index 1 saddle point p the level curve $L(x) = L(p) + \varepsilon$ intersects the stable manifold of p in an $n-2$ dimensional sphere S_ε when $\varepsilon > 0$ is small. As $t \to -\infty$ every trajectory on S_ε leaves R and hence intersects ∂R transversally (since ∂R a level surface of L) at a single point. The points on the intersection of the unstable manifold with ∂R are connected to those of S_ε by the trajectories of X and this provides a diffeomorphism between them. □

A. Four attractor configurations. When there are four attractors there are two possible configurations. There will be three cancelling saddles and the stable manifolds of these will intersect the $(n-1)$-sphere ∂R in three $(n-2)$-spheres, S_1, S_2 and S_3. Each of the S_i will separate ∂R and clearly for two of them, say S_1 and S_2, ∂R is separated into two components one of which D_i, $i = 1, 2$, does not intersect S_3. In this case, D_i is a $(n-1)$-disk and is contained in the basin of one of the attractors A_i with $A_1 \neq A_2$. The third $(n-2)$-sphere S_3 may or may not have this property.

If it does, then there is a $(n-1)$-disk D_3 with similar properties. In this case the saddle s_i in the stable manifold W^s_i corresponding to S_i, $i = 1, 2, 3$ does not escape to A_j for $j = 1, 2, 3, j \neq i$. Since every saddle escapes to two different attractors, every saddle s_i must escape to the fourth attractor A_4. Thus the configuration in phase space is that there is an attractor A such that each of the three saddles escapes to A and also to one other of the three other attractors. We call this configuration *EU-like* since it is what occurs in the compact elliptic umbilic.

In the other configuration one of the components of $\partial R \setminus S_3$ contains S_1 and the other S_2. Let Q_i denote the component of $R \setminus W^s_3$ containing S_i, $i = 1, 2$. Then Q_i contains the unique saddle s_i in W^s_i, the attractor A_i and one other attractor B_i that s_i escapes to. Since $B_i \in Q_i$, $B_1 \neq B_2$. It follows that the saddle s_3 in W^s_3 must escape to the attractors B_1 and B_2. Thus in this configuration the saddles are ordered so that $A_1 \prec s_1 \succ B_1 \prec s_3 \succ B_2 \prec s_2 \succ A_2$. We call this the *linear configuration*.

B. No folds at cuspoidal joining attractors

Lemma 6. *Consider a 3-attractor system as in Sect. A. If the connector is not smooth then a fold bifurcation of the central attractor is impossible.*

Proof. We need to check that there cannot be a fold at a cuspoidal join. If there is a fold there it is at a point θ on a fold bifurcation curve B_C. In the generic case we can move θ an arbitrary small amount in B_C to ensure that the eigenvalues at the fold point are non-resonant. if the move is small enough the connection will still be non-smooth and cuspoidal.

Note that this new fold point in n dimensions for $r > 2$ one can find C^r coordinates $(x, y) \in \mathbb{R} \times \mathbb{R}^{n-1}$ in which the differential equation takes the form of equation (5) ((3) Sect. 5.7). Without loss of generality we can assume that this bifurcation takes place at $\theta = 0$. Consider the case $+x^2$. Then for $\theta > 0$ small there are two saddles s_1 and s_2 only one of which (say s_1) is involved in the bifurcation. The unstable manifold of these are asymptotic to the attractor taking part in the fold bifurcation where they meet cuspoidally. Because they meet in this way we must have that for points starting on the unstable manifold of s_2, $\dot{x}(t) < 0$ as they converge onto the attractor. However, from equation (5) $\dot{x}(t) \geq 0$ in a neighbourhood of $x = 0, y = 0$ which gives a contradiction. □

C. Proof that the connected components of $\mathcal{M}$ are disks

A. The interior of a fold circle is a disk. If $\mathbf{x}_i = (x_i, \theta_i)$, $i = 1, 2$ are in $\mathcal{M}$ write $\mathbf{x}_1 \sim \mathbf{x}_2$ if there exists a connected neighbourhood U in $\mathcal{M}$ containing both points and not intersecting any fold curves. This is clearly an equivalence relation and the equivalence class of a point $\mathbf{x} \in \mathcal{M}$, which we denote by $[\mathbf{x}]$, is connected.

Take a small tubular neighbourhood N of C and consider the two components of $N \setminus C$. Any two points in one of these are equivalent under $\sim$ and not equivalent if they are in different components.

If one of the components N^{ext} contains in its closure a boundary point of $\mathcal{M}$ we say C that is at *depth* 0. Then, if N^{int} is the other we denote by M_C and V_C the equivalence classes of $\mathbf{x} \in N^{\text{ext}}$ and $\mathbf{x} \in N^{\text{int}}$. We are thinking of V_C as being part of the inside of C.

Now for an arbitrary fold circle C we define depth, M_C and V_C by induction: C has depth $n > 0$ if for some tubular neighbourhood N the equivalence class of one of the components of $N \setminus C$ is $V_{C'}$ for a fold curve C' of depth $n-1$. Then that equivalence class is denoted M_C and V_C is the other equivalence class.

Proposition 15. *Each fold curve C separates $\mathcal{M}$ into two components. One of them I_C is a disk with boundary C and is such that $\chi|I_C$ is injective on a neighbourhood of C in I_C. The other has the property that it contains in its closure either boundary points of $\mathcal{M}$ or singularities of χ which are not in C.*

Proof. We prove this by induction on height.

Suppose C has height 0 by which we mean that V_C contains no other fold points. Then $\chi : V_C \to U_C = \chi(V_C)$ is injective. Consequently, by invariance of domain $\chi|V_C$ is a homeomorphism between V_C and U_C and $\chi(C)$ separates $\mathbb{R}^2$ into two components only one of which is bounded. It follows that this is U_C and that it and V_C are disks.

Now suppose the height is n. Then for each fold circle C' in the closure of V_C of height $n-1$, $I_{C'}$ is a disk with boundary C' and $\chi|I_{C'}$ is injective on a neighbourhood of C' in $I_{C'}$. Moreover, V_C is a surface with boundary C and the union of the C' in V_C of height $n-1$. Therefore, to obtain I_C one just glues the disks $I_{C'}$ into V_C to obtain a disk with boundary C. □

B. Proof of Prop. 1. Consider a connected component $\mathcal{M}_0$ and let $J(\mathbf{x})$ be the Jacobian of χ at $\mathbf{x}$ and let $\mathcal{M}_1$ denote the set of points $\mathbf{x} \in \mathcal{M}_0$ where $J > 0$. Since $J > 0$ on a neighbourhood of the boundary, it follows by Prop. 15 that, in the generic case, the sets where $J < 0$ are disks bounded by fold circles. Therefore, if $\mathcal{M}_0$ is not orientable $\mathcal{M}_1$ must contain a Möbius band. But that is impossible as then χ must have a singularity in $\mathcal{M}_1$ contradicting $J > 0$.

To show that $\mathcal{M}_0$ is a disk we must prove that $\mathcal{M}_1$ does not contain any handles. Then the result follows from the classification of surfaces (e.g. (16)).

Suppose that there is a handle. Then there is an embedding $f : S^0 \times D^2 \to \mathcal{M}_0$ such that the handle is given by using f to glue the cylinder $K = D^1 \times S^1$ into $\mathcal{M}_0 \setminus f(K)$. But then the induced orientation on K induces an orientation on $1 \times D^2$ that is opposite to that on $-1 \times D^2$. Hence the two circles bounding these have opposite orientations. It follows that $\chi|\mathcal{M}_0$ has singularities as otherwise it would map the handle to an annulus and induce opposite orientations on its inner and outer boundary circles. □

D. Bifurcation curves: Proof of Prop. 2

We use the fact that every connected component of $\mathcal{M}$ is diffeomorphic to a disk. One can prove the results of this section without this assumption using ideas such as those employed in Sect. A. From this assumption it follows that we can talk about the interior and exterior of a fold circle and we have that the restriction of χ to the interior of a fold circle is injective.

That B_C is smooth except at cusp points follows from the generic local structure of fold points as described above.

Suppose that B_C has a self-intersection. By genericity the intersection will be transverse. Then there are two points $\mathbf{x}_1, \mathbf{x}_2 \in C$ such that $\chi(\mathbf{x}_1) = \chi(\mathbf{x}_2)$ and that there is an open segment γ in C that has $\mathbf{x}_1$ and $\mathbf{x}_2$ as its end points such that $\chi|\gamma$ is an embedding. γ might contain cusp points. Let N be a small tubular neighbourhood of C and let N^{int} be the connected component of $N \setminus C$ contained in the interior of C. If N is small enough $\chi|N^{\text{int}}$ is injective. Because of the transversality of the intersection the thin ribbon $\chi(N^{\text{int}})$ in $\mathbb{R}^2$ has self-intersection and so there are distinct points in N^{int} with the same image under χ. This contradicts the injectivity of χ on N^{int}.

Now the result follows from the Jordan-Brouwer Separation Theorem which implies that $\mathbb{R}^2 \setminus B_C$ has exactly two components, one of which is bounded and the other not. □

E. Proof of Prop. 5

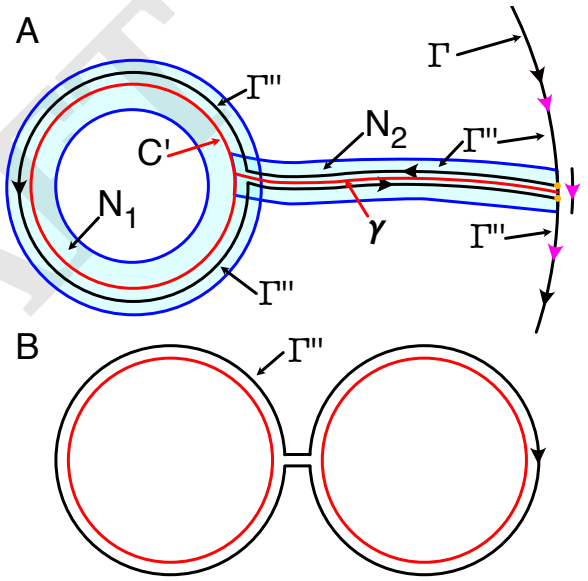

Fig. S16. (A) We connect C' (red) to Γ (black) and then take a small neighbourhood $N_1 \cup N_2$ as shown (light blue). Then we take the black curve in $N_1 \cup N_2$ as shown that joins the two orange points on Γ either side of γ. By following the black arrows instead of the pink ones we get a loop Γ''' that has an odd index as Γ (because the index round the new part is even) but now has C' in the exterior part. (B) How to move two odd index fold circles to the exterior.

Proof. Let $\mathcal{G}$ be the interior of Γ. Let C' be a fold circle in $\mathcal{G}$ that is not contained in any other fold circle and is such that $\mathcal{C}_{C'}$ is trivial. We firstly prove that we can find a simple closed curve whose interior contains exactly the fold circles that are in $\mathcal{G}$ except for C'.

Let $\mathcal{M}_0$ be the connected component of $\mathcal{M}$ that contains Γ and let γ in $\mathcal{M}_0$ be a curve that connects C' to Γ (see Fig. S16A). Since all fold points inside $\mathcal{G}$ must be on fold curves we can choose γ so that it intersects no other fold points. Also choose γ so that the endpoint on C' is not a cusp point. Let N_1 be a small annular tubular neighbourhood of C' and N_2 a small annular tubular neighbourhood of γ and let $N = (N_1 \cup N_2) \setminus (C' \cup \gamma)$. Choose a point in each of the components of $N \cap \Gamma$ and let Γ' denote the short part of Γ between them.

Then there is a curve Γ'' in N that connects these points. Let Γ''' be the closed curve obtained by combining $\Gamma \setminus \Gamma'$ with Γ''. Moreover, since N encloses a disk, Γ''' separates $\mathcal{M}$ into two components as required. But now C' is in the exterior component. Now $\Gamma' \cup \Gamma''$ is a closed curve for which the saddle bundle is trivial. Since $\Gamma''' = (\Gamma \setminus \Gamma') \cup \Gamma''$ it follows that if Γ' is short enough the saddle bundle of Γ''' is a Möbius band. Moreover, Γ''' separates $\mathcal{M}_0$ into two components and one of the components contains less fold circles with trivial saddle bundle than $\mathcal{G}$ did.

Repeating this process for all such fold circles we obtain a closed curve which must contain in its interior component a fold circle since it has a Möbius saddle bundle but which contains no non-Möbius fold circles at top level.

To see that one can also remove any even number of Möbius fold circles note that one can find a closed curve Γ'' around any two Möbius fold circles with the property that its bundle $E^c_{\Gamma''}$ is a cylinder (see Fig. S16B). Then one can proceed as above to use Γ'' to adjust Γ to obtain a curve with a Möbius saddle bundle whose interior component does not contain these two fold circles. □

Note that this proof also shows that any curve Γ_0 satisfying the conditions of the proposition contains an odd number of Möbius fold circles.

F. Justification of Condition (*) for Theorem 2

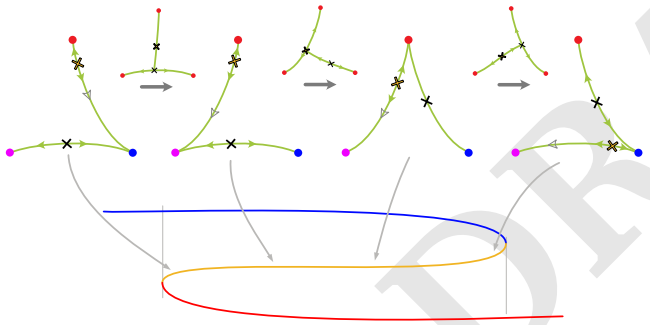

Fig. S17. This shows how over a 1-dimensional parameter space one can have a seemingly bistable Z shaped system which does not flip the orientation of the folds. This involves generic flip bifurcations and violates Condition (*) thus illustrating why bistability is not sufficient in Theorem 2. Note that the lines could cross depending on the projection considered.

Part II
Examples

1. Three state system has elliptic-umbillic parameter space

For three cells or genes $i, j = 1..3$ define mutual repression among them by the rational functions

$$\dot{x}_i = \frac{2}{\prod_{j\neq i}(1+\frac{x_j^n}{k_{i,j}^n})} - x_i, \qquad [7]$$
$$k_{i,j} = 1 + c_i - c_j$$

with the Hill exponent $n = 4$ ($n = 2$ does not generate 7 restpoints at the symmetry point).

Each of the c_i favors x_i by dividing x_i by a number smaller than 1 and $x_{j\neq 1}$ by a number larger than 1. We confine ourselves to a two dimensional parameter space by imposing $\sum_i c_i = 0$ and then projecting onto two orthogonal directions such that permutation among the i corresponds to a rotation by $2\pi/3$. Rational functions are technically useful in this example since Mathematica routines are guaranteed to find all the rest points, and one can also include the zero Jacobian condition to find the fold lines. We believe the same phase diagram would emerge from Eq.11 for $N = 3$ but the root finding is more difficult with transcendental functions. We again emphasize that imposing the 3-fold symmetry simplifies the parameter search but the phase diagram is invariant in a neighborhood in the complete parameter space. One presumably would find the same phase diagram if the interactions were completely symmetric and the parameters controlled the degradation rates. With an exponent $n = 4$ the states are reasonably close to binary, i.e., at the corners A in Fig.6b the stable point is at $x_i = (2.00, 0.03, 0.03)$ + permu, while along the inner black curve the stable points are $x_i \sim (2.00, 0.2, 0.2)$ + permu and the saddle point is at $(1.00, 1.00, 0.44)$

2. A flow defines a potential

We use the flows which are later used for the activator-inhibitor pair showing Turing patterns.

$$\dot{a} = \frac{a^2}{(1+a^2)(1+h)} - \nu a + D_a\partial_x^2 a, \qquad [8]$$

$$\dot{h} = \rho\frac{a^2}{1+a^2} - h + D_h\partial_x^2 h. \qquad [9]$$

Parameter values, which are also used later, are $\nu = 0.2$ and $\rho = 5$. There are two stable fixed points on either side of the inset. The potential is defined as $\int_0^\infty(\dot{a}^2+\dot{h}^2)dt$ in accordance with the one dimensional definition i.e. it is the integral of the of the vector field along the trajectory. To define the metric, we need to project the flows given by the potential onto the actual flow. This can be done with a projection operator, which, however is not a proper metric because it has determinant zero. Let $\vec{a} = (\dot{a}, \dot{h})$ represent the vector flows. Let $\vec{u}$ be the flows which derive from the derivative of the constructed potential. Let $\vec{u}_P$ be the vector perpendicular to $\vec{u}$ with the same magnitude. Now define the inverse metric as the sum of two projection operators

$$g = \frac{1}{(\vec{u}.\vec{a})}\left(\vec{a}\vec{a}^T + \vec{u}_P\vec{u}_P^T\right) \qquad [10]$$

Evidently, when operating on $\vec{u}$, this gives $\vec{a}$. Though these two independently have determinant zero, their sum can be shown to have positive determinant as long as the angle between them is less than $\pi/2$ i.e. $\vec{u}.\vec{a} > 0$. Other linear combinations of these two operators are possible reflecting the redundancy in the definition of the metric.

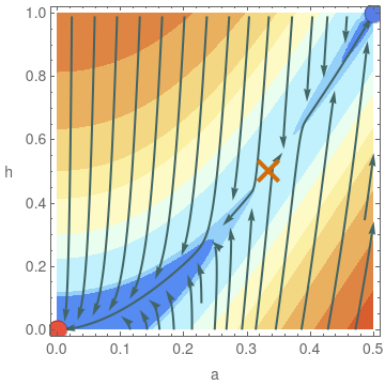

Fig. S18. Contours of the potential defined in the text are shown going from low (blue) to high (red). The flow defined by the potential multiplied by the metric is shown in green as streamlines.

Near the fixed points, this construction chooses the potential to be the symmetric part of the Jacobian. In two dimensions, it can be shown that a matrix cannot be written as the product of two symmetric matrices where the second matrix is the symmetric part of the matrix being represented. Therefore, the potential and the metric need to be defined independently near the fixed points. Near the fixed point, one can approximate the dynamics by its linear part. The Jacobian matrix is not symmetric but can be written as the product of two symmetric matrices, one of which is positive definite. Hence, we can approximate the metric as constant and the potential as parabolic near the fixed points and glue this together with the global construction above. The gluing is done with a sigmoidal function $1/(1+\exp(((a-a_0)^2+(h-h_0)^2-m)/c)$. a_0 and h_0 are just the value at the fixed points whereas m and c are chosen to be 0.001 and 0.00001 in this example but can be chosen appropriately.

3. Patterning by lateral inhibition

The model in question describes a field of cells, subject to mutual inhibition via the Notch-Delta pathway (17). Each cell is described by a single variable a between $0-1$ and when a cell is ON it forces its neighbors to be OFF. The biological data consists of the time course of expression beginning with all cells off and ending when a sparse random subset are on. An elegant minimal model describing this situation reads:

$$\tau\dot{a}_i = \sigma(a_i - h_i) - a_i,$$
$$\sigma(a) = (\tanh(4a)+1)/2,$$
$$h_i = \sum_{j\neq i} K_{i,j}d(a_j), \qquad [11]$$
$$d(a) = 0.05a + \frac{2.85a^4}{1+2a^2}$$

where $K_{i,j}$ is a Gaussian function of the spacing between cells i, j and $d(a)$ maps the interval $[0, 1]$ onto itself. The system

is initialized with all $a_i \sim 0$ and positive. In the terminal configuration only a sparse set of the $a_i \sim 1$ with a spacing set by the $K_{i,j}$ and the rest are zero. The mean field inhibition h_i from the neighbors of i slides the sigmoid function σ along the axis giving rise to two saddle-node bifurcations that destabilize the upper and lower fixed points.

The behavior of the system is most easily understood by solving it in one dimension for cells uniformly positioned around a circle Fig. S19. We have omitted additive Gaussian noise to better understand the underlying dynamics.

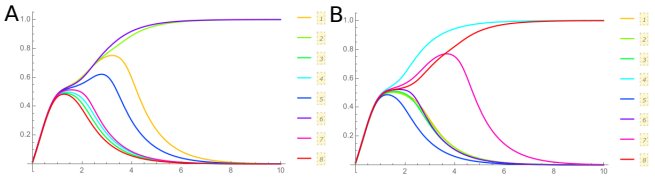

Fig. S19. Solution $a_i(t)$ for the model of Eq.11 for 8 cells evenly spaced around a circle with slightly different initial conditions shown in (A) and (B). The range of the inhibitory interactions is adjusted to allow only two cells to be on in the final state, which are always on opposite sides of the circle.

Note the cells all rise together and then when $a \sim 0.5$ cells peal off. Most go to zero but a few persist to larger a when they too peal off leaving the two survivors. The intuitive reason for this is already apparent when observing the flow field with just two cells Fig. S20.

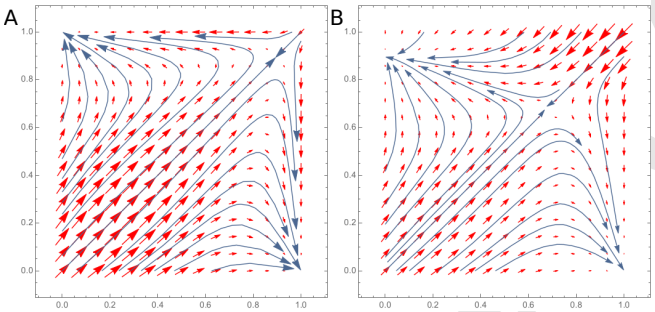

Fig. S20. Vector field and stream lines from Eq.11 for (A) two cells and (B) three cells with a_1 on the x-axis and $a_2 \equiv a_3$

In fact for any number of particles there is a saddle point along the diagonal in a space at $a \approx 0.89$ for two cells which decreases down to $a \approx 0.51$ (for $K_{0,1} \approx 0.841$) when the number of cells N exceeds the range of interactions. There is one strongly stable eigenvalue along the diagonal and $\mathcal{O}(N)$ unstable directions. The pattern repeats as suggested in Fig. S20B, namely for $N = 3$ there are secondary saddle points around $\vec{a} \approx (0, 0.89, 0.89)$ + permu with two stable and one unstable directions. Thus the dynamics in Fig. S19 is qualitatively explained by a tree or star-burst of saddle points with an increasing number of stable directions.

Can we capture the essentials of this behavior in a potential model of the form of Eq.12 where both $K_{i,j}$ and $d(a)$ agree with Eq.11?

$$\begin{aligned} \dot{a}_i &= -g(a_i)\nabla_{a_i} F \\ F &= \sum_i s(a_i) + \frac{1}{2}\sum_{i\neq j} d(a_i) K_{i,j} d(a_j) \end{aligned} \qquad [12]$$

We first impose that the location of the critical point along the diagonal in a space agrees with Eq.11:

$$\begin{aligned} &s'(a) + d'(a)h(a) = 0 \Leftrightarrow \sigma(a - h(a)) = a \text{ where} \\ &h(a) \equiv \sum_j K_{0,j} d(a) = a - \frac{1}{8}\ln(\frac{a}{1-a}) \end{aligned} \qquad [13]$$

where the expression involving ln in Eq.13 is the inverse of σ in Eq.11. Thus we have an explicit expression for $s'(a)/d'(a)$ in terms of a at the critical point which falls in the range $0.51 - 0.89$ depending on N.

To make the Jacobians $J_{i,j} = \partial \dot{a}_i / \partial a_j$ agree compare the expressions in Eq.11 and Eq.12:

$$\begin{aligned} J_{i,j} =& \delta_{i,j}(\sigma'(a - h(a)) - 1) - (1 - \delta_{i,j})\sigma'(a - h(a))\partial h_i/\partial a_j \\ J_{i,j} =& -\delta_{i,j} g(a)(s''(a) + d''(a)h(a)) \\ & - (1 - \delta_{i,j}) g(a) d'(a) \partial h_i / \partial a_j \end{aligned} \qquad [14]$$

Note at the critical point the term involving the derivative of the inverse metric vanishes, and we can calculate $\sigma'(a - h(u)) = 8a(1-a)$. Thus the off diagonal terms are equivalent if $g(a)d'(a) = 8a(1-a)$, and it can be shown the diagonal ones follow, as we also checked numerically. Thus we have determined both $s'(a)$ and $g(a)$ in Eq.12 in terms of $d(a)$ and explicit functions of a.The vector field for N=2 and the dynamics for N=8 are shown in Fig. S21. The most obvious problem is that the potential model has vanishing velocity in the neighborhood of the origin since $g(a) \sim a$.

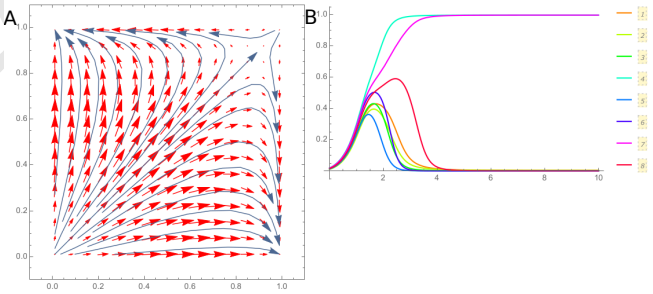

Fig. S21. The potential model from Eq.12 with a metric satisfying $g(a)d'(a) = 8a(1-a)$. (A) The vector field and streamlines (B) The dynamics. Note the dynamics around the origin are not correct as is clear in both (A) and (B).

The origin is a completely unstable critical point well removed from the saddle on the diagonal which is restricted to $a > 0.51$. So in particular we can define the metric for $a \geq 0.5$ as before, but modify the definition for $a < 0.5$ so that $\tau \dot{a} = \frac{1}{2}$ at $a = 0$ to agree with Eq.11. For instance the following choice illustrates the idea:

$$g(a) = 8a(1-a) - (1-2a)^4(4/\ln(a) + 8a(1-a))\eta(\frac{1}{2} - a) \qquad [15]$$

where expression involving the step function η is C^4 around $a = \frac{1}{2}$ ($\eta(x < 0) = 0$) and the $\ln(a)$ term subtracts the singularity in $s'(a)$ near the origin that's implicit in Eq.13. Its overall coefficient together with the singular expression for $h(a)$ in Eq.13, guarantees the desired value at $a = 0$

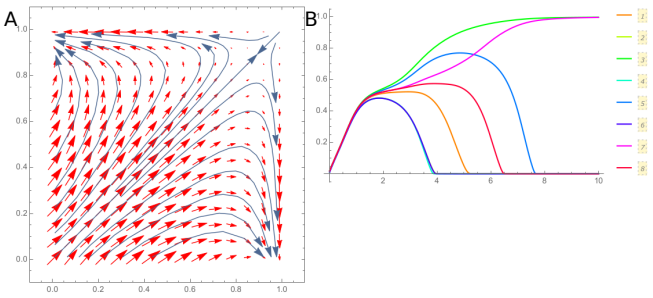

Fig. S22. The potential model from Eq.12 with the metric from Eq.15. (A) The vector field and stream lines. (B) The dynamics.

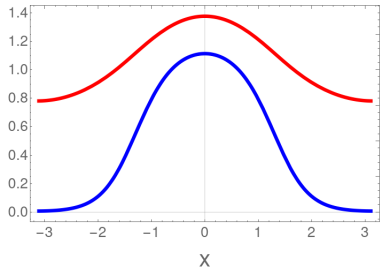

Fig. S23. The typical behavior of a (blue) and h (red) in the model. Parameter values are $\nu = 0.2$, $\rho = 5$, $D_a = 0.02$, $D_h = 2$.

Inspection of Fig. S22 reveals that the velocity field is nearly 2x too large around $\vec{a} \approx (\frac{1}{2}, \frac{1}{2})$ and that $\dot{a}_1$ is too large for $\vec{a} \approx (a_1 < 0.6, 1)$ which affects how the curves tend to 0 for times larger than two. This problem can also be fixed within the context of Eq.12 if we smoothly interpolate between two values of $s'(a)$ for $a \ll 1$ and $a \sim 1$ as in Eq.15, and make a consistent choice of the two free constants to get appropriate values of $\vec{a}$ around the origin and $(0, 1)$. The choices are now dependent on N and we will not go further in matching a potential model to Eq.11, since at this stage the agreement is better than the fit of Eq.11 to the corresponding data, which unfortunately for the system in question does not yet include quantitative time lapse data. With such data, one can hope to initialize the model specifically to each embryo and then follow the dynamics for some period of time and compare trajectories. We suggest that our potential and metric formulation will be a more principled way to fit dynamic data. Note that we got rather far with a diagonal metric.

4. The Turing Model in potential form

The model we use relies on local activation by an activator a and long range inhibition by an inhibitor h. The dynamical equations are

$$\dot{a} = \frac{a^2}{(1+a^2)(1+h)} - \nu a + D_a \partial_x^2 a, \qquad [16]$$

$$\dot{h} = \rho \frac{a^2}{1+a^2} - h + D_h \partial_x^2 h. \qquad [17]$$

We have modified the classic Gierer-Meinhardt form of the model (18) to remove the singularity at $h = 0$ and saturate the production of a. Parameters have been rescaled or set to 1 so that the behavior of the model depends only on two parameters ν and ρ along with the diffusion coefficients D_a and D_h. The typical behavior of the model is to produce a bump in a and h as shown in in Figure S23.

This matrix can not be written as the product of a metric and a potential without introducing k^2 into the metric. The expression for the Jacobian matrix at the homogenous fixed point is quite involved. The essence of the argument can be seen by taking the limit of small ν (i.e. dynamics of h being quicker than dynamics of a).

$$\begin{pmatrix} 2\nu^2 - D_a k^2 & -2\nu^2 \\ 1/(2\nu) & -1 - D_h k^2 \end{pmatrix} \qquad [18]$$

It is easy to show that the opposite signs on the off-diagonal elements implies an off-diagonal metric. One can therefore take the generic form of a metric inverse times a potential

$$g.V = \begin{pmatrix} g_{11} & g_{12} \\ g_{12} & g_{22} \end{pmatrix} \begin{pmatrix} V_{11} + U_{11}k^2 & V_{12} + U_{12}k^2 \\ V_{12} + U_{12}k^2 & V_{22} + U_{22}k^2 \end{pmatrix} \qquad [19]$$

Setting this expression to be equal to the Jacobian and solving the equations and matching the k^2 terms leads to a contradiction: there is no solution of these equations with the components of g independent of k^2 with $D_a \neq D_h$ and $g_{12} \neq 0$ which we require to fix the sign problem. Making the metric a function of k^2 is not disallowed but it is an overly cumbersome route which we do not pursue.

Another alternative is to saturate the production of h which gives $h = \rho \oint a^2/(1+a^2)$. Treating this equation as a constraint, one can write down a long range potential for a

$$V(a(x), h) = \int dx (\nu \frac{a(x)^2}{2} + H(a(x)) + \frac{D_a}{2}(\partial_x a(x))^2 - \frac{1}{2}a(x)^2 h + 2\rho a(x)^2 \oint dx' a(x')^2) + \nu \frac{h^2}{4} \qquad [20]$$

where $H(a) = \int da\, a^2/(1+a^2)$. What this does in essence is to put a long range anti-ferromagnetic potential to compensate for the h which is introduced into the potential with the wrong sign thus resolving the sign difficulty. This works in practice but is biologically implausible and does not get us much more than the original formulation of the problem.

Finally, the solution as discussed in the main text is to focus only on the unstable manifold where it is much easier to write down a potential formulation. We can do the analysis in a general form (19) writing the equations as

$$\dot{\vec{a}}(k) = M(k)\vec{a}(k) + \vec{f}(a(\vec{k})), \qquad [21]$$

where we have combined the variables into the vector $\vec{a} \equiv (a - a^*, h - h^*)$. We assume that we are working in coordinates around the homogeneous fixed point and the linearization is given by the matrix $M(k)$ which is dependent on the Fourier mode k. $\vec{f}$ contains all nonlinearities. We can find eigenvectors of the matrix $M(k)$ which we denote by $\vec{u}_k^j$ where the index on top denotes the eigenvector and k denotes the Fourier coefficient. Let us make the decomposition

$$\vec{a}(x) = \sum_j \sum_k \vec{z}_k^j e^{ikx}. \qquad [22]$$

$\vec{a}$ is real, so $\vec{z}_k^j = (\vec{z}_{-k}^j)^*$. Then, putting this form in the expression above, we get

$$\sum_{j,k} \dot{\vec{z}}_k^j e^{ikx} = M(k) \sum_{j,k} \vec{z}_k^j e^{ikx} + \vec{f}(a(\vec{k})). \qquad [23]$$

We have two eigenvectors for each value of k, one of which has a large and negative eigenvalue (corresponding to relaxation of h) and the other has an eigenvalue which is relatively small but either positive (if the mode is unstable) or negative (if the mode is stable). We can neglect the large and negative eigenvalue and convert the above vector equation into a scalar equation with the understanding that scalar z and scalar f refer to the dominant eigenvectors and the component of the nonlinearity in its direction respectively. Then we get the equation

$$\sum_k \dot{z}_k e^{ikx} = \sum_k \lambda_k z_k e^{ikx} + f(\sum_{k'} z_{k'} e^{ik'x}). \quad [24]$$

We can project out the coefficient k with the operator $1/(2\pi)\oint dx e^{-ikx}$ on both sides

$$\dot{z}_k = \lambda_k z_k + \frac{1}{2\pi}\oint dx e^{-ikx} f(\sum_{k'} z_{k'} e^{ik'x}). \quad [25]$$

Let the nonlinearity be of the form $f(x) = \tilde{f}_2 x^2/2 + \tilde{f}_3 x^3/3$ to cubic order. Further, using the fact that $\frac{1}{2\pi}\oint e^{-ikx}dx = \delta_k$, we get

$$\begin{aligned}\dot{z}_k =& \lambda_k z_k + \sum_{k',k''} \frac{\tilde{f}_2}{2} z_{k'} z_{k''} \delta_{k'+k''-k} \\ &+ \sum_{k',k'',k'''} \frac{\tilde{f}_3}{3} z_{k'} z_{k''} z_{k'''} \delta_{k'+k''+k'''-k}. \end{aligned} \quad [26]$$

Consider now a single mode $k = 1$ to be unstable with all other modes stable. Evidently there are no quadratic terms possible. A single cubic term is possible with $k' = 1, k'' = -1, k''' = 1$ and corresponding permutations. This gives the equation

$$\dot{z}_1 = \lambda_1 z_1 + \tilde{f}_3 z_1 |z_1|^2. \quad [27]$$

Now, suppose there are two unstable modes $k = 1, 2$. At cubic order it is now possible to have $k' = 1, k'' = -2, k''' = 2$ with permutations in the equation for z_1. There are twice as many permutations of this than with $k' = 1, k'' = -1, k''' = 1$. At the quadratic order, it is possible to have $k' = 2, k'' = -1$ in the equation for z_1. One can thus count all possibilities to get the equation

$$\dot{z}_1 = \lambda_1 z_1 + \tilde{f}_3 z_1(|z_1|^2 + 2|z_2|^2) + 2\tilde{f}_2 z_1^* z_2, \quad [28]$$

$$\dot{z}_2 = \lambda_2 z_2 + \tilde{f}_3 z_2(|z_2|^2 + 2|z_1|^2) + \tilde{f}_2 z_1^2. \quad [29]$$

Notice that this happens to be potential, not requiring a metric. We can rename parameters to put them in the same form as in the main text.

$$\begin{aligned}\dot{z}_1 &= \lambda_1 z_1 - \beta z_1(|z_1|^2 + 2|z_2|^2) - 2\gamma z_1^* z_2, \\ \dot{z}_2 &= \lambda_2 z_2 - \beta z_2(|z_2|^2 + 2|z_1|^2) - \gamma z_1^2. \end{aligned} \quad [30]$$

For our simulations, we start with initial conditions close to the homogenous state with a few Fourier modes added with small random coefficients. The $a(x,t)$ obtained for several different initial conditions is linearly projected on to $\exp(ix)$ and $\exp(2ix)$ to obtain our numerical approximation to z_1 and z_2. We then fit to the parameters λ_1, λ_2, β and γ which are independent of the initial conditions by fitting our projection to the dynamics in Equation 30. These parameters are not difficult to fit for they are directly related to the linear growth rate and the height of the final stable equilibrium. With these values of the parameters, we can then approximate the continuous dynamics as the real part of $z_1(t)\exp(ix) + z_2(t)\exp(2ix)$. Note that we are using a very simple linear projection on to Fourier modes as an approximation to the unstable manifold which is quite flat. For early times, our approximation suffices.

For mid to late times, the inaccuracies in our Fourier approximation have to do with the other modes, and higher order terms in Equation 30. There are several different possibilites to improve the fit. The final stable state is given by a Jacobi Elliptic function which also have a natural interpolation from trigonometric functions. It is possible to use some such interpolation but in practice, we find that an adequate solution is simply to saturate our sum of two modes with a simple sigmoidal function. The sigmoidal function is made a function of the real radial part of z_1 and z_2 which we denote by r_1 and r_2. It is defined as $\sigma(y, r_1, r_2) = \sigma_0(r_1, r_2)/(1 + \exp(-\Lambda(r_1, r_2)(y - y_0(r_1, r_2))) + 1)$ whose parameters Λ, σ_0 and y_0 are functions of r_1 and r_2 and are fit as explained below. Note that y_0 and σ_0 simply reflect the center and the height of the function. Hence our final approximation to the function $a(x)$ is $\sigma(\mathrm{Re}[z_1(t)\exp(ix) + z_2(t)\exp(2ix)])$ with parameters in σ a function of r_1 and r_2. The sigmoidal function ensures that the function remains positive and was empirically found to fit well. While the final form of the fit may look complicated to do exactly, it can be approximated in practice as follows.

First we take the linear form of the fit mentioned above for one initial condition which gives us an approximation $a_l(x,t) = \mathrm{Re}[z_1(t)\exp(ix) + z_2(t)\exp(2ix)]$. We then plot the actual value of the function $a(x,t)$ for the same initial condition as a function of $a_l(x,t)$ for a particular time point t. This data can be fit to a sigmoidal function $\sigma(y)$ as defined above. We can then find the parameters of the sigmoidal function as a function of t for discrete time points chosen appropriately. The parameters can then be plotted as a function of r_1 and r_2 by using our known form for $r_1(t)$ and $r_2(t)$ from our linear fit. We can then approximate the parameters as functions of r_1 and r_2. In practice we found that σ_0 could be taken to be constant. The parameter y_0 was either kept constant (done when fitting either 1 or 2 modes in one spatial dimension) or taken to linearly vary with radius (done when fitting 1 mode in 2 spatial dimensions). Finally the parameter Λ was also fit as a polynomial in r_1 and r_2. Details for the particular cases considered in the paper are given in the captions. We emphasize that our fits are only meant for the precision of a few percent which suffices for the biology under consideration. It is possible that other functional forms may work equally well or even better but in essence we require a mapping from the abstract coordinates z_1 and z_2 to the physical coordinates where the only time-dependence enters through z_1 and z_2 themselves. For the case of just one unstable mode, the discussion is entirely analogous to the one above. In summary, we have reduced a very high dimensional problem to a relatively simple fitting exercise in two dimensions involving only Fourier coefficients and a simple sigmoidal saturation function.

If a different set of Fourier modes are unstable, then one could work out the equations as above. Some couplings between the two modes depend on the specific wave number but

others are allowed for all pair of modes.

For the two spatial dimensional version of the problem, we use a slightly different set of equations

$$\dot{a} = \frac{a^2}{(1+Ka^2)(1+h)} - \nu a + D_a(\partial_x^2 a + \partial_y^2 a) - \alpha a s(y), \quad [31]$$

$$\dot{h} = \rho(x,y)a^2 - h + D_h(\partial_x^2 h + \partial_y^2 h) - \alpha h s(y) \quad [32]$$

equal diffusion coefficients in x and y. The system has length $L_x = 6\pi$ in the x direction and $L_y = 2\pi$ in the y direction both with the center at 0. There are periodic boundary conditions in the x and y directions albeit with a sink at the y boundaries to localize the blobs. Parameter values are $D_a = 0.032, D_h = 5, \nu = 0.2, K = 0.2, \alpha = 0.005, s(y) = \exp(-(L_y^2 - y^2))$ and $\rho(x,y) = 5 + \epsilon \sum_{n=5}^{7} a_n/n \cos(2\pi n x)\exp(-y^2)$ with $\epsilon = 0.1$ and a_n randomly chosen from a uniform distribution between -1 and 1. For the projection and fitting, we first average over the angular variable from the center of each blob. We then fit the function to a Fourier-Bessel series keeping only the first mode. The comparison between the fit and the actual dynamics is shown in Figure S25.

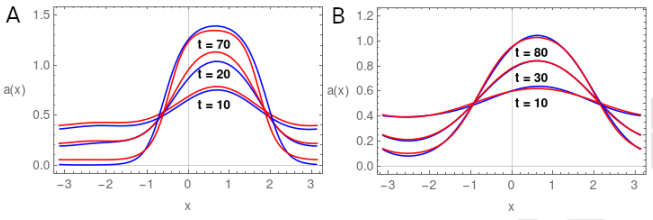

Fig. S24. A comparison between having one unstable mode or multiple unstable modes shown for random initial conditions. The simulated Turing system is shown in blue and the potential fit is shown in red. (A) There are three unstable modes in the actual system with $D_a = 0.01$ but a model with 2 unstable modes does a good job of fitting it. Other parameter values are $\nu = 0.2, \rho = 5, D_h = 20$. The parameters for the potential fit are $\alpha = 0.128, \alpha_2 = 0.0796, \gamma = 0.042, \beta = 0.125$. The saturation function is chosen to have $\sigma_0 =$ maximum of $a(x)$, $y_0 = \sigma_0/2$, $\Lambda(r_1, r_2) = 1$, $\sqrt{r_1^2 + r_2^2} <= 0.52$ and $\Lambda(r_1, r_2) = 1 + 4(\sqrt{r_1^2 + r_2^2} - 0.52)^2$ otherwise. (B) There is only one unstable mode with $D_a = 0.05$. The parameters for the potential fit are $\alpha_1 = 0.061$, $\beta = 0.155$. Here the saturation function has parameters values $\sigma_0 = 1.27$, $y_0 = 0.66$ and $\Lambda = 1.26 + 0.46 r_1$.

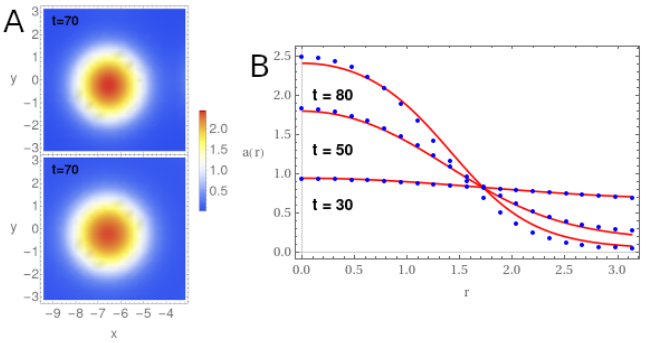

Fig. S25. A comparison is shown between the actual dynamics and the potential fit to the two dimensional Turing system. A) The first blob is shown on top at time $t = 70$ along with the comparison to the potential fit at the same time below it. B) The radial cross-section is shown at three different times. The actual data is shown at discrete time point in blue and the potential fit is shown in red. The function fit is of the form $0.8 + r_1(t)\sigma(1.5 J_0(r))$ where r is the radial coordinate in physical space, $r_1(t)$ is the abstract radius and σ is the saturation function as defined in the text. For the saturation function we use $y_0 = 1.26 + 0.5 r_1(t)$ and $\Lambda = 1 + 0.2 r_1(t)$.

5. Spreading the pattern by a wave

The model solved in Fig. 13 is defined by

$$\begin{aligned} u(a,b) &= \int_a (a(a-s)(a-p_1)) + p_2(b-a^2)^2/2 - p_3 ab, \\ U &= \sum_{i=1}^{N} u(a_i, b_i) + D_b \sum_{1}^{n+1} (b_i - b_{i-1})^2/2 \\ &\quad + \frac{p_4}{2} \sum_{i \neq j} d(a_i) K_{i,j} d(a_j), \\ K_{i,j} &= \exp(-(i-j)^2/(2\sigma^2)). \end{aligned} \quad [33]$$

where $s = 0.3, p_{1,2,3,4} = (2, 0.3, 0.2, 0.5), D_b = 4, \sigma^2 = 2$.

There are a total of 7 possible parameters modulo rescalings in the functional form of Eq.33 and it is fairly simple to adjust them. The origin is a stable point of $u(a,b)$ so we impose $sp_1p_2 - p_3^2 > 0$; σ controls the spacing between the cells with $a \sim 1$; $p_1 > 1$ increases the value of a in active cells and thus makes the potential in the symmetry broken state more negative (making p_3 larger has the same effect but is limited by the determinant condition. The p_2 parameter weights the induction of h by a. Too large a value damps b and prevents the wave from propagating, a low value of 0.05 activates extra sites. A larger value of s destroys the wave since cells do not get over the saddle to activate, too small a value and the sites well ahead of the furrow are susceptible to noise. The diffusion constant should be increased until the wave begins to propagate. The parameters shown in Fig. 13 were adjusted by inspection following these rules.

The flow around the saddle controls how the diffusive spreading of b interacts with the repulsion from the previous active cell to select the next active cell. The inset to the saddle can be substantially manipulated by a constant metric, Fig. S26. If we lower its intersection with the b axis for $a \sim 0$ less diffusive transport of b is required to trigger the ON state.

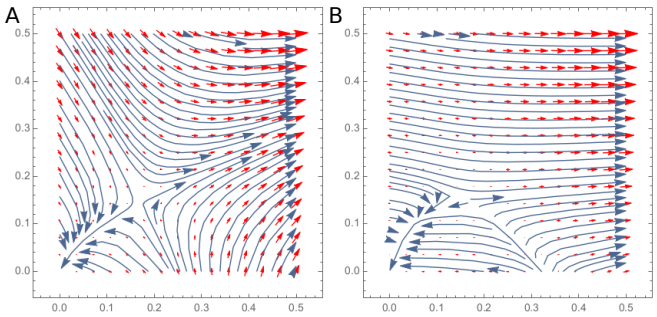

Fig. S26. The flow around the saddle point defined by $u(a,b)$ in Eq.33 for two values of the metric, $g=(1,1)$ in (A), and (10,1) in (B) for the same potential. The saddle point occurs at $a,b\sim(0.17,0.14)$ and the upper fixed point for u at $(2,7,9.2)$. In the coupled system $a,b\lessapprox(1.5,1)$ so the diffusion has a substantial impact on the realized levels.

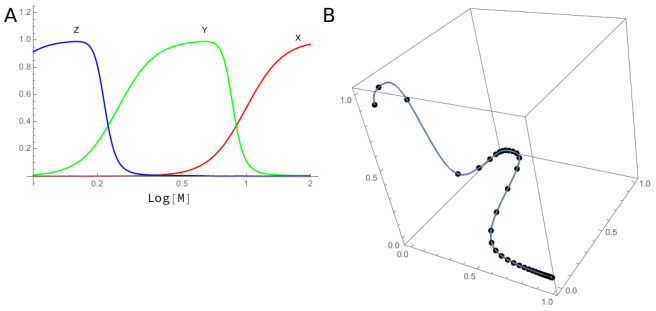

Fig. S27. Expression of three genes in an exponential morphogen gradient. (A) Expression as a function of position which is equivalent to log of the morphogen. (B) The same data as in (A) shown in three dimensions with the points uniformly spaced in morphogen level from 0.1 to 2 giving a sense of the 'speed' of the orbit in the configuration space.

6. Morphogen models

An embryo has to solve the problem of expressing the genes that define cellular fates in the correct position. A classic model for establishing a one dimensional pattern posits a static protein gradient that activates target genes as a function of concentration (aka "French flag") (20) . Within this simple paradigm are several different dynamical models as we now enumerate in the minimal case of three target genes, X,Y,Z that are positioned from high to low morphogen respectively.

The simplest model assumes the morphogen activates all three genes with different thresholds and in addition X inhibits Y,Z and Y inhibits Z i.e.,

$$\begin{aligned}\dot{x}&=\frac{M^n}{M^n+1}-x,\\ \dot{y}&=\frac{M^n}{M^n+\lambda^n}\frac{1}{1+(\frac{x}{\lambda})^n}-y,\\ \dot{z}&=\frac{M^n}{M^n+\lambda^{2n}}\frac{1}{(1+(\frac{x}{\lambda^2})^n)(1+(\frac{y}{\lambda})^n)}-z.\end{aligned}\qquad[34]$$

that we solve with $n=5$ and $\lambda=\frac{1}{4}$. The inhibition is necessary in Eq.34 so that the gene most sensitive to the morphogen is only expressed furthest away from the morphogen source. The scale factors are organized to make the domains of x,y,z occupy equal regions in $\log(M)$ or position assuming an exponential profile of morphogen as has been accurately shown for Bicoid in the fly blastoderm (21). Thus the scale at which x inhibits z is the square of the point at which x inhibits y. The result is shown in Fig.S27,

Dynamically the model in Fig.S27 is very boring, there is a single fixed point that is pushed around in three dimensions by the morphogen. New phenomena arise when the interactions among targets of the morphogen interact to generate bi or multi-stability. One such model for the mouse neural tube, (22), considers three genes patterned as a function of distance from a ventral signaling source. To fit their data which includes mutating the gene Y positioned at intermediate morphogen levels, they needed to include more cross repressions that resulted in bistability at intermediate morphogen levels. As a result they observed hysteresis, so that the boundaries in the final pattern depend on the temporal profile of the morphogen. Their model is,

$$\begin{aligned}\dot{x}&=\frac{5M}{M+1}\frac{1}{1+y+z}-x,\\ \dot{y}&=\frac{5M}{M+1}\frac{1}{1+x^5}-y,\\ \dot{z}&=\frac{3}{1+x^6+y^2}-z.\end{aligned}\qquad[35]$$

where x,y,z represent the genes Nkx2.2, Olig2, and Pax6.

Figure S28 represents the solution. The bistability is a function of the coupled system, hence in a plot of gene level vs morphogen the saddle node bifurcations appear at the same abscissa for all genes. From the plot we infer that large X strongly inhibits Y,Z and Y inhibits the other two. We can directly replot plot Fig.S28A in 3D as three curves parameterized by the morphogen. However it is more informative to represent the the two dimensional stable manifold of the saddle point, which divides the basins of the high and low X. Then as the morphogen changes, this surface and the two attracting fixed points move as does the state of the cell, which may transit between basins. An impression for the basins of attraction at fixed morphogen is conveyed by intersecting the two dimensional inset to the saddle with the plane defined by the saddle and two fixed points. It does not suffice to compute the stable and unstable manifold of the saddle restricted to this plane since in the case shown in Fig.S28B the planar equations have 9 restpoints in contrast to the 3 restpoints in the complete system. We thus adapt the expedient of just showing a projection.

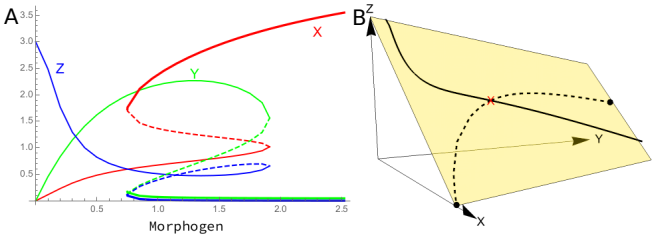

Fig. S28. Three genes in a morphogen gradient with bistability, Eq.35. (A) The branch extending from low morphogen disappears at 1.91, while the upper branch disappears at 0.75. The unstable solution is shown dashed. (B) For the morphogen equal to 1.5, the two fixed points (dots) and the saddle (X) define a plane. The 1D unstable manifold of the saddle (dashed), and the most stable mode of the saddle (black) are projected onto the plane.

The segmental patterning of the blastoderm in *Drosophila*

is the paradigm gene regulatory network, and the control of the gap genes by the anterior morphogen Bicoid has been the subject of several modeling papers (23–25). Only the second of these makes any mention of bistability. We consider multistability or its absence a salient feature of any gene network model.

7. Adaptive systems

One would be hard pressed to find a static morphogen gradient in the early developmental stages in any vertebrate system. However, in the embryo positional information can perfectly well be transmitted to the cell by morphogen spreading from a source if the cellular response is adaptive, i.e., a smoothed time derivative (26–28).

In mathematical terms an adaptive system is one with a single attracting fixed point at which one of the variables is independent of a parameter representing the external input and the others act as a buffer. A simple example from (29) will fix the ideas,

$$\begin{aligned} \dot{a} &= 1 - sa, \\ \dot{h} &= sa - h. \end{aligned} \qquad [36]$$

where s is a time dependent signal and h is the adaptive response and a the buffer. When s is constant, $h = 1$ irrespective of s. The system is linear so by matrix manipulations it can be written as the product of a positive definite metric times the gradient of a quadratic polynomial. But in the case of Eq.36 rewriting it in this way will put s in both the metric and potential, thereby obscuring the simplicity of Eq.36. Better is to write families of adaptive systems based on Eq. 36 by using the potential $U = a - sa^2/2 + (1-h)^2$ and a metric with an off diagonal term. The potential naturally makes the fixed point of h independent of s, and the metric couples a and h when they vary.

1. John Guckenheimer and Philip Holmes. *Nonlinear oscillations, dynamical systems, and bifurcations of vector fields*, volume 42. Springer Science & Business Media, 2013.
2. S. Smale. On gradient dynamical systems. *Annals of Mathematics*, pages 199–206, 1961.
3. V. I. Arnold, V. S. Afrajmovich, Yu. S. Il'yashenko, and L. P. Shil'nikov. *Dynamical Systems V: Bifurcation Theory and Catastrophe Theory*, volume 5. Springer Science & Business Media, 2013.
4. M. W. Hirsch, C. C. Pugh, and M. Shub. *Invariant manifolds*, volume 583. Springer Lecture Notes in Mathematics, 1977.
5. E. C. Zeeman and D. Trotman. The classification of elementary catastrophes of codimension ≤ 5. In *Structural stability, the theory of catastrophes, and applications in the sciences*, pages 263–327. Springer, 1976.
6. E. C. Zeeman. *Catastrophe Theory: Selected Papers, 1972-1977*. Advanced Book program. Addison-Wesley, 1977.
7. I. N. Stewart. Catastrophe theory and equations of state: Conditions for a butterfly singularity. *Mathematical Proceedings of the Cambridge Philosophical Society*, 88(3):429–449, 1980.
8. T. Poston. On deducing the presence of catastrophes. *Mathématiques et Sciences humaines*, 64:71–99, 1978.
9. Geert Vegter. Bifurcations of gradient vector fields. *Astérisque*, 98-99:39–73, 1982.
10. B. A. Khesin. Bifurcations in gradient dynamic systems. *Journal of Soviet Mathematics*, 52 (4):3279–3305, 1990.
11. Stephen Smale. Generalized poincare's conjecture in dimensions greater than four. *Annals of Mathematics*, 74(2):391–406, 1961. ISSN 0003486X. URL http://0-www.jstor.org.pugwash.lib.warwick.ac.uk/stable/1970239.
12. Stephen Smale. On the structure of manifolds. *American Journal of Mathematics*, 84(3): 387–399, 1962.
13. J. Milnor. *Lectures on the h-Cobordism Theorem*. Princeton University Press, 1965.
14. S Newhouse and M Peixoto. There is a simple arc joining any two morse-smale flows. *Asterisque*, 31:15–41, 1976.
15. K. R. Meyer. Energy functions for morse smale systems. *American Journal of Mathematics*, pages 1031–1040, 1968.
16. Morris W Hirsch. *Differential topology*, volume 33. 'Springer Science & Business Media', 2012.
17. Francis Corson, Lydie Couturier, Hervé Rouault, Khalil Mazouni, and François Schweisguth. Self-organized notch dynamics generate stereotyped sensory organ patterns in drosophila. *Science*, 356(6337), 2017.
18. Hans Meinhardt. Models of biological pattern formation. *New York*, page 118, 1982.
19. H Haken and H Olbrich. Analytical treatment of pattern formation in the gierer-meinhardt model of morphogenesis. *Journal of Mathematical Biology*, 6(4):317–331, 1978.
20. Lewis Wolpert, Cheryll Tickle, and Alfonso Martinez Arias. *Principles of development*. Oxford University Press, USA, 2015.
21. Thomas Gregor, Eric F Wieschaus, Alistair P McGregor, William Bialek, and David W Tank. Stability and nuclear dynamics of the bicoid morphogen gradient. *Cell*, 130(1):141–152, 2007.
22. Nikolaos Balaskas, Ana Ribeiro, Jasmina Panovska, Eric Dessaud, Noriaki Sasai, Karen M Page, James Briscoe, and Vanessa Ribes. Gene regulatory logic for reading the sonic hedgehog signaling gradient in the vertebrate neural tube. *Cell*, 148(1-2):273–284, 2012.
23. Johannes Jaeger, Maxim Blagov, David Kosman, Konstantin N Kozlov, Ekaterina Myasnikova, Svetlana Surkova, Carlos E Vanario-Alonso, Maria Samsonova, David H Sharp, John Reinitz, et al. Dynamical analysis of regulatory interactions in the gap gene system of drosophila melanogaster. *Genetics*, 167(4):1721–1737, 2004.
24. Dmitri Papatsenko and Michael Levine. The drosophila gap gene network is composed of two parallel toggle switches. *PLoS One*, 6(7):e21145, 2011.
25. Mariela D Petkova, Gašper Tkačik, William Bialek, Eric F Wieschaus, and Thomas Gregor. Optimal decoding of cellular identities in a genetic network. *Cell*, 176(4):844–855, 2019.
26. Benoit Sorre, Aryeh Warmflash, Ali H Brivanlou, and Eric D Siggia. Encoding of temporal signals by the tgf-β pathway and implications for embryonic patterning. *Developmental cell*, 30(3):334–342, 2014.
27. Anna Yoney, Fred Etoc, Albert Ruzo, Thomas Carroll, Jakob J Metzger, Iain Martyn, Shu Li, Christoph Kirst, Eric D Siggia, and Ali H Brivanlou. Wnt signaling memory is required for activin to function as a morphogen in human gastruloids. *Elife*, 7:e38279, 2018.
28. Idse Heemskerk, Kari Burt, Matthew Miller, Sapna Chhabra, M Cecilia Guerra, Lizhong Liu, and Aryeh Warmflash. Rapid changes in morphogen concentration control self-organized patterning in human embryonic stem cells. *Elife*, 8:e40526, 2019.
29. Paul François and Eric D Siggia. A case study of evolutionary computation of biochemical adaptation. *Physical biology*, 5(2):026009, 2008.